

UNIVERSITY OF CAPE TOWN

IYUNIVESITHI YASEKAPA • UNIVERSITEIT VAN KAAPSTAD

Heat transfer analysis on the growth of artificial sea ice using dynamic temperature profiles in an idealised environment

Prepared by:
Mr Felix Ashton Guni

Supervisor:
Dr Tokoloho Rampai

Co-supervisors:
Prof Klaus Moller
Prof Marcello Vichi

DISSERTATION SUBMITTED TO THE UNIVERSITY OF CAPE TOWN IN FULFILMENT OF THE REQUIREMENTS FOR THE DEGREE OF MASTER OF SCIENCES IN:

CHEMICAL ENGINEERING

November 2022

University of Cape Town

The copyright of this thesis vests in the author. No quotation from it or information derived from it is to be published without full acknowledgement of the source. The thesis is to be used for private study or non-commercial research purposes only.

Published by the University of Cape Town (UCT) in terms of the non-exclusive license granted to UCT by the author.

University of Cape Town

Plagiarism declaration

- I know the meaning of plagiarism and declare that all the work in the document, save for that which is properly acknowledged, is my own. This thesis/dissertation has been submitted to the Turnitin module (or equivalent similarity and originality checking software) and I confirm that my supervisor has seen my report and any concerns revealed by such have been resolved with my supervisor.
- I know that plagiarism is wrong. Plagiarism is to use another's work and pretend that it is my own.
- I have used the Harvard referencing system for citation and referencing. In this report, all contributions to, and quotation from, the work(s) of other people have been cited and referenced.
- This report is my own work. I have not allowed, and will not allow, anyone to copy my work.

PeopleSoft No.	Sign
1562231	Signed by candidate

Abstract

Heat exchange between the atmosphere and the ocean plays a significant role over the Earth's climate, such that despite its complexity, it is essential to fully characterise it. Notably, sea ice growth occurs both in the Northern and Southern Hemisphere. It covers approximately 7% of the global surface area and reflects 40% of the radiation back into the atmosphere. However, over the past few decades there has been an increase in the global temperatures. This has led to the decrease in sea ice extents, and this continues to be accelerated by the positive-ice albedo effect. This effect of sea ice extents on the global climate requires research into models that can accurately predict sea ice growth. Sea ice growth is directly related to the heat exchanged at the ice-atmosphere interface. which can be approximated as the conductive heat flux at the top of the ice.

The objectives of the project were to characterise the vertical conductive heat flux by developing models that can be used to solve the ice growth problem. The techniques developed would then be used to investigate the effect of varying the air temperature, starting solution salinity and tank size on the growth dynamics and conductive heat flux in artificial sea ice. Lastly, the project was aimed at predicting the temperature field in artificial sea ice through estimation of the thermal conductivity.

The project therefore focuses on the development of a 1-D analysis model for the prediction of the vertical conductive heat flux, ice surface temperature and the average thermal conductivity using the temperature distribution of the ice. This was performed by assuming pseudo steady state and treating the ice growth problem as a moving boundary problem. The method for the prediction of the temperature field was based on solving the 1-D dynamic heat diffusion equation showing that the linear pseudo steady state assumption can be used to approximate the dynamic growth of ice and to estimate the model parameters.

The results presented showed the assumption of pseudo steady state is valid for artificial sea ice that has a linear temperature profile with depth. As such the average thermal conductivity, ice surface temperature and heat linearly conducted through the ice were computed through regression of experimental temperature output data by linearisation of the heat diffusion equation. Regression of the temperature profile was performed at each measured time point. Lastly, it was shown that using the model parameters obtained from the linear analysis, a 1-D constant parameter dynamic model with a variable boundary was able to predict the dynamic growth of ice, within a least squares error of 0.31^{o}C between the experimental and model data.

Acknowledgements

This project was sponsored by the National Research Foundation of South Africa (NRF).

I would like to thank my supervisor Dr Tokoloho Rampai for recognising my potential during my undergraduate studies. This was during my second year in 2017. It was from this point that I was scouted to partake in sea ice research.

I would also like to extend my gratitude towards Professor Klaus Moller. He worked with me tirelessly and provided all the support that he could. The extensive knowledge that he shared with me on heat and mass transfer is invaluable.

To Prof Marcello Vichi, thank you for for making funding provisions as well as providing guidance when it was needed.

Nigel Guni, you are the best brother that I know. I am grateful that you are in my life, we are bound by more than blood. Thank you for being a good listener, adviser, for believing in me when I couldn't and for all the support that you continuously give to me. Lisa Kumadiro and Boitumelo Matlakala, you give the word friendship meaning. Thank you for being such a good support system.

Dillon Craig Roberts, thank you for being a kind soul and for all the support.

My deepest gratitude goes towards my late mother, Mrs Maggie Guni Matizanadzo. I wish you had lived to see through all the preliminary hard work that you put through. I am what I am today because of what you instilled in me from a young age.

Special thanks to Hailey Swait, Safiyyah Moos, Curwin Nomdoe, Ameen Jakoet, the preceding Chemical Engineering MARis research students and the Chemical Engineering department for all the help. I would also like to extend my gratitude towards my family and friends. The list is long to get through by name.





Table of Contents

Plagiarism declaration ..... **i**

Abstract ..... **ii**

Acknowledgements ..... **iii**

List of illustrations ..... **vii**

Figures vii

Tables xii

Nomenclature ..... **xiii**

Chapter 1 : Introduction **1**

1.1 Background 1

1.2 Problem statement 1

1.3 Scope and Limitations 2

Chapter 2 : Literature Review **3**

2.1 Morphology and formation of sea ice 4

2.1.1 Sea ice structure 4

2.1.2 Sea ice classification and its formation stages 4

2.1.3 Brine channels and brine drainage 7

2.2 Temperature and salinity profiles of sea ice 7

2.2.1 Temperature 7

2.2.2 Salinity profiles 8

2.3 General thermodynamics of sea ice 9

2.3.1 Sea ice as a “mushy layer” 9

2.3.2 Effect of salinity on sea ice thermodynamics 10

2.3.3 Sea ice phase equilibrium 13

2.4 Thermal Properties of sea ice 14

2.4.1 Thermal conductivity 14

2.4.2 Heat capacity 16

2.4.3 Latent heat of fusion 16

2.5 Modelling the thermodynamic growth of ice and conductive heat flux 17

2.5.1 Thermodynamics of ice growth 17

2.5.2 Heat flux at the ice-atmosphere interface 20
2.6 Artificial sea ice for the study of ice growth dynamics 21
2.6.1 Temperature control in the tank 24
2.6.2 Considerations for the saline solution 24
2.6.3 Nucleation in artificial sea ice tanks 25
2.6.4 Artificial sea ice temperature profiles 25
2.7 Measurement techniques of artificial sea ice variables 26
2.7.1 Ice depth measurement 26
2.7.2 Temperature measurement 27
2.7.3 Salinity measurement 27
2.8 Rationale of study 28

Chapter 3 : Research Objectives 29

3.1 Overall aim and objectives 29
3.2 Key Questions 29

Chapter 4 : Methodology 30

4.1 Mathematical modelling of ice growth 30
4.1.1 Ice growth rate from the energy balance 32
4.1.2 Solution of the dynamic model 32
4.1.3 Development of linear temperature profile model through pseudo steady state 33
4.1.4 Application to temperature profile measurements during ice growth 34
4.1.5 Limitations to the pseudo steady state model 35
4.2 Experimental matrix and tank configuration 37
4.2.1 Temperature and salinity measurements with the inclusion of uncertainties 38
4.2.2 Experimental procedure 40

Chapter 5 : Analysis of temperature- time data using the linearised model 42

5.1 Method of analysis 42
5.2 Interpretation of results 50

Chapter 6 : Investigation of system parameters on the growth rate of artificial sea ice 53

6.1 Variation of the air temperature 53
6.2 Variation of the starting solution salinity 60
6.3 Variation of the tank size 68

Chapter 7 : Dynamic model to solving the temperature field for sea ice 72

7.1 Method of analysis for the dynamic model 72
7.2 Comparison of dynamic model data and experimental data 76
7.2.1 Sensitivity analysis of the linearised model in the determination of the thermal conductivity 78
7.3 Effect of varying parameters on the average instantaneous thermal parameters (k and h) 80
7.3.1 Effect of varying the starting salinity on the thermal parameters 80
7.3.2 Effect of varying the ambient temperature on the thermal parameters 81
7.3.3 Summary of trends in k upon variation of air temperature and starting solution salinity in a 30 L tank 82

Chapter 8 : Conclusions and Recommendation 84

8.1 Conclusions 84
8.2 Recommendations 85

References 86

Appendices 92

Appendix A: Scilab CODES 92
A1: Code for proof-of-concept analysis 92
A2: Code for the dynamic model of solving for the temperature field 97
Appendix B: Experimental temperature output data 102
B1: Uncertainty in temperature measurements 102
B2: Temperature profiles to analyse the effect of varying the air temperature on the growth dynamics and conductive heat flux of artificial sea ice 104
B3: Temperature profiles to analyse the effect of varying the starting solution salinity on the growth dynamics and conductive heat flux of artificial sea ice 105
B4: Temperature profiles to analyse the effect of varying the tank on the growth dynamics and conductive heat flux of artificial sea ice 106
B5: Dynamic model output data 107
Appendix C: Cross polarised images for artificial sea ice 109
Appendix D: Ethics Approval 111

List of illustrations

Figures

Figure 2.1:Crystal structure of ice (Weeks & Ackley,1982) 4

Figure 2.2:Vertical cross section of sea ice (Schwarz and Weeks, 1977) 6

Figure 2.3:Normalised salinity curves where A shows a C-type curve, B shows an S-type curve, C shows an opposite of the S-type, the ?-type. D shows the I-type curve (Eicken,1992) 9

Figure 2.4: Representation of the relationship of saltwater density maximum to temperature and salinity....12

Figure 2.6: Summary of the heat fluxes experienced through sea ice (adapted from Wiese,2012) 17

Figure 2.7: Modelled sea ice growth profile as a function of the cumulative number of freezing days (Anderson, 1961) 19

Figure 2.8: Temperature evolution with time profile for artificial sea ice grown at -20^{o}C in a 15 L tank where the temperature was measured using thermistors (Wettlaufer et at., 1997) 26

Figure 4.1: Ice growth model problem definition schematic....30

Figure 4.2: Tank configuration for artificial sea ice grown inside a cold laboratory at UCT ...38

Figure 4.3: Tank schematic showing temperature probe placement and tank dimensions ...39

Figure 5.1: Experimental temperature profile for artificial sea ice grown at -20^{o}C at 10PSU 43

Figure 5.2: Temperature profile with depth for artificial sea ice grown at -20^{o}C at 10PSU 45

Figure 5.4:Ice growth profile for artificial sea ice grown at -20^{o}C and 10PSU 47

Figure 5.5 : Smoothed ice growth rate profile for artificial sea ice grown at -20^{o}C and 10 PSU for a period of 160 hours. 48

Figure 5.6: Estimation of h/k from the slope of 1/alpha vs ice thickness using regressed data for artificial sea ice grown at -20^{o}C and 10 PSU for a period of 160 hours 48

Figure 5.7: Conductive heat flux with time for artificial sea ice grown at -20^{o}C at 10PSU using the pseudo steady state method 49

Figure 5.8: Salinity profile for artificial sea ice grown at 10PSU at -20^{O}C after 160 hours 50

Figure 6.1: Temperature profiles for artificial sea ice grown at 10 PSU where the blue curves are for the experimental run at -10°C, green is for the experimental run at -15°C and red/orange is for the experimental run at -20°C.....54

Figure 6.2: Temperature with depth profile for artificial sea ice that was grown at 10 PSU to show the effect of varying air temperature where the air temperature for (a) is -10°C, the air temperature for (b) is -15°C and the air temperature for (c) is -20°C 54

Figure 6.3: Variation in the change in the slope of dT/dz with units in °C/cm to show the effect of varying the ambient temperature.....55

Figure 6.4: Growth profile for artificial sea ice that was grown at 10 PSU but at different air temperatures 55

Figure 6.5: Smoothed ice growth rate profiles for artificial sea ice that was grown at 10 PSU but at different air temperatures to show the effect of varying the ambient temperature 56

Figure 6.6: Evaluation of the driving force for artificial sea ice that was grown at 10 PSU but at varied air temperatures.....57

Figure 6.7: Estimation of h/k from the slope of 1/alpha vs ice thickness using regressed data for artificial sea ice that was grown at 10 PSU but at varied air temperatures 57

Figure 6.8: Salinity profile for artificial sea ice that was grown at 10 PSU at varied air temperatures 58

Figure 6.9: Conductive heat flux of artificial sea ice that was grown at 10PSU at varied air temperatures 59

Figure 6.10: Temperature with time profile for artificial sea ice grown at -20°C to show the effect of varying the starting solution salinity. The solid lines are profiles for artificial sea ice at a depth of 3 cm and the dashed lines temperature profiles at 5 cm 60

Figure 6.11: Temperature with depth profile for artificial sea ice that was grown at -20°C to show the effect of varying initial solution salinity where the starting solution salinity for (a) is 10 PSU, the starting solution for (b) is 20 PSU and the starting solution for (c) is 30 PSU 61

Figure 6.12: Variation in the change in the slope of dT/dz with units in °C/cm to show the effect of varying the starting solution salinity.....62

Figure 6.14: Smoothed ice growth rate profiles for artificial sea ice that was grown at -20°C but at different starting solution salinity 63

Figure 6.15: Evaluation of the driving force for artificial sea ice that was grown at -20°C to show the effect of varying the starting salinity 64

Figure 6.16: Estimation of h/k from the slope of 1/alpha vs ice thickness using regressed data for artificial sea ice that was grown at -20°C to show the effect of varying the starting solution salinity 65

Figure 6.17: Conductive heat flux of artificial sea ice that was grown at -20°C to show the effect of varying the starting salinity 66

Figure 6.18: Salinity profile for artificial sea ice that was grown at -20°C to show the effect of varying starting salinity 66

Figure 6.19: Temperature profile with depth for artificial sea ice grown at -20°C and 30 PSU to show the effect of tank size where the tank size for (a) is 3 L, the tank size for (b) is 30 L and the tank size for (c) is 300 L.....68

Figure 6.20: Growth profile for artificial sea ice that was grown at -20°C to show the effect of varying the starting salinity 69

Figure 6.21: Salinity profile for artificial sea ice grown at -20°C and 30 PSU to show the effect of tank size on the growth dynamics of artificial sea ice.....70

Figure 7.1: Simulated temperature with depth profile for artificial sea ice growing at -20°C where all the temperature nodes are within the ice.....73

Figure 7.2: Simulated temperature evolution with time for artificial sea ice growing at -20°C where all the nodes are within the growing ice. The nodes are always at the same position relative to the length of ice, L(t).....74

Figure 7.3: Simulated temperature evolution with time for artificial sea ice growing at -20°C where the temperature profiles are reported at the same fixed locations within the tank as were used in the experimental measurements. 75

Figure 7.4: Simulated temperature with depth profile for artificial sea ice growing at -20°C where the thermocouples stationary and the growing ice front is moving past them 75

Figure 7.5: Modelled ice growth profile for artificial sea ice that was simulated at -19.5°C at a starting solution salinity of 10 PSU.....76

Figure 7.6: Modelled growth rate for artificial sea ice that was simulated at -20°C at a starting solution salinity of 10 PSU.....77

Figure 7.7:Comparison of the modelled vs experimental temperature time profile 77

Figure 7.8: Estimation of the thermal conductivity from the linearised model using the dynamic model data and the experimental data for artificial sea ice grown at -20°C at 10 PSU 78

Figure 7.9: Estimation of the convective heat transfer coefficient from the linearised model using the dynamic model data and the experimental data for artificial sea ice grown at -20°C at 10 PSU 79

Figure 7.10: Average instantaneous variation of thermal conductivity for artificial sea ice that was grown at -20°C to show the effect of varying the starting salinity.....80

Figure 7.11: Average instantaneous variation of the convective heat transfer coefficient for artificial sea ice that was grown at -20°C to show the effect of varying the starting salinity.....81

Figure 7.12: Average instantaneous variation of thermal conductivity for artificial sea ice that was grown at 10 PSU to show the effect of varying the ambient temperature.....81

Figure 7.13: Average instantaneous variation of the convective heat transfer coefficient for artificial sea ice that was grown at 10 PSU to show the effect of varying the ambient temperature 82

Figure 7.14: Variation of the average thermal conductivity across the duration of the experiment for artificial sea ice that was grown at -20°C in a 30 L tank but at varied starting solution salinities.....83

Figure 7.15: Variation of the average thermal conductivity across the duration of the experiment for artificial sea ice that was grown at 10 PSU in a 30 L tank but at varied temperatures 83

Figure B1: Zoomed in temperature time profile for artificial sea ice showing the temperature fluctuations as recorded by the temperature probe located 1 cm within the growing ice- to show the uncertainty in the temperature measurements.....102

Figure B2: Zoomed in temperature time profile for artificial sea ice showing the temperature fluctuations as recorded by the temperature probe located 1 cm above the ice surface to measure the air temperature within the growing ice- to show the uncertainty in the temperature measurement.....102

Figure B3: Temperature time profile showing the defrost cycles as recorded by the temperature probe located 1 cm above the ice surface to measure the air temperature within the growing ice.....103

Figure B4: Variation of the correlation coefficient of the linear regression of the temperature vs depth data at each time point in Figure 5.2. (this is for the experiment that was performed at -20°C at 10 PSU).....103

Figure B5: Temperature-time profile for artificial sea ice grown at 10 PSU at -15°C for 160 hours.....104

Figure B6:Temperature- time profiles for artificial sea ice grown at 10 PSU at -10°C for 94 hours.....104

Figure B7:Temperature-time profile for artificial sea ice grown at 10 PSU at -20°C for 140 hours in 30 L tank.....105

Figure B8:Temperature-time profile for artificial sea ice grown at 20 PSU at -20°C for 125 hours in 30 L tank.....105

Figure B9:Temperature-time profile for artificial sea ice grown at 30 PSU at -20°C for 248 hours in 30 L tank.....106

Figure B10: Temperature-time profile for artificial sea ice grown at 30 PSU at -20°C for 25 hours in a 3 L tank.....106

Figure B11: Temperature-time profile for artificial sea ice grown at 30 PSU at -20°C for 350 hours in a 300 L tank.....107

Figure B12: Simulated temperature with normalised depth profile for artificial sea ice growing at -20°C where all the temperature normalised nodes are within the ice.....107

Figure C1: Cross polarised sample for artificial sea ice that was grown at -20°C at 30 PSU in the 30 L tank where (a) represents the top section of the ice and (b) represents the bottom segment of the ice.....109

Figure C2: Cross polarised sample for artificial sea ice that was grown at -20°C at 20 PSU in the 30 L tank where (a) represents the top section of the ice and (b) represents the middle segment of the ice and (c) represents the bottom segment of the ice.....109

Figure C3: Cross polarised sample for artificial sea ice that was grown at -20°C at 10 PSU in the 30 L tank where (a) represents the top section of the ice and (b) represents the bottom segment of the ice.....110

Figure C4: Cross polarised sample for artificial sea ice that was grown at -10°C at 10 PSU in the 30 L tank.....110

Tables

Table 2.1: Thermal conductivity of pure ice at 0°C 15

Table 2.2: Summary of ice properties for artificial sea ice 22

Table 2.3: Summary of advantages and disadvantages of artificial using saline ice experiments in the study of sea ice, (Haas, 1999) 23

Table 4.1: Experimental matrix for experiments that were performed in the 30 L tank to assess for the effect of varying the air temperature and the starting solution salinity artificial sea ice. The effect of tank size is reflected in C1, C2 and C3. 37

Table 6.1: Estimation of h/k from temperature measurements for artificial sea ice 58

Table 6.2: Salinity uptake data for artificial sea ice that was grown at 10 PSU at varied air temperature 59

Table 6.3: Thermal conductivity estimation from temperature measurements for artificial sea ice 65

Table 6.4: Salinity uptake data for artificial sea ice that was grown at -20°C to show the effect of varying starting salinity 67

Table 6.5: Salinity uptake data for artificial sea ice that was grown at -20°C and 30 PSU to show the effect of varying the tank size.....70

Table 7.1: Parameters used in the dynamic model 72

Nomenclature

h : Convective heat transfer coefficient of air

k : Thermal conductivity of sea ice/ artificial sea ice

PSU : Practical Salinity Units where 1 PSU is 1g of salt in 1 kg of water

Q_a : Atmospheric heat flux at the ice-atmosphere interface (W/m^2)

$Q_{c,b}$: Conductive heat flux at the bottom of the ice (W/m^2)

$Q_{c,t}$: Conductive heat flux at the top of the ice (W/m^2)

Q_e : Heat loss through evaporation (W/m^2)

Q_H : Latent heat released during ice formation (W/m^2)

Q_{lw} : Longwave radiation (W/m^2)

Q_{sw} : Incoming short-wave radiation from the sun (W/m^2)

Q_w : Ice-Oceanic interface heat flux (W/m^2)

T_a : Air temperature

T_o : Ice surface temperature

T_f : Freezing point temperature (°C)

T_w : Freezing temperature of pure water (0°C)

S_{bu} : Bulk in-ice salinity (PSU)

S_{br} : interstitial brine salinity (PSU)

L : Ice length (cm)

φ : Solid volume fraction of solid ice crystals

∇ : vector differential operator del acting on the space coordinates

Chapter 1 : Introduction

1.1 Background

Sea ice plays an important role in the Earth's climate due to its insulative and reflective power. Furthermore, sea ice at the poles maintains the global ocean circulation and this can be referred to as thermohaline circulation (Allison, 1981). However, sea ice is susceptible to changes in atmospheric temperatures which have been observed to be steadily increasing since the late 1980's (IPCC, 2019). This has resulted in more studies being conducted to improve knowledge on sea ice and to incorporate its effect on the Earth's climate system (Notz, 2005).

There has been extensive research on the growth patterns of the sea ice in the Northern hemisphere, the Arctic region. The research was largely done due to prospects into offshore oil and gas operations. The Arctic ice exists in a dynamic state and the presence of the open ocean affects its growth and melt rate. The sea ice in the Antarctic takes on a different form due to the combination of turbulent waters and low temperatures. It is important to note that in the Southern hemisphere, the growth and melt rate of the sea ice in the Antarctic Marginal Ice Zone (MIZ) has been unresearched (Weeks & Hibler, 2010).

The growth and melt sea of ice is dependent on the heat exchange between the atmosphere and the ocean. As such the value of knowing the heat flux lies in its ability to determine regional and seasonal variations in the ice thickness(McPhee & Untersteiner, 1982). Investigating the relationship between the heat exchanged and the growth conditions of sea ice on its growth dynamics is important as the information can be used as input to global climate models.

The MARiS in Chemical Engineering Research group at the University of Cape Town has embarked on studies that are aimed at understanding the growth of sea ice. However, it is costly to conduct field experiments. As such, the research team has sought to grow artificial sea ice as the base case for understanding how different variables affect the growth of sea ice. This is because the study of artificial sea ice offers greater control over sea ice growth variables such as the initial starting solution salinity, air temperature, and the cooling rate.

1.2 Problem statement

It has been established that the growth of sea ice is largely dependent on the growth conditions of the ice. In addition, sea ice growth is directly related to the heat flux liberated by the ocean

into the atmosphere. The value of knowing the heat flux lies in its role in determining the regional and seasonal variations in ice thickness (McPhee & Untersteiner, 1982). However, it is difficult to directly measure the heat flux of in-situ ice. Furthermore, it has been established that the growth rate of sea ice is dependent on variations in the ocean's heat flux. Models that quantify the conductive heat flux have been established. These models have a dependency on the thermal properties of the growing ice. However, the relationship between the conductive heat flux and the growth conditions of artificial sea ice is an area that requires further research.

1.3 Scope and Limitations

The focus of the project was to therefore investigate the effect of growth conditions on the growth dynamics and vertical conductive heat flux of artificial sea ice. Growth conditions in this case refers to the starting solution salinity, air temperature, and tank size. It is important to note that, the artificial sea ice was grown under calm conditions, hence it mimics the conditions in the Arctic for columnar ice. However, it was grown at constant air temperature, unlike in the open ocean where the air temperature changes periodically. The work on this project therefore serves as a base case to understand sea ice growth by analysis of artificial sea ice that was grown under calm conditions. This project is devoted towards the modelling of artificial sea ice. It does not extend towards the modelling of real natural sea ice.

The investigation is limited to varying the air temperature between -5^{o}C and -20^{o}C and the starting solution salinity between 10 PSU and 30 PSU. Moreover, the study is limited to three tanks, 3 L, 30 L and 300 L. The saline ice properties under investigation include the average thermal conductivity, driving force for heat transfer and growth profiles. This information will be obtained from experimentally determined temperature profiles. Lastly, this project aims to find a simplified solution that can predict the temperature field of sea ice. The continuous salinity profile could not be measured, as such this study is limited towards the analysis of the vertical salinity profile that was measured at the end of the experiment.

The study begins with a literature review on sea ice and the application of artificial sea ice studies to supplement field experiments for sea ice. The research objectives are in Chapter 3. These are followed by the methodology section in Chapter 4. The analysis technique for the treatment of results is presented in Chapter 5 and the results and discussion in Chapter 6. The development of the dynamic model to predict the temperature field in artificial sea ice is presented in Chapter 7. The conclusions and recommendations are given in Chapter 8. Appendices are presented in the last section

Chapter 2 : Literature Review

Heat exchange between the atmosphere and the oceans plays a significant role over the Earth's climate, such that despite its complexity, it is essential to fully characterise it (Trodahl et al., 2001). Notably, sea ice growth occurs in the polar regions in the Northern and Sothern hemispheres during the winter period. Sea ice has an extensive surface area accounting for as much as 7% of the global surface area in winter months (Weeks, 2010). Its presence is a major limiting factor for heat exchange for two main reasons. Firstly, it acts as an effective insulator at the ice atmosphere interface, decreasing the rate of heat exchange at the air-ice interface (Semtner Jr, 1976). Secondly, it reflects as much as 40% of the radiation back into the atmosphere (Rinke et al., 2006).

Sea ice at the poles maintains the global circulation systems where the denser water that is generated from the sea ice is circulated to the poles. However, in the last few decades the global air temperatures have steadily been increasing and have thus resulted in a decrease in sea ice extents (IPCC, 2019). Furthermore, the decrease in sea ice extents accelerates the rate of sea ice extent decrease. This is due to the positive sea-ice albedo effect (Rinke et al., 2006). The sea ice albedo effect is described as the decrease in sea ice extent which results in an increase in global air temperatures and consequently an increase in the rate of sea ice reduction (Curry, Schramm & Ebert, 1995). Considering the effect that sea ice has on the global climate, this has resulted in research into models that can predict and incorporate for the sea ice decrease.

The distribution of sea ice thickness is controlled by thermal processes that lead to growth and melting of the ice and mechanical processes that are induced by internal, oceanic and wind stresses which drive deformation (Thorndike, 1992). The most common approach in the numerical simulation of these processes is to treat the thermal evolution one dimensionally and couple this to the motion of sea ice (Thorndike, 1992). The thermal evolution of the ice is dependent on the thermal properties of the ice and one of the thermal parameters that is required by the climate models is the thermal conductivity of sea ice. This parameter has been reported to be a function of temperature and salinity. As such it is important to investigate how heat exchange and the growth rate of ice is affected by the growth conditions that the sea ice is subjected to. These growth conditions include the atmospheric temperature and salinity of the saltwater (Middleton et al., 2016). On the other hand it has become common practice to supplement natural sea ice field experiments with artificial sea ice experiments due to the advantages that this has (Haas, 1999).

2.1 Morphology and formation of sea ice

2.1.1 Sea ice structure

Sea ice has a tetrahedral arrangement of H_2O molecules in which a central H_2O molecule is bonded to four other water molecules through hydrogen bonding. The hydrogen bonding is between an electronegative oxygen atom of one H_2O molecule and a hydrogen atom from another water molecule. The extensive tetrahedral arrangement of the H_2O molecules leads to the open hexagonal crystal structure of sea ice. This hexagonal arrangement allows ice to be less dense than its melt. Figure 2.1 shows a schematic of the hexagonal crystal structure of sea ice (Weeks & Ackely, 1982).

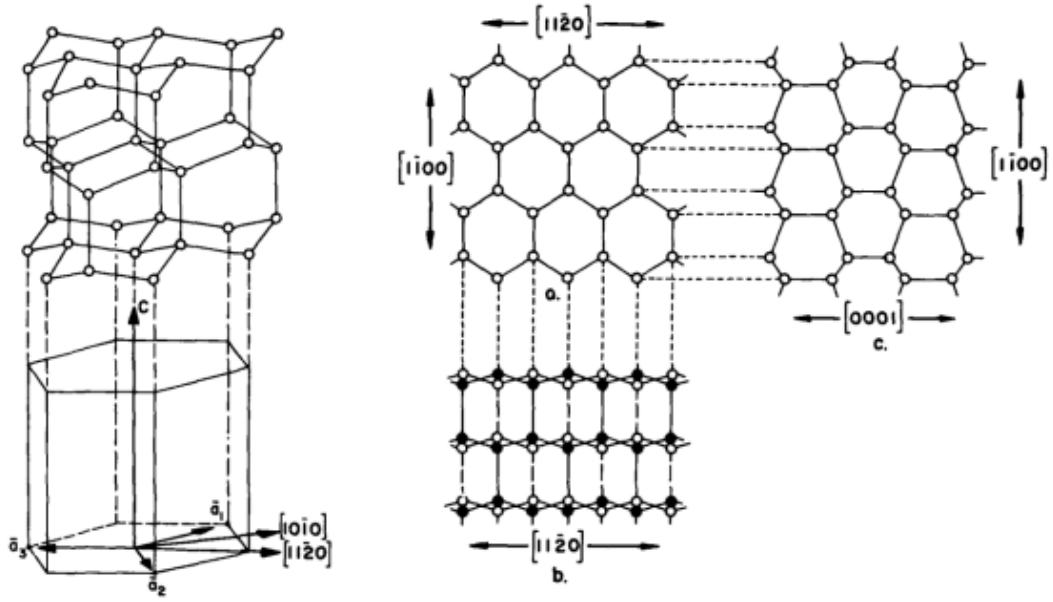


Figure 2.1:Crystal structure of ice (Weeks & Ackley,1982)

Figure 2.1 shows the hexagonal arrangement of the crystal faces of sea ice. The arrangement of oxygen atoms allows for easy fracture to occur along the basal plane which is shown as [0001] in Figure 2.1. There is easy fracture along the basal plane as there are fewer bonds that need to be broken. The basal plane is the axis that shows the hexagonal symmetry of sea ice. The axis normal to the basal plane of sea ice is known as the crystallographic axes or c-axis and it is shown by the arrow labelled c in Figure 2.1. Light passes through the c-axis without being diffracted. Hence, the c-axis is also known as the optical axis (Fransson, 2009). Moreover, the hexagonal faces of ice lie parallel to the c- axis (Maykut, 1985a)

2.1.2 Sea ice classification and its formation stages

Sea ice formation occurs through atmospheric cooling and it is most predominant during winter months at the polar regions (Wiese, 2012). Sea water has been reported to have a salt content of 34 PSU (Worster & Jones, 2015). Hence, freezing of the ocean surfaces starts to occur at temperatures around -1.7ºC (Talley, 2002). Sea ice begins as small spherical ice crystals on the surface of open water. These small crystals are randomly oriented, growing into hexagonal discs. When these crystals have sufficiently grown their preferred crystal orientation will be in the basal plane. The initial small ice platelets are termed as frazil ice and these occur when the surface layer of the ocean is supercooled (Weeks & Ackely, 1982). Frazil ice is described as a suspension of ice crystals on the ocean surface exhibiting a slush like appearance. Moreover, it has a granular ice texture and is formed from the agglomeration of individual frazil ice crystals. Granular ice is isotropic in that its properties do not vary according to the direction of measurement (Eicken & Lange, 1989). The initial granular ice has a c-axes that is predominantly oriented in the vertical direction.

Once frazil ice has formed on the ocean surface, the growth pathways and appearance of the sea ice becomes dependent on two prevailing environmental conditions namely turbulent and calm conditions. Under calm conditions frazil ice freezes to form a thin flexible sheet of ice known as nilas. Frazil ice and nilas are both termed as new ice, as the ice continues to grow it is termed as young ice. In the ocean, when the ice has reached a thickness beyond 30 cm it is termed as first-year ice (Weeks & Hibler, 2010). However, under turbulent conditions, in high winds and a rough sea state the frazil ice grows through consolidation rather than growth in individual crystal size. The frazil ice crystals are churned into a thick soupy layer known as grease ice. The ice crystals of grease ice are not bonded well together, and they lose their shape when taken out of the water (Weeks & Hibler, 2010).

As the grease ice continues to thicken, the frazil ice crystals freeze together to form small conglomerate masses of ice. These conglomerates grow through adherence of the frazil crystals whilst bumping into each other due to the rough sea state. The bumping action rounds the edges of the ice. This results in the formation of pancake ice (Doble, Coon & Wadhams, 2003; Løset et al., 2006). Pancake ice continues to grow through agglomeration and rafting. They eventually congeal to form consolidated ice. As consolidated ice begins to grow, anisotropic growth occurs and this facilitates the process of geometric selection in the direction of the preferred crystal orientation (Maykut, 1985b). The growth stages of sea ice cause differences in the vertical structure of the ice. The vertical structural differences of sea ice are shown in Figure 2.2.

Figure 2.2 shows that there are four main layers that can be distinguished from the vertical structural profile of sea ice for the case where there is no snow. These include the initial ice layer, the transition zone, the columnar zone and the skeletal layer (Schwarz & Weeks, 1977).

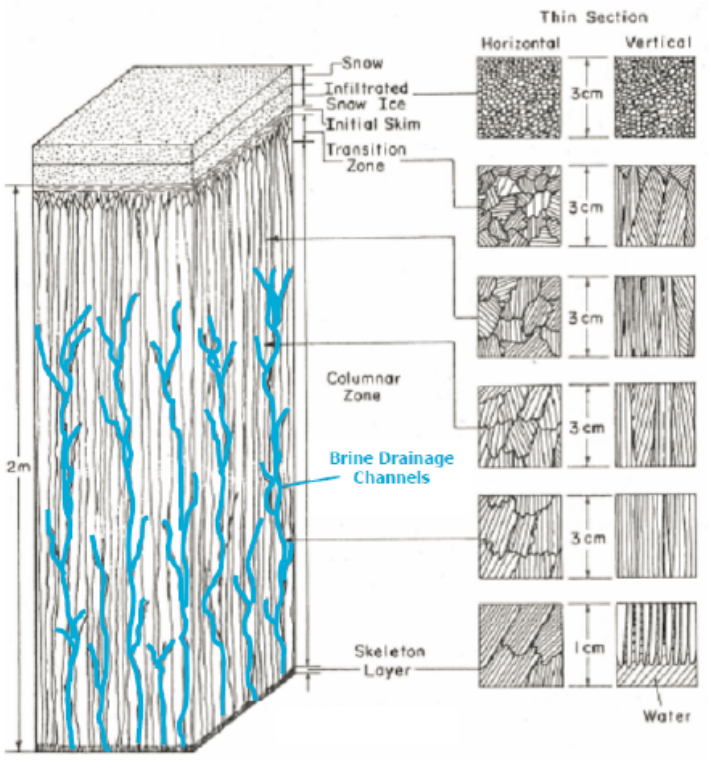


Figure 2.2:Vertical cross section of sea ice (Schwarz and Weeks, 1977)

The formation stages of the initial layer have been described above. In natural sea ice the direction of heat flow is dominant in the vertical direction. Hence, as the ice growth progresses, the c-axes that are parallel to the direction of the heat flow grow faster. These intersect with the crystal that have a less favoured direction and inhibit their growth. The layer where this shift occurs is known as the transition layer (Weeks & Ackely, 1982) and its location is shown in Figure 2.2.

The layer following the transition layer is called the columnar layer wherein the preferred direction of downward crystal growth is dominant. The crystals are therefore oriented downwards with the c-axis oriented horizontally (Weeks & Ackely, 1982). Thus at depths of 50-100 mm the c-axes have a horizontal orientation (Kawano & Ohashi, 2009). The last layer is the skeletal layer and this layer is highly porous and it is found between the ice-ocean interface (Light, Maykut & Grenfell, 2003)

The hexagonal crystal structure of sea ice that is displayed in Figure 2.1 does not allow the incorporation of any additional molecules within its crystal matrix, thus, salts are expelled from the growing ice and they are expelled through brine drainage channels that are shown in blue in Figure 2.2. These are discussed in detail in section 2.1.3.

2.1.3 Brine channels and brine drainage

When ice is forming the salt is expelled into the underlying solution. The rejected salt is concentrated in the surrounding liquid because the solubility limit of the salt in the ice crystal lattice is small (Weissenberger et al., 1992. With growing ice, the salty liquid or brine gets subsequently trapped within the ice inclusions or channels which are shown in Figure 2.2. In the case of granular ice, the brine and salt inclusions are found between the ice crystals, trapped by surrounding ice crystals (Weissenberger et al., 1992). However, in columnar ice, the salt and brine inclusions occur within the crystals at the grain boundaries in vertically oriented planes. Interconnection of the brine inclusions leads to the formation of the brine channels, and these can grow or shrink as a function of temperature. Brine channels occur because of the various convective processes that occur. The convective processes occur due to the vertical temperature and salinity gradients that occur as the ice is growing (Worster, 1996; Neufeld & Wettlaufer, 2008). It has been reported that brine channels allow for brine convection to occur within the ice and young ice has been found to experience significant brine drainage (Notz & Grae Worster, 2008).

2.2 Temperature and salinity profiles of sea ice

2.2.1 Temperature

The temperature profile has been reported to follow a linear trend with depth (Notz, 2005; Wiese, 2012; Petrich & Eicken, 2017). The linear temperature profile follows from the direction of heat flux in the ocean. There is top-down cooling between the underlying water and the atmosphere. The direction of heat exchange in sea ice can be approximated using the heat flux in the vertical direction only. This is because horizontal gradients in sea ice are small compared to vertical gradients. Hence, these can be ignored as their effects are negligible (Maykut & Untersteiner, 1971).

During the early stages of ice growth when the ice crystals have not completely covered the sea surface, a supercooled layer forms on the ice surface as mentioned in earlier sections. As a result, the growth rate of the ice is faster in the horizontal direction than in the downward direction with crystal growth occurring mostly on the surface(Weeks & Ackely, 1982). The

diffusivity of heat is higher in the ice crystals than in seawater therefore the temperature in and around the ice crystals becomes lower (Kawano & Ohashi, 2009). Once the ice crystals have covered the sea surface and the thickness of the ice has increased, the temperature distribution in the horizontal direction becomes uniform. This means that fluctuations of temperature in the horizontal direction become minimal, with temperature decreasing with depth as the sea ice grows downwards (Kawano & Ohashi, 2009).

2.2.2 Salinity profiles

Brine is removed from the ice through four desalination processes. These include gravity drainage, brine expulsion, brine-pocket diffusion and flushing (Notz, 2005). These processes result in the creation of a salinity profile within the sea ice. As such there exists horizontal and vertical variations in the distribution of brine in sea ice. The horizontal variations are attributed to the changes in the snow cover and ice thickness whereas the vertical variations are due to brine drainage and brine entrapment from the four aforementioned desalination processes (Vancoppenolle, Fichefet & Goosse, 2009; Gough et al., 2012) with gravity drainage being the main mechanism for salt expulsion (Notz, 2005). There are four possible vertical salinity profiles that sea ice can exhibit, and these are shown in Figure 2.3.

The vertical salinity profile of sea ice typically resembles a “C” shaped profile with a high salinity at the top and bottom of the ice and lower salinity at the middle of the ice as shown in Figure 2.3. The “C” shaped vertical salinity profile is typical of growing young sea ice. The reason for the c-shaped profile in young ice is because salt expulsion is dependent on the growth rate and temperature distribution of the ice (Eicken, 1992). Moreover, ice salinity has been reported to be a linear function of the ice growth rate. Hence, the surface salinity of the ice is high as the surface layer is formed during the period of rapid ice growth. The middle layer is formed when the growth of the ice starts to slow down, hence it has a lower salinity (Weeks & Assur, 1967; Cox & Weeks, 1975). The high salinity experienced at the bottom of the ice is due to the open structure of the ice at the bottom and the brine drainage from the ice above.

The second salinity profile is the “S” type where the salinity of the ice is high at the top and reaches a minimum at the bottom. The “S” type salinity profile is usually found in first year ice. Its ice surface salinity is lower than that of the “C” shaped profile. The “?” salinity profile mirrors the opposite of the “S’ shaped profile with the ice salinity increasing towards the bottom of the ice. This salinity profile is found in sea ice at the beginning of the melt season where the melt water at the surface of the ice lowers its surface salinity.

The last salinity profile displays an “I” shape and is typically found in multi-year ice. This profile shows a decrease in ice salinity towards the bottom of the ice, displaying a characteristic linear shape (Eicken, 1992). The, formation processes of sea ice, salinity and temperature profiles are dependent on the thermodynamics underpinning sea ice.

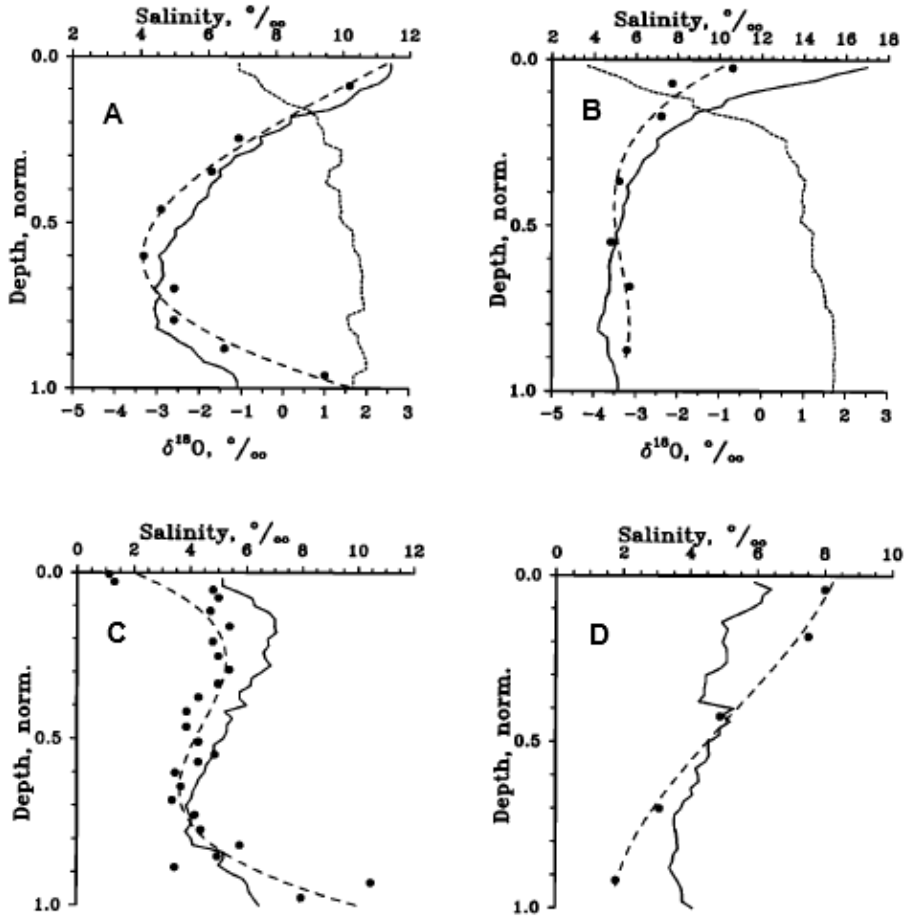


Figure 2.3:Normalised salinity curves where A shows a C-type curve, B shows an S-type curve, C shows an opposite of the S-type, the ?-type. D shows the I-type curve (Eicken,1992)

2.3 General thermodynamics of sea ice

2.3.1 Sea ice as a “mushy layer”

The solidification of a multicomponent fluid may result in the formation of a porous medium through which interstitial fluid may flow (Worster, 1996). In the sea, solidification of the seawater results in the formation of finger-like structures which then form convective currents (De Paoli, Alipour & Soldati, 2020). A porous layer is thus formed from the convoluted interface and it is made out of dendritic crystals that would have been formed during the solidification process of the multi-component solution (Schulze & Worster, 2005; Neufeld & Wettlaufer, 2008). This porous medium that contains the interflowing fluid is known as the

mushy layer. The structure of sea ice has been likened to that of the mushy layer (Middleton et al., 2016). Furthermore, mushy layers can also be found in metallic alloys and in aqueous solutions (Peppin et al., 2007). Thus the “mushy” layer is a reactive, porous two–phase component system. It is not a layer as the name suggests. It is a rigid matrix of solid ice bathed in its impurity rich melt termed brine (Feltham et al., 2006).

Nuefeld & Wettlaufer, (2008), have reported that natural buoyancy forces are one of the mechanisms that drive fluid flow in the mushy layer. These buoyancy forces emanate from salinity and temperature gradients. Worster, (1996) further mention that the buoyant convection results in the formation of vertically elongated vents that are known as chimneys. In the context of sea ice these chimneys represent the brine channels whose formation has been previously mentioned. Moreover, thermal convection that occurs as a result of the temperature decrease during the solidification process, mainly contributes to salt expulsion through gravity drainage (Middleton et al., 2016). Lastly, the “mushy layer” theory is the most widely used thermodynamic description of sea ice.

2.3.2 Effect of salinity on sea ice thermodynamics

The presence of salt in seawater results in freezing point depression and it affects the density of the saltwater. The bulk salinity of ice S_{bu} is related to the salinity of the brine S_{br} by the following correlation (Equation 2.1) where φ is the volume fraction occupied by the solid crystals (Worster & Jones, 2015).

$$S_{bu} = (1 - \phi)S_{br} \qquad \text{Equation 2.1}$$

It therefore follows that the thermodynamic properties of mushy layers are a combination of its different phases (Notz, 2005). The theory of mushy layers makes use of the assumption that sea ice is in local thermodynamic equilibrium. However, this assumption holds when the rate of phase change within the growing ice is rapid enough to maintain thermodynamic equilibrium between the solid and liquid elements. Furthermore, the assumption of local thermodynamic equilibrium implies that the brine concentration and temperature lie on the liquidus curve on the equilibrium phase diagram for sea ice (Feltham et al., 2006).

The liquidus temperature is the temperature at which a multi component material starts to form a solid. The liquidus temperature for pure materials is the same as the material’s freezing temperature and is therefore a constant at constant pressure. However, for solutions where saltwater is an example, it is a function of concentration and pressure (Notz, 2005). The

liquidus curve can be approximated by Equation 2.2 which relates the equilibrium freezing temperature or liquidus temperature T_f of brine to its salt concentration. It follows from the liquidus relationship that when the salinity of brine is high, the liquidus temperature is low. When a slight change in the local temperature occurs, to maintain phase equilibrium a simultaneous change in the interstitial brine occurs. As an example, when there is a drop in the local temperature, some of the water in the brine refreezes to form ice. This increases the salinity of the remaining brine which then re-establishes a new phase equilibrium at a lower temperature. Through this mechanism the mushy layer maintains phase equilibrium and the local brine salinity can be inferred from the local temperature field (Notz, 2005).

Equation 2.2 is analogous to the one presented by Worster and Rees Jones, (2015) for the calculation of the freezing temperature of saltwater as a function of salinity. When S is used, this refers to T_f of the saltwater but when S_{br} is used, it refers to T_f of the interstitial brine.

$$T_f = T_w - mS \qquad \text{Equation 2.2}$$

Where T_f is the expected freezing temperature, m is a constant (0.05°C/PSU) and T_w is the freezing temperature of pure ice and S is the saltwater salinity in PSU. A further correlation for the calculation of the freezing temperature as a function of temperature and pressure is given by Fofonoff and Millard, (1983) which is presented below as Equation 2.3, where p represents the pressure. However, the effect of pressure can be neglected as ice formation occurs at sea level.

$$T_f = -0.0575S_{br} + 0.0017{S_{br}}^{\frac{3}{2}} - 0.0002{S_{br}}^{2} - 0.0007p^4 \qquad \text{Equation 2.3}$$

The complex phase composition of sea ice influences its physical properties during freezing and melting. The heat capacity, thermal conductivity and latent heat of fusion are dependent on the bulk salinity and temperature of sea ice (Wiese, 2012). The solid fraction and the bulk salinity are linked using Equation 2.1. Interstitial brine salinity profiles are usually obtained from temperature measurements with the assumption that the brine salinity is given by the liquidus temperature. Weast, (1971) gave a correlation for NaCl solutions where the brine salinity is calculated using Equation 2.4 for concentrations between 1 and 230 PSU.

$$S_{br\,(NaCl)} = -0.00361T^3 - 0.388T^2 - 17.6T \qquad \text{Equation 2.4}$$

Equation 2.4 was derived from the freezing temperature of NaCl solutions which is shown in Equation 2.5

$$T_{f(NaCl)} = -0.0592S_{br} - 9.37x10^{-6}{S_{br}}^2 - 5.33x10^{-7}{S_{br}}^3 \qquad \text{Equation 2.5}$$

The addition of salt to freshwater not only causes a freezing point depression but it also results in an increase in the density of the solution. The increase in the solution density as the salinity of the solution increases is shown in Figure 2.4 which shows the temperature of maximum density and the corresponding freezing point of the seawater.

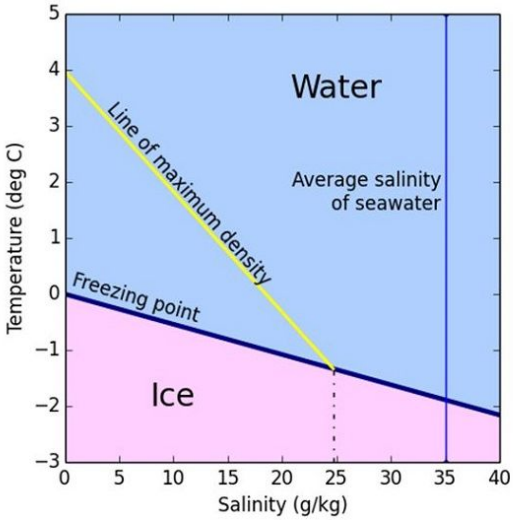


Figure 2.4: Representation of the relationship of saltwater density maximum to temperature and salinity

Figure 2.4 shows that the line of maximum density intersects the freezing point at approximately 25 PSU. This gives the threshold salinity of seawater after which the behaviour of the solution changes with regards to convective processes (Wadhams, 2000). Moreover, Figure 2.4 shows that below the threshold salinity of 25 PSU, as the seawater cools, it reaches its temperature of maximum density before reaching its freezing temperature. Thus, beyond its temperature of maximum density seawater becomes stratified with the colder less dense water being above the warmer denser water. The colder water will begin to freeze even though the water below it has not reached its freezing temperature.

However, above 25 PSU, seawater reaches its freezing point before it has reached its temperature of maximum density. This means that as the solution cools, the density of seawater will continue to increase. This causes the colder water to sink, and the warm less water will rise. This sets up convective overturning. This convection continues until the whole

water column is at the same temperature. Thereafter freezing will begin. Thus, at higher salinities above 25 PSU, more convection occurs, and this causes a delay in the freezing of the seawater compared to lower salinities.

The effect of salinity on density is noticed in the freezing of natural sea ice. As seawater has a salinity of 34 PSU, it does not reach its maximum density before it reaches its freezing point of -1.7°C. As such the upper cooler layer of seawater is always denser than the underlying solution. The resulting convective overturning results in the entire water column needing to reach the freezing temperature before ice formation can occur.

2.3.3 Sea ice phase equilibrium

Phase equilibrium in sea ice is dependent on the degree of cooling. As the temperature of the solution decreases and the sea ice is growing, the salt is trapped within the ice, and this leads to the multiphase structure of sea ice (Hunke et al., 2011). Further decrease in the temperature causes the brine channels to become more concentrated so as to maintain freezing equilibrium within the growing ice (Butler et al., 2016). However, as the temperature further decreases, more ice forms and the brine pockets become more concentrated until a point where salt precipitation begins to occur. The phase equilibria of ice, brine and brine salts has been shown in Figure 2.5.

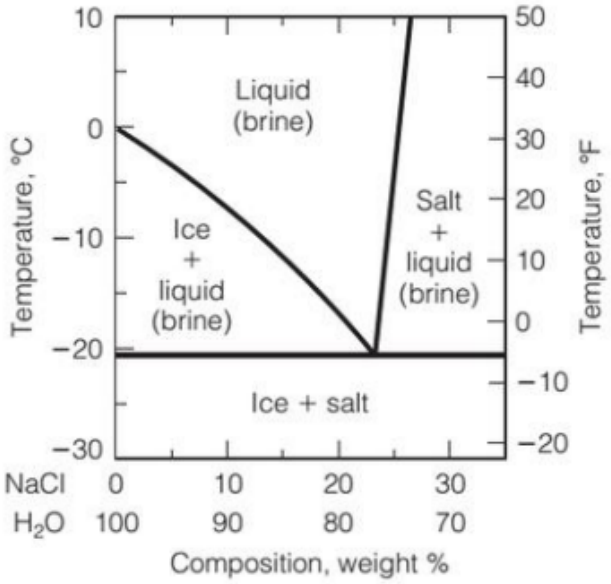


Figure 2.5: Phase diagram of ice, brine and brine salts (Mamlouk & Zaniewski, 2010)

Figure 2.5 shows the phase diagram of ice, brine and brine salts where the salt is NaCl. It should be noted that NaCl is not the only salt found in seawater. The combination of other

salts in the sea makes the phase equilibria of sea ice more complex due to the changes in the freezing point depression and the precipitation of the salts at different temperatures depending on their weight fraction as shown in Figure 2.5.

2.4 Thermal Properties of sea ice

2.4.1 Thermal conductivity

The thermal conductivity is a measure of the material's ability to allow heat to flow from its warmer surface through the material to its colder surface. This parameter is required when modelling the growth of sea ice (Weeks & Ackley, 1986). Despite its importance, a few measurements have been taken to quantify this parameter (Trodahl et al., 2000). As a result, sea ice growth models rely on the theoretical predictions based on existing correlations (Trodahl et al., 2001). It has been reported that sea ice incorporates air bubbles in addition to the brine channels and inclusions (Weeks & Ackley, 1986). Hence, the theoretically predicted values for the thermal conductivity are unreliable for such an inhomogeneous material as it depends on the geometric arrangement of these various components.

The theoretical models for predicting the thermal conductivity are based on the assumption of a parallel arrangement of ice components and brine (Schwerdtfeger, 1963). Yen, (1981) mentions that the thermal conductivity of the sea ice is a function of temperature, density and ice salinity. Schwerdtferger, (1963) further adds that, at high temperatures, the thermal conductivity is determined by the salinity of the sea ice. However, at lower temperatures, it is determined by the density of the ice. Trodahl et al., (2001) have reported that the thermal conductivity of air is significantly smaller than that of pure ice. As such its presence in sea ice is predicted to reduce the thermal conductivity of sea ice by its volume fraction contribution. The same is true for the brine. Weeks and Ackley, (1986) have reported that, there is a predicted fall in the thermal conductivity of sea ice as the temperature is raised above -5^{o}C due to the increase in the brine volume of the ice. As such an increase in brine volume is expected to reduce heat flow (Trodahl et al., 2001).

The rigorous treatment of the thermal conductivity has been performed by Schwerdtferger, (1963). On the contrary, Untersteiner, (1982) gave a classic simplified expression for the thermal conductivity of sea ice which is shown in Equation 2.6.

$$k = k_s + \beta\left(\frac{S_{bu}}{T}\right) \qquad \text{Equation 2.6}$$

Where k_s is the thermal conductivity of pure ice (2.04 W/m.K) and β is a constant (0.1173 W/m).The thermal conductivity of pure ice can be calculated using the formulation presented by Yen et al., (1991) as shown in Equation 2.7 where T is temperature in °C.

$$k_s = 2.21 - 1.00x10^{-2}T + 3.44x10^{-5}T^2 \quad \text{Equation 2.7}$$

Table 2.1 shows values for the thermal conductivities of pure ice at 0°C. The difference in these values has been attributed to a difference in anisotropy of 5% (Slack, 1980).

Table 2.1: Thermal conductivity of pure ice at 0°C

Thermal conductivity (W/m°C)	Author
2.14	Slack, 1980
2.23	Pounder, 1965
2.07	Yen, 1981
2.21	Yen et al,1991
2.00	Thomas and Dieckmann, 2010

Recently however, Pringle et al., (2007) suggested a more accurate method of determining the thermal conductivity of sea ice. This is shown in Equation 2.8, where T is temperature in °C, ρ and ρ_s are the densities of sea ice and pure ice respectively in kg/m^3.

$$k = \left(\frac{\rho}{\rho_s}\right) x(2.11 - 0.011T + 0.09\frac{S_{bu}}{T} - \left(\frac{\rho-\rho_s}{1000}\right) \quad \text{Equation 2.8}$$

Notz, (2005) accounts for the solid fraction in their derivation of the effective thermal conductivity. In the formulation presented, the effective thermal conductivity is a combination of the heat conductivity of the pure ice matrix (k_s) and that of the liquid interstitial brine (k_{br}) which are both functions of temperature. This heat conductivity of the interstitial brine is given by the Equation 2.9 (Schwerdtfeger, 1963).

$$k_{br}(T,S) = 0.52325\left(1 - \frac{S_{br}}{10^3}\right) + 0.01256T \quad \text{Equation 2.9}$$

Moreover, they assume that sea ice and NaCl consist of platelets that can be approximated to be in a parallel arrangement. Hence, the thermal conductivity of the resulting mushy layer

can be approximated as the weighted average of the different phases as shown in Equation 2.10.

$$k = \phi k_s + (1 - \phi) k_{br} \qquad \text{Equation 2.10}$$

Equation 2.10 is an approximation, however given the one-dimensional growth of ice where the ice crystals are well aligned, the error induced by it is relatively small. Lastly, the thermal conductivity can be determined from measured temperature profiles. This has been described as an inverse heat transfer problem (Tervola, 1989; Yang, 1999). In the case of a steady state approach, the thermal conductivity can be identified directly using a direct approach. The direct approach in this case refers to directly solving the heat diffusion equation. In the direct analysis of the problem, the thermal conductivity is assumed to be known and it is then used to solve for the temperature field of the heat conduction equation via numerical methods. Then optimisation methods are used to iterate for the thermal conductivity (Yang, 1999).

2.4.2 Heat capacity

The heat capacity describes the relationship that exists between a given amount of energy that is added per unit mass to a system to cause a temperature change in the system. Schwerdtfeger, (1963) highlights that the specific heat for sea ice (C_p) is a function of its salinity. The specific heat is calculated according to Equation 2.11.

$$C_p = \frac{S_{bu}}{\alpha T^2} H_s + \frac{S_{bu}}{\alpha T} (C_w - C_s) + C_s \qquad \text{Equation 2.11}$$

Notz, (2005) has given a rigorous treatment of the heat capacity by incorporating the theory of mushy layers. The model developed is analogous to the initial one developed by Untersteiner, (1961) which was derived from an empirical fit of the data obtained by Malmgren, (1927) which is shown in Equation 2.12 where Ɣ is 17.2 kJ/KgK

$$\rho C_p = \rho C_s + \frac{\gamma S_{bu}}{T^2} \qquad \text{Equation 2.12}$$

2.4.3 Latent heat of fusion

The latent heat of fusion considers the transfer of sensible heat between the ice and brine and the reduction of the latent heat due to finite porosity (Thomas & Dieckmann, 2010). It describes the energy that is released when loosely attached molecules in the liquid phase become

bounded to each other to form solid (Notz,2005). Schwerdtfeger, (1963), theorised that the latent heat of sea ice formation is dependent on the relative proportions of the ice and brine in the newly formed ice. In this case, the latent heat (H) can be calculated using Equation 2.13 where S_w is the mixed–layer salinity and it has been estimated to be 32 PSU.

$$H = [1 - S_{bu} - \frac{S_{bu}}{S_w}(1 - S_w)]H_s \qquad \text{Equation 2.13}$$

2.5 Modelling the thermodynamic growth of ice and conductive heat flux

2.5.1 Thermodynamics of ice growth

The growth of sea ice is dependent on the heat exchange that occurs at the air-ice interface noting that as soon as an initial layer of ice has formed, conduction rather than convection becomes the dominant mechanism of heat transfer. The different forms of heat flux that are exchanged through sea ice are shown in Figure 2.6

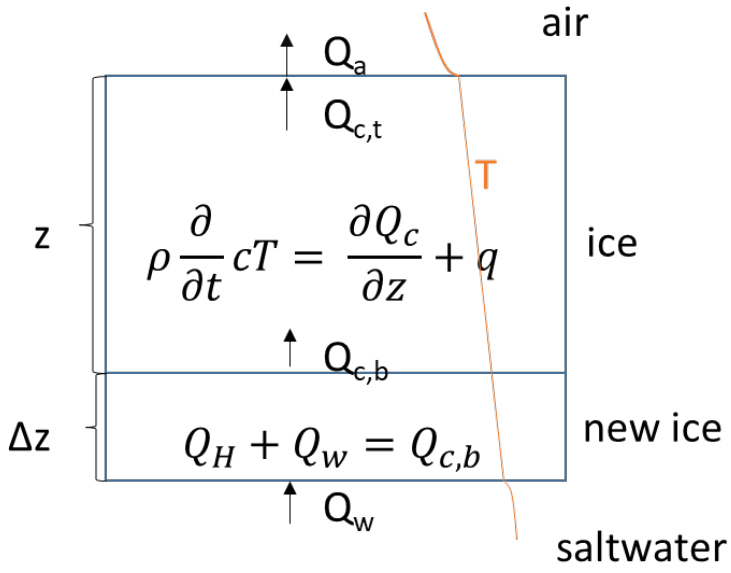


Figure 2.6: Summary of the heat fluxes experienced through sea ice (adapted from Wiese,2012)

Figure 2.6 is a summary of the heat flux at the air-ice/ice-water interface in the vertical direction. Q_w represents the heat flux at the ocean to ice interface. This is the layer around which the new ice is forming. Q_w is the least known heat flux and several studies have been performed to develop models that can accurately quantify its magnitude. Q_H is the latent heat released during ice formation and the sum of Q_w and Q_H gives $Q_{c,b}$ which is the conductive heat

flux at the bottom of the ice. $Q_{c,t}$ is the conductive heat flux at the top of the ice that is exchanged to the atmosphere. Qa is the net atmospheric heat flux (Wiese, 2012).

The thermodynamic growth of sea ice is a classic problem in geophysics. Traditionally it is treated one dimensionally in the vertical direction. This is due to the large variation of the temperature gradients in the vertical direction which represent much greater heat fluxes in the vertical direction than in the horizontal direction. Ice growth occurs mostly at the bottom. The latent heat released during freezing is conducted through the ice and is released to the atmosphere through radiative and turbulent heat fluxes (Lepparanta, 1993). The general sea ice growth model follows a classic heat conduction model (Equation 2.14).

$$\rho \frac{\partial}{\partial t} C_p T = \nabla Q_c + q = \nabla(k \nabla T) + q \qquad \text{Equation 2.14}$$

In Equation 2.14, the term on the left side gives a description of the warming or cooling of the ice. This is as a result of the gradient in the conductive heat flux Qc and internal heat sources q, i.e. solar radiation penetrating into the ice (Lepparanta, 1993). As the horizontal gradients in sea ice are much smaller than vertical gradients, heat exchange primarily occurs in the vertical direction. Assuming that the heat flux is only in the vertical direction due to negligible variations in the temperature gradients across the horizontal axes results in Equation 2.15

$$\rho \frac{\partial}{\partial t} C_p T = \frac{\partial Q_c}{\partial z} + q \qquad \text{Equation 2.15}$$

Where z is the direction of ice growth and represents the ice thickness. The ice growth of ice can be modelled using classic work presented by Stephan, (1891) by making simplifying assumptions. The model assumes that heat released by freezing ice at the bottom is conducted through the ice by a constant linear temperature gradient. This is the same as assuming that the temperature of the seawater is equal to the temperature of the ice at the water-ice interface Thus, heat linearly conducted through the ice is exactly balanced by the latent heat of fusion of the newly formed ice (Allison, 1981).

The Stephan model works well for landfast ice growing in shallow water where the water column remain thermally quiescent as the assumption of a linear temperature gradient is accurate (Anderson, 1961). However, the boundary condition chosen at the water- ice interface in the Stefan's Law overestimates ice thickness as it does not consider the role of heat transport from the ocean to the ice at the lower boundary. Therefore, the Stefan's Law

can be taken to be the upper boundary for favourable ice growth conditions (Lepparanta, 1993).

$$\rho H \frac{\partial z}{\partial t} + Q_w = \frac{k \partial T}{\partial z} \qquad \text{Equation 2.16}$$

Assuming that there is no heat flux from the water yields Equation 2.17 which can be used for calculating the ice thickness. In this case the ice thickness is proportional to the square root of time.

$$z^2 = \frac{2k(T_o - T_f)}{\rho H} t \qquad \text{Equation 2.17}$$

In Equation 2.17, T_o and T_f represent the temperature difference between the upper and lower ice surfaces respectively. The assumption for no heat flux from the water holds true if T_o and T_f are independent of time. Moreover, the Stefan's law has limitations in that it neither allows for changes of heat content within the ice nor for the time taken for boundary surface temperatures to vary the heat flux at the lower boundary (Allison, 1981). Schwerdtfeger, (1964) corrected for the change in the heat content of the ice by introducing the effective latent heat.

The net heat flux can be used to derive the theoretical growth rate of sea ice. In a study carried out by Anderson (1961) in North Star Bay over the winter period 1956-1957, ice samples that had very little snow with a thickness in the range 20-150 cm were taken. These were evaluated as a function of the cumulative number of freezing days. The observed trend for the ice growth profile is shown in Figure 2.7.

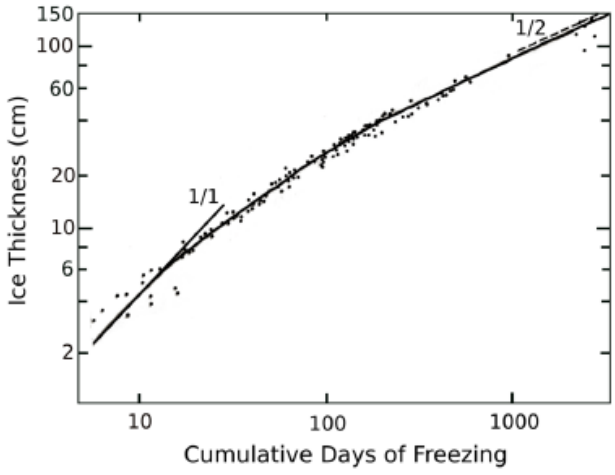


Figure 2.7: Modelled sea ice growth profile as a function of the cumulative number of freezing days (Anderson, 1961)

Anderson, (1961) reported that the growth profile shows an initial linear relationship which over a longer time period was approximated as parabolic. The decrease in the growth of the ice has been attributed to the insulative properties of the ice which slows down the conductive heat flux from the growth location at the ice-ocean interface.

2.5.2 Heat flux at the ice-atmosphere interface

Heat exchange between the ice and the atmosphere can be modelled using the convective heat transfer model (Maykut, 1986). In the absence of a snow cover, the convective heat flux at the air-ice atmosphere interface is given by

$$Q_a = H_{ia}(T_o - T_a) \qquad \text{Equation 2.18}$$

$$H_{ia} = \max\left(11.6, 5.7{V_w}^{0.8}\right) \qquad \text{Equation 2.19}$$

Where T_o is the surface temperature at the snow-ice interface, T_a is the air temperature and H_{ia} is the convective heat transfer coefficient which is a function of the wind speed as shown in Equation 2.19. However in the absence of snow cover, it can be assumed that the temperature of the atmosphere is approximately the same as the surface temperature of the ice (Allison, 1981) The above correlation is analogous to the one presented by (Thomas & Dieckmann, 2010), where they presented that as a first approximation, the net heat flux can be linearised with respect to the temperature difference between the air and ice surface temperature by setting Qa° to zero. In Equation 23 h_{eff} is the effective heat transfer coefficient.

$$Q_a = -h_{eff}(T_a - T_o) + Qa^0(T_a, T_o \ldots.) \qquad \text{Equation 2.20}$$

The surface temperature of the ice can be calculated by solving the general energy balance shown in Equation 2.21, where the sum of the outgoing turbulent, radiative and conductive heat flux balances incoming longwave and shortwave radiation (West et at., 2016).

$$(1 - \alpha)Q_T - I_0 + Q_I - Q_E + Q_{sen} + Q_H + Q_c + Q_m = 0 \; if \; T_s < 273\,°K \qquad \text{Equation 2.21}$$

Where α is the surface albedo, I_0 represents flux of radiative energy penetrating into the interior of the ice, Q_E is the outgoing long-wave radiation, Q_c is the conductive heat flux, Q_T is incoming shortwave radiation, Q_L incoming long-wave radiation, F_{sen} is the fluxes of sensible heat, Q_H is the latent heat and Q_m is the heat loss due to ice melting. Assuming negligible radiative effects

and the absence of melting, Equation 2.21 can be simplified to calculate the net atmospheric heat flux using Equation 2.22. This is because the sum of the incoming sensible, latent and radiative heat fluxes coming from above into the ice surface is equal to the conductive heat flux travelling downwards into the ice (West et at., 2016).

$$Q_a = Q_{sen} + Q_H = Q_c \qquad \text{Equation 2.22}$$

The sensible heat flux is expressed as

$$Q_{sen} = \rho_a C_a C_m W(T_a - T_o) \qquad \text{Equation 2.23}$$

Where ρa is the average air density (1.29 kg/m^3), C_a is the specific heat of the air at constant pressure (1006 J/kgK), C_m is the sensible heat transfer coefficient (0.003), W is the wind speed in m/s. The latent heat flux is expressed as

$$Q_{lat} = \rho_a H_e C_e W(f_a - f_s) \qquad \text{Equation 2.24}$$

Where H_e is the specific heat of the vaporisation (2.5 x 10^6 J/kg), Ce is the evaporation coefficient (0.00175), and (f_a-f_s) represent the difference in humidity 10 m above the ice and at the ice surface respectively.

The vertical conductive heat flux within the ice is directly proportional to the vertical temperature gradient. Thus, the overall heat flux can be calculated given a record of temperature distribution and ice growth. This method is based on using the temperature gradient and thermal conductivity in a horizontally homogeneous ice sheet (McPhee & Untersteiner, 1982). This is the classical way of determining heat flux through air temperature and ice thickness measurements as was done at Mawson for several years (Allison, 2007). The proportionality constant in the Fourier's field equation for heat conduction is the thermal conductivity (Yen, 1981).

2.6 Artificial sea ice for the study of ice growth dynamics

Artificial sea ice has been used in the analysis of sea ice as it offers greater control over sea ice growth variables such as the initial starting solution salinity, air temperature, and the cooling rate. This allows for the analysis of the effect of one variable. Moreover, artificial sea ice has been used to analyse the different properties and characteristics of sea ice such as the thermal properties, brine channels and brine drainage (Weeks, 1962). However, for artificial sea ice to be used to assess for these properties, it must closely resemble natural sea

ice. This is difficult to judge due to the variation of sea ice properties (Maykut, Grenfell & Weeks, 1992). The focus of previous artificial sea ice set-ups has been on the growth of artificial columnar sea ice as this is the most prevalent form of sea ice (Weeks & Ackley, 1986). When considering the previous artificial sea ice set-ups, a list of key properties has been identified that can be used to categorise that the laboratory grown ice is columnar.

Table 2.2 gives a summary of artificial sea ice properties. The direction of the heat flux plays a large influence on these properties (Lepparanta, 1993). The direction of the heat flux can be known through the temperature profile. The temperature profile is an important variable to measure as temperature affects all the other properties of the ice (Weeks & Cox, 1974). The growth profile of ice is a property that is affected by the temperature and it has been approximated to be parabolic in nature for sea ice (Anderson, 1961). The trend in the growth profile is attributed to the uni-directional top-down conductive heat flux, with the corresponding increase in ice thickness causing the growth of the ice to slow down due to the increased insulating effect of the thickening ice. Furthermore, the direction of the conductive heat flux affects the crystal morphology with the vertical elongation of the crystals occurring in the direction of the heat flux (Cox & Weeks, 1975).

Table 2.2: Summary of ice properties for artificial sea ice

Property	Expected trend	Supporting studies
Temperature profile	Linear temperature profile with depth with unidirectional top-down cooling	Wiese, 2012 Marks et al., 2017 Haas, 1999 Cottier and Wadhams, 1999
Ice growth profile	as shown in Figure 2.7	Cox and Weeks, 1975
In-ice salinity profile	C-shaped salinity profile, - highest salinity found at the top and bottom of the ice samples	Notz et al., 2005
Crystal morphology	Vertically elongated ice crystals with c-axes with the c-axis located in the horizontal plane	Schulson et al., 2015 Haas, 1999

The vertical salinity profile of natural sea ice has been found to have a “C” shaped salinity profile, with the same profile observed for artificial sea ice (Cottier, Eicken & Wadhams, 1999; Notz, 2005). However, it is important to note that laboratory experiments cannot replace the

need for field experiments. The growth rates and temperature gradients that are experienced in the artificial sea ice are much higher than for the thicker natural sea ice. Moreover, the small achievable thicknesses make comparisons in older natural sea ice much more complex (Haas, 1999). Outlined in Table 2.3 is a summary of the advantages and disadvantages of using artificial sea ice in the study of sea ice as adapted from Haas, (1999).

In previous studies the growth of artificial sea ice has been carried out in temperatures that range from -5^{o}C (Naumann et al., 2012) to -30^{o}C (Perovich & Grenfell, 1981). Anderson, (1961) has reported that a linear relationship exists between the atmospheric temperature and the growth rate. A lower atmospheric temperature creates a greater temperature gradient and consequently a higher growth rate. The growth rate in turn affects the crystal size and the ice salinity (Weeks & Assur, 1967). Fast growth rates are associated with smaller crystal sizes and more brine inclusions (Weeks & Ackley, 1986). The popular choice for the growth temperature is -20^{o}C since it closely resembles the temperature that is experienced in winter in the polar regions. Moreover, this temperature facilitates for relatively fast ice growth (Cox & Weeks, 1975; Wiese, Griewank & Notz, 2015; Middleton et al., 2016). When choosing the air temperature to operate at, another fact to consider is the precipitation of salts out of solution. According to Assur, (1960), -20^{o}C is below the precipitation temperature of most salts.

Table 2.3: Summary of advantages and disadvantages of artificial using saline ice experiments in the study of sea ice, (Haas, 1999)

Advantages	Disadvantages
▪ Allows for controlled studies of specific sea ice properties ▪ The growth history of the ice is well understood and the ice has a greater degree of homogeneity ▪ Multiple samples can be taken with comparable properties ▪ Allows for the separation of primary processes of ice formation from the secondary processes that follow for example algal activity ▪ Simpler logistics and experiments are repeatable ▪ Cheaper than field experiments	▪ Experiments cannot replace the need to investigate natural sea ice ▪ Higher temperature gradients and growth rates than those for natural ice ▪ Smaller ice thicknesses which make it more complex to compare with natural sea ice

2.6.1 Temperature control in the tank

The common method of adjusting the air temperature is through the use of a temperature controlled room (Weeks, 1962; Cottier, Eicken & Wadhams, 1999). Thus, the primary freezing mechanism will be the heat transfer that occurs between the solution surface and the cold air. However, the disadvantage with this is that air has poor heat transfer properties. This results in slow ice growth rates and a variable air temperature when measured above the solution surface (Nomura, Yoshikawa-Inoue & Toyota, 2006). This effect has been negated through the use of a fan that blows the cold air above the tank surface to improve circulation and improve the heat transfer rate (Perovich & Grenfell, 1981; Marks, Lamare & King, 2017).

Furthermore, it is common practice to install a temperature control or apply constant heating rate for the underlying solution (Weeks & Cox, 1974; Roscoe et al., 2011; Wiese, Griewank & Notz, 2015; Marks, Lamare & King, 2017). This is meant to simulate the oceanic heat flux which is highly variable. It has been reported to average between 10-15 $W.m^2$ in the Antarctic (Allison, 1981). Moreover, the use of a heat input prevents supercooling, and this allows ice formation to only occur at the ice-water interface with Wiese et al., (2015) reporting that a heat input of 15 $W.m^2$ was enough to prevent supercooling.

Artificial sea ice setups agitate or circulate the underlying solution to prevent salinity and temperature stratification. As shown in Figure 2.4, the relationship between freezing point and the solution density maximum should ensure that convective mixing occurs in seawater. However, Haas, (1999) noted that artificial sea ice setups experience much greater temperature gradients and growth rates than those experienced in natural sea ice. This requires the need for mixing to minimise the large degree of temperature variation in the underlying saline solution. Mixing can be induced using pumps or magnetic stirrers ((Wiese, 2012; Schulson, Renshaw & Snyder, 2015; Marks, Lamare & King, 2017).

2.6.2 Considerations for the saline solution

The saline solution that is used for the growth of the artificial sea ice should closely resemble natural seawater. This can be achieved using natural seawater that is found in the polar regions as has been used by researchers such as Weissenberger et al., (1992) and Nomura et al, (2006). However, Weeks and Cox, (1974) noted that this is expensive when one is located far from the polar regions. Moreover, this method is better suited when wanting to conduct experiments with the same salinity as that of seawater. Hence, this problem can be overcome by formulating saline water using salt and deionised water. Deionised water is used as it does not add undesired components to the system. Some researchers such as Weeks,

(1962) use single component salts such as NaCl to formulate the saline solution. NaCl accounts for more than 60% of the salts in seawater. As such the ice that is formed from NaCl solutions closely resembles that of natural sea ice. The added advantage is that the simple composition allows for the modelling and prediction of the ice growth dynamics as a function of salinity and temperature (Assur, 1960).

2.6.3 Nucleation in artificial sea ice tanks

The freezing point of the saline solution is the thermodynamically defined temperature at which freezing will occur. However, in reality it is possible for a solution to remain a liquid even though the saline solution would have reached temperatures that are much lower than the predicted thermodynamic limit (Freitag, 1999). The process of nucleation needs to occur for ice formation to begin. There are two types of nucleation namely primary and secondary nucleation. Primary nucleation occurs due to the spontaneous nucleation of ice from the solution, and it occurs at temperatures much lower than the thermodynamically predicted crystallisation temperature.

Secondary nucleation involves the addition of a small amount of ice crystals to act as a nucleation site and is possible within a very small degree of supercooling. This process of adding ice crystals is known as seeding (Randall, Nathoo & Lewis, 2009). In natural sea ice secondary nucleation occurs from the readily available heterogeneous nuclei (Weeks, 2010). However, in the absence of natural seeding, the dominant ice form occurs with crystals oriented with a vertical c-axis, which is the opposite of what is observed in natural sea ice (Tucker III, Gow & Weeks, 1987). Hence in artificial sea ice setups where secondary nucleation is not present it is common to artificially seed the solution at the predicted freezing point to control the grain orientation and to promote columnar growth (Cottier, Eicken & Wadhams, 1999).

2.6.4 Artificial sea ice temperature profiles

The temperature evolution with time profiles for artificial sea ice have been found to exhibit a non-linear trend (Wettlaufer, Worster & Huppert, 1997). Figure 2.8 shows the temperature data for the artificial sea ice experiment that was performed at -20^{o}C by Wettlaufer et al., (1997) from seven thermistors.

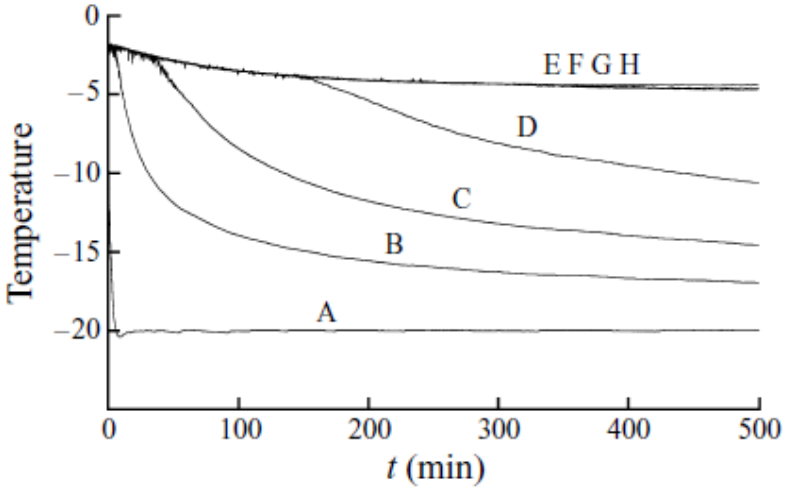


Figure 2.8: Temperature evolution with time profile for artificial sea ice grown at -20°C in a 15 L tank where the temperature was measured using thermistors (Wettlaufer et at., 1997)

Thermistor A measured the air temperature and thermistors B-D measured the temperature within the ice whilst thermistors E-H measured the temperature in the underlying freezing solution. Probe B-D show that the temperature shows a non-linear decrease with time where the decrease is steep at the onset of the experiment. However, thermistors E-H show a slight decrease in temperature and thereafter remain constant.

2.7 Measurement techniques of artificial sea ice variables

2.7.1 Ice depth measurement

The measurement of the ice depth is important as it allows for the determination of the growth rate and the endpoint of the freezing experiment. Weeks and Cox, (1974) noted that the salinity of the underlying solution increases as the experiment progresses. Hence, they have recommended that the ice should not exceed 50 % of the tank depth. Recently, artificial sea ice experiments have seldom exceeded 20% of the tank volume (Cottier, Eicken & Wadhams, 1999; Wiese, Griewank & Notz, 2015). The easiest method to measure the ice thickness is through visual inspection. However, this method is possible if the tank is transparent (Wiese, Griewank & Notz, 2015).

Weeks (1962) presents an alternative method to measure the ice thickness where a metal crossbar is frozen into the ice. The metal rod is then heated to allow it to slide freely within the ice when taking ice depth measurements. On the other hand, Notz et al., (2005) presents a measurement device that records the ice depth continuously without the need for human input. Feltham et al., (2006) mentioned that the ice depth can be inferred from the temperature profile of ice. They note that the inference of ice depth from a linear temperature profile provides a

reasonable approximation for depth up to 0.8 m. As such, Marks et al., (2017) have used temperature as a means of continuous ice depth approximation.

2.7.2 Temperature measurement

Temperature is an important variable to measure during the growth period of artificial sea ice. Quantification of the conductive heat flux is only possible knowing the temperature evolution of the growing ice. A good temperature record gives a good description of the growth history of the ice and this gives an understanding of its properties (Haas, 1999). Temperature can be measured using three probe types. The choice of the probe depends on the degree of accuracy required. These probes include thermistors, resistive temperature detectors (RTD's) and thermocouples. Thermistors require a voltage to be applied over the resistor, the corresponding voltage drop is then converted into a temperature reading. They have a small footprint, have high accuracy and fast response. However, they experience drift overtime (0.02^{o}C/year) and hence require frequent calibration to ensure their measurement accuracy (Wiese, 2012).

The RTD's also require a voltage to be applied to the resistor and the wire that is chosen to cover the temperature probe has a known resistance at 0^{o}C. The wire that is commonly used is platinum. RTD's experience higher resistances than thermistors and they have a linear relationship with temperature. The higher resistances of RTD's requires a higher current to be supplied and this has the problem of leading to self-heating of the RTD probes. The commonly used RTD probes are PT100 and PT1000 where PT is an abbreviation for platinum. PT100 provide highly stable measurements overtime with a drift of 0.05^{o}C/year (Texas Instruments, 2019). Thermocouples measure the voltage difference between two wires. They are simple and have a robust design. However they are not commonly used in artificial sea ice experiments (Texas Instruments, 2019).

2.7.3 Salinity measurement

The measurement of salinity is important as the salt content in the saltwater determines the extent of freezing point depression (Cottier, Eicken & Wadhams, 1999). The salinity is calculated through the measurement of temperature and conductivity using a conductivity meter. The conductivity and temperature are then converted to salinity using the Practical Salinity Scale that was developed in 1978 (PSS-78). In situ salinity can be measured using the salinity harp that was developed by Notz, (2005). However, in the absence of in-situ salinity measurement methods, the in-ice salinity can be measured at the end of the experiment to

obtain the vertical salinity profile. This is done by removing and cutting an ice sample into vertical sections and melting each section prior to using a portable conductivity meter or salinometer. This is done to measure the bulk salinity of the melt ice (Weeks, 2010). The main disadvantage with this method is that there is loss of brine during the extraction of the ice from the tank and this affects the accuracy of the results (Notz & Grae Worster, 2008).

2.8 Rationale of study

The review of literature outlines that modelling the growth of sea ice is important as sea ice plays a significant role in the global climate. However, to be able to model the growth of sea ice, an understanding of the growth processes that affect the formation of sea ice and its associated thermal properties is important.

The models that currently exist show a dependency on temperature and salinity. Hence, it is important to determine the effect that these growth conditions have on sea ice growth dynamics and on the heat that is linearly conducted through the ice. Additionally, artificial sea ice experiments have the potential to be used to supplement natural sea ice studies as the full growth history of the ice is known and it allows for the investigation of the effect of one variable at a time. However, artificial sea ice experiments have been conducted in varying tank sizes. The effect that this has on the growth dynamics and conductive heat flux has not been thoroughly investigated. Moreover, the previously conducted artificial sea ice experiments have had their focus on columnar ice. The temperature, growth and salinity profiles provide a guiding reference of how to characterise artificial sea ice. Lastly, it has been reported that relatively few measurements have been conducted in the determination of the thermal conductivity, yet this parameter is required in the modelling of the growth of ice and in the determination of the conductive heat flux. However, it has been reported that the thermal conductivity can be estimated from experimental temperature measurements.

The work in this project will therefore be to develop a base case analysis technique for the quantification of the growth rate of artificial sea ice and the extrapolation of the thermal conductivity. The developed technique will be used to assess for the effect of varying the air temperature, starting solution salinity and tank size on the growth dynamics in artificial sea ice. The growth profile will be inferred from the temperature measurements.

Chapter 3 : Research Objectives

3.1 Overall aim and objectives

The primary aim of the project is to investigate the effect of growth conditions on the growth dynamics and conductive heat flux of artificial sea ice. This will be achieved through the following objectives:

- Develop an analysis technique that allows for the determination of the overall thermal conductivity, ice surface temperature, ice growth rate and conductive heat flux in artificial sea ice
- Apply the developed technique to investigate the effect of air temperature, starting solution salinity and tank size on the growth dynamics and vertical conductive heat flux in artificial sea ice
- Develop a base case model that can predict the temperature field of artificial sea ice

3.2 Key Questions

The key questions that arise from the outlined objectives are:

1. Is the assumption of pseudo steady state heat conduction valid to model artificial sea ice growth?
2. How does the air temperature affect the growth dynamics and vertical conductive heat flux of artificial sea ice?
3. How does the tank size affect the growth dynamics and vertical conductive heat flux of artificial sea ice?
4. How does the starting solution salinity affect the growth conditions and vertical conductive heat flux of artificial sea ice?
5. Is it possible to have a model that can predict the temperature field and growth profile of artificial sea ice through the assumption of constant thermal properties of sea ice?

Chapter 4 : Methodology

4.1 Mathematical modelling of ice growth

It has been emphasised in previous sections that quantification of the heat flux is important as it can be used to model ice growth. Figure 4.1 shows the schematic diagram of the growth of ice. The parameters that influence the growth of the ice are specified in Figure 4.1. The ice was grown at constant air temperature. The underlying solution (brine) was maintained at or very close to its freezing temperature. The air temperature and brine solution temperature formed important boundary conditions from which the model for the ice growth was developed.

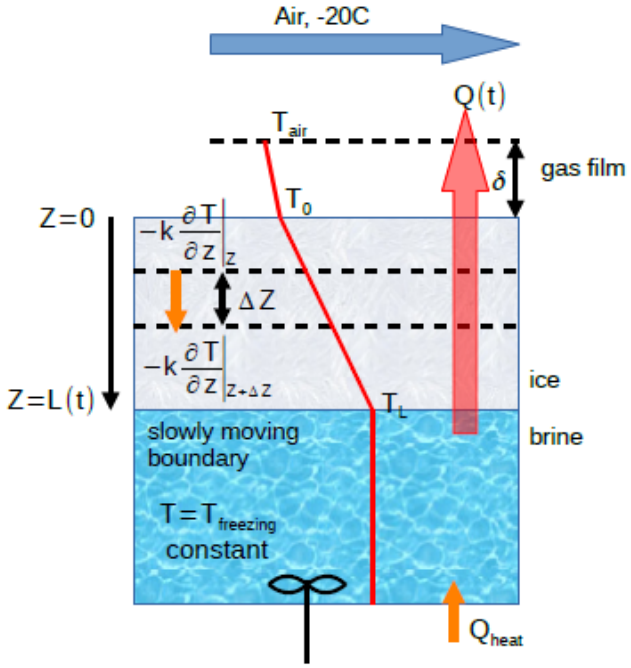


Figure 4.1: Schematic showing the variables that were considered in modelling artificial sea ice that was grown in an idealised environment, where z represents the direction of heat flow in the axial direction, L(t) represents the change in the length of the growing ice as a function of time

The basis of the ice growth model was derived from the heat diffusion equation, noting that ρ and C_p are independent of time. However, they are dependent on position through temperature.

$$\rho C_p \frac{\partial T}{\partial t} = \nabla(k\nabla T) + q \qquad \text{Equation 4.1}$$

The heat diffusion equation was expanded further to incorporate the geometry. The experiments were conducted in a cylindrical tank. Hence, the heat diffusion equation for cylindrical coordinates was employed.

$$\rho C_p \frac{\partial T}{\partial t} = \frac{1}{r}\frac{\partial}{\partial r}\left(kr\frac{\partial}{\partial r}\right) + \frac{1}{r^2}\frac{\partial}{\partial \emptyset}\left(k\frac{\partial T}{\partial \emptyset}\right) + \frac{\partial}{\partial z}\left(k\frac{\partial T}{\partial z}\right) + q \qquad \text{Equation 4.2}$$

Where r is the radial direction, z is the axial direction and ∅ is the angular direction. It was assumed that heat conduction was mostly dominant in the z direction due to the sides of the tanks being insulated and further assuming that the ice was homogenous in the radial direction. The temperature gradients in the radial and angular direction were therefore neglected. This simplified the problem to one-dimensional heat transfer at unsteady state with respect to the spatial coordinates. It was assumed that that the thermal conductivity, density, and the heat capacity were constant over the given temperature range. Furthermore, the absence of sink or source terms simplified the problem to Equation 4.3.

$$\rho C_p \frac{\partial T}{\partial t} = \frac{k}{L^2}\left(\frac{\partial^2 T}{\partial x^2}\right) \qquad \text{Equation 4.3}$$

where $x = \frac{z}{L}$ Equation 4.4

Equation 4.4 was used to make the position dimensionless. This means that the dimensionless temperature coordinates remain unchanged as the length of the ice (L) increases. This forms an important assumption towards the modelling of the ice growth problem. Moreover, L is a function of time and the boundary condition at the air-ice interface was given by the convective boundary condition. In this case the convective heat flux at the surface balances the conductive heat flux. This expression resulted in the formulation of the first boundary condition

$$Q(t) = hA(T_a - T_o) = -\frac{k}{L} A \left.\frac{\partial T}{\partial x}\right|_{x=0} \qquad \text{Equation 4.5}$$

The second boundary condition was given by:

$$T_f = T_L \qquad \text{Equation 4.6}$$

It is important to note that Equation 4.6 highlights that the ice and brine temperature are the same at the interface freezing. Thus, there is no conductive heat flux through the film and

there is no salt gradient at the film. It is important to note that L varies with time, the problem then becomes a moving boundary problem.

4.1.1 Ice growth rate from the energy balance

As an initial estimate, it was assumed that the brine concentration does not change significantly to depress the freezing point. Consequently, by experimental design this implied that the heat passing through the ice-brine interface was equivalent to the heat required to freeze the water at the interface. This is the infinite body of water assumption, which holds true when the amount of ice growth is small in comparison to the volume of brine. This led to a coupling of the energy balance to the ice growth rate and hence the variation of L with time as shown:

$$-\frac{k}{L}\,A\,\frac{\partial T}{\partial x}\Big|_{x=1} = \frac{dm}{dt}\Delta H_c = \rho A\frac{dL}{dt}\Delta H_c \qquad \text{Equation 4.7}$$

Thus $L(t)$ can be modelled as

$$\frac{dL}{dt} = -\frac{k}{\rho \Delta H_c L}\,\frac{\partial T}{\partial x}\Big|_{x=1} \qquad \text{Equation 4.8}$$

The solution to this dynamic problem was solved through orthogonal collocation and the use of differential algebraic equation dasrt() solvers in Scilab. The details can be found in Appendix A2.

4.1.2 Solution of the dynamic model

The solution vector for the temperature profiles was given by the following vector:

$$X_{1:N} = [T_a \;\; T_1 \;\; T_2 \ldots\ldots T_{n-1} \;\; T_n \;\; T_L] \qquad \text{Equation 4.9}$$

Equation 4.9 is a matrix for temperatures at every time step, where Tn = T_L and T_1 = T_0. Here *N* are the vector *X* elements and n are the temperature nodes in the ice. It is important to note that although the set point of the air temperature was kept constant, there were slight variations in the air temperature. The detailed code for the dynamic model is shown in Appendix A2, where Aij and Bij are collocation matrices of size n = nc + 2, where nc is the number of internal collocation points.

4.1.3 Development of linear temperature profile model through pseudo steady state

To develop a model for pseudo steady state, it was first assumed that the temperature and L remain constant over a small-time range (delta t). It then follows that:

$$\frac{k}{\rho C_p L^2}\left(\frac{\partial^2 T}{\partial x^2}\right) = 0 \qquad \text{Equation 4.10}$$

Integrating this twice yields;

$$T = a + bx \qquad \text{Equation 4.11}$$

Evaluating the expression at the two boundary conditions, at $x = 0$:

$$T_o = a \qquad \text{Equation 4.12}$$

at $x = 1$:

$$T_L = a + b \qquad \text{Equation 4.13}$$

Hence:

$$b = T_L - T_0 \qquad \text{Equation 4.14}$$

Hence the temperature profile is given by:

$$T = T_0 + (T_L - T_0)x \qquad \text{Equation 4.15}$$

However, T_o was unknown, and was evaluated using the film boundary condition:

$$hA(\,T_0\, -\, T_a\,) \,=\, \frac{k}{L}\, A\, \frac{\partial T}{\partial x}\Big|_{x=0} \qquad \text{Equation 4.16}$$

and using the profile through the ice,

$$\frac{\partial T}{\partial x}\Big|_{x=0} = (T_L - T_0) \qquad \text{Equation 4.17}$$

And defining a dimensionless parameter

$$\alpha = \frac{k}{hL}$$ Equation 4.18

This resulted in

$$T_0 = \frac{\alpha T_L + T_a}{1+\alpha}$$ Equation 4.19

The linear temperature profile at any instant in time was then given by

$$T = \frac{\alpha T_L + T_a}{1+\alpha} + \left(\frac{T_L - T_a}{1+\alpha}\right)\frac{Z}{L} = a + \frac{b}{L}Z$$ Equation 4.20

4.1.4 Application to temperature profile measurements during ice growth

As the temperature profile through the ice had been measured at a particular time instant *t* such that: $T = [\,T_1 \;\; T_2 \ldots\ldots T_m]$ and $Z = [\,Z_1 \;\; Z \ldots\ldots Z_m]$

It then followed that by linear regression of T vs Z using Equation 4.21 only for the temperature measurements in the ice. This means that not all points in the vectors T, Z are used.

$$T = \beta_1 + \beta_2 Z$$ Equation 4.21

$$a = \beta_1 = T_0 = \frac{\alpha T_L + T_a}{1+\alpha}$$ Equation 4.22

where T_L and T_a are given by the experiment

$$\frac{b}{L} = \beta_2 = \frac{\left(\frac{T_L - T_a}{1+\alpha}\right)}{L}$$ Equation 4.23

This meant that from β_1, α could be found which then also gave b and thus the value of L, the depth of the ice. Thus, the ice growth as a function of time can be inferred by the application of the linearised model at each time instance. This was further checked by noting that α is a function of time through L and that $\frac{h}{k}$ should be approximately constant, then rearranging Equation 4.18 as follows

$$\frac{1}{\alpha} = \frac{h}{k}L$$ Equation 4.24

Equation 4.24 yields a straight line when $\frac{1}{\alpha}$ is plotted against L. Application of the regression solution to $\frac{dT}{dx}$ in Equation 4.7 then yields Equation 4.25 which calculates the instantaneous heat flux. Moreover, it follows from Equation 4.25 that having calculated $\frac{Q(t)}{A}$ from the growth rate, the average instantaneous thermal conductivity for ice that has formed at that particular point in time and convective heat transfer coefficient can be calculated.

$$\frac{Q(t)}{A} = \frac{dm}{dt}\Delta H_c = \rho \Delta H_c \frac{dL}{dt} = h(\,T_0\, -\, T_a\,) = \frac{k(T_L - T_0)}{L}$$ Equation 4.25

The expanded form of $\frac{Q(t)}{A}$ is shown in Equation 4.26

$$\frac{Q(t)}{A} = \frac{A(T_a - T_L)}{\frac{1}{h} + \frac{L(t)}{k}}$$ Equation 4.26

It should be noted that the ratio of $\frac{h}{k}$ from Equation 4.24 requires specification of h for quantification of k. The k calculated using this approach is the average across the duration of the experiment. The approach of calculating k from $\frac{h}{k}$ used in this work assumes that h is constant and independent of the starting solution salinity and air temperature. This argument is based on studies by Ashton, (1989) where the author argues that h varies with wind speed. The author prescribes the range of h as between 1 W/m^2. ºC and 30 W/m^2.ºC. Consequently, h has been assumed to be 23 W/m^2.ºC. This value was considered appropriate for forced cooling which is applicable in this work.

4.1.5 Limitations in the data analysis as a consequence of experimental procedure

The pseudo steady state models use the experimental temperature profiles as input. However, it is important to note that three regions need to be avoided in the regression of the data. These include:

1. At the start of the experiment, the air and ice surface temperature required a few hours to stabilise. This is the initial stabilising zone at the onset of the experiment which corresponds to frazil ice formation before the formation of a cohesive ice sheet at the top of the freezing solution. These data points are discarded in the analysis that is in accordance with the pseudo steady state assumption in the model that will be used to

analyse the data. This is because as long as the temperature probe remains in the brine solution, its temperature remains constant. However, once the temperature probe has been embedded in the ice, its temperature decreases non -linearly after a short lag phase. The lag phase is possibly a result of the transition between the brine and the ice. This is because the transition does not occur instantaneously with position and time. This leads to a smudging of the temperature profile. Hence, this region of the temperature profiles needs to be neglected in the analysis as it does not conform to the assumptions of the model. This point must be found manually from the temperature vs time data.

2. Linear regression requires data with two or more points, which means that there must be at least 2 temperature probes embedded in the ice for a valid regression. The time at which this occurs can be estimated from the temperature vs time data plot.
3. Only the internal points are regressed. To is estimated from the intercept and L is obtained by assuming that at Z=1, $T=T_L$ which is the brine temperature. The starting ice temperature (T_{ice}), for linear regression must be estimated from the temperature vs time data plot and lies between -1^{o}C and -2^{o}C for a typical growth experiment
4. The linearised model does not account for resistance to mass transfer at the ice-brine interface
5. The artificial sea ice temperature profile at the growing ice-brine boundary is non-linear (Worster & Jones, 2015). This section has been neglected in the analysis. It is important to note that the linearised model is not aimed at replacing the numerical techniques of natural sea ice.

4.2 Experimental matrix and tank configuration

The effect of air temperature and salinity was assessed by conducting experiments in the 30 L tank. The experimental matrix that was used is shown in Table 4.1. An air temperature of -20^{o}C was selected as the temperature of choice to assess the effect of starting solution salinity for experiments A-C1. Moreover, 10 PSU was selected as the starting solution salinity for the assessment of the effect of temperature for experiments A and D-F. Lastly, assessment of the effect of tank size was done through experiment C1-C3.

Table 4.1: Experimental matrix for experiments that were performed in the 30 L tank to assess for the effect of varying the air temperature and the starting solution salinity artificial sea ice. The effect of tank size is reflected in C1, C2 and C3.

Temperature	Salinity				
	10 PSU	20 PSU	30 PSU		
			30 L	300 L	3 L
-20 °C	A	B	C1	C2	C3
-15 °C	D				
-10 °C	E				
-5^{o}C	F				

The tank configuration is shown in Figure 4.2. The tanks were each insulated to prevent heat loss or addition through the walls. The insulation used had a thickness of 10 cm. This thickness was based on previous artificial sea ice experiments performed at UCT by the MARiS research group (Hall, 2021). Moreover, the tanks were placed on a wooden board that was raised 10 cm from the floor and additionally they were placed on 100 mm Styrofoam columns. This was done to prevent cooling of the tanks from the bottom.

Magnetic stirrers were placed inside the tanks. Their purpose was to provide homogenous mixing of the saline solution. Side heating was added to the tanks. The purpose of the side heating was to prevent cooling of the tank from the sides. Moreover, the use of a heat input was done to prevent supercooling (Wiese et al., 2015). The fan was placed adjacent to the tanks, and it blew air directly the tanks. This was done to improve convective heat transfer above the solution surface.

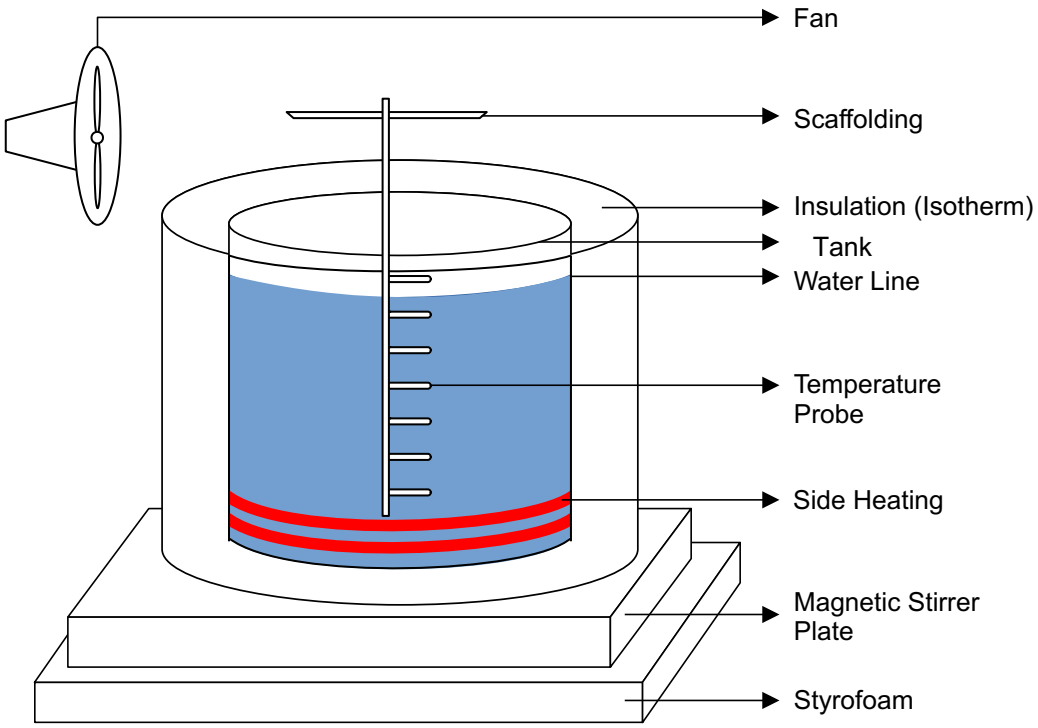


Figure 4.2: Tank configuration for artificial sea ice grown inside a cold laboratory at UCT

4.2.1 Temperature and salinity measurements with the inclusion of uncertainties

Figure 4.3 shows the tank dimensions and the placement of the temperature probes. The temperature probes used were all class A PT100 (±0.15°C) and these were connected to a Campbell Scientific CR5000 datalogger. The datalogger recorded temperature measurements every 6 seconds and the values were averaged over 150 seconds. Since the recorded measurements were an average of 25 points, no further smoothing of the temperature data was performed and these were used to plot the relevant temperature profiles. Calibration of the temperature probes at 0°C was performed only once. The temperature measurements were taken using a maximum of 13 temperature probes that spanned the length of the tank (refer to Figure 4.3 for temperature probe positioning).

The temperature probes measured the centre temperature of the ice as they were located at the centre of the tank. However, it is important to note that temperature variations in the horizontal direction were not measured as these were found to be negligible (Hambrock, 2021). Hence this implies that the measured temperature at the centre was therefore the average temperature of any brine or ice that was contacting the temperature probes. The objective was to grow the ice until it covered at most half of the tank height. This was because,

the tank system had no pressure relief system, hence there would be pressure build up from the bottom of the tank if the ice was allowed to grow all the way to the bottom of the tank.

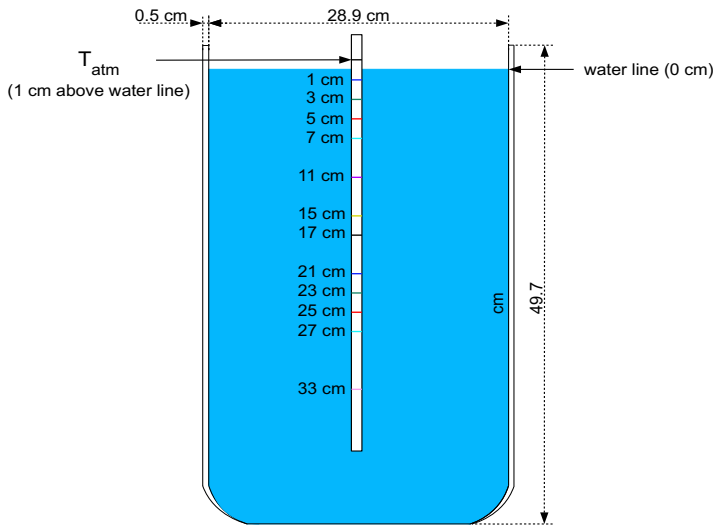


Figure 4.3: Tank schematic showing temperature probe placement and tank dimensions

The probe spacing at the top was chosen based of the configuration by Notz, (2005). This is because this probe spacing gives a good resolution for temperature measurements during the initial stages where there is the fastest growth of ice. The first temperature probe measured the air temperature at 1 cm above the water surface. The ice temperature was measured using in-ice temperature probes. The probes located 33 cm was used to measure the solution temperature.

The techniques employed to measure the experimental parameters presents points of uncertainty. Firstly, the placement of the temperature probes at the respective depths. The probes had to be correctly placed at the desired depths to obtain accurate temperature profiles with depth. Slight changes in the position would cause some degree of error in the profiles.

Secondly, the temperature probes show oscillations between 0 and -1.0°C. The systematic deviations of some 0.5°C seen at the start of the experiment were treated as calibration error. Thus, the temperature probes benefitted from calibration. The temperature probes were each calibrated before the onset of each experiment at 0°C in the cold laboratory.

It is important to note that there are two types of oscillations:

1. The oscillations with a period of approximately 19 minutes are particularly visible in the air temperature as shown in Figure B1 and Figure B2 (Appendix B1). These are due to the air-cooler's ON/OFF control algorithm. These oscillations are of the order of

1.0^{o}C, the dead band of the ON/OFF control. These oscillations reflect in the first few temperatures measured in the ice, but the variation is greatly reduced (damped) as the depth of the ice increases. It is important to note that the 25-point sample averages are not able to damp out these oscillations. Moreover, since these oscillations penetrate the ice, they are not smoothed out.

2. There are large spikes of some ±5.0^{o}C and do not occur at the after the same time interval (Figure B3 in Appendix B1) This is the de-icing (thawing) cycle of the cooler. The defrost cycle occurs because the cold laboratory uses compressors to cool the temperature down to the desired temperature. Hence to prevent overheating of the system, the laboratory undergoes defrost cycles to also prevent freeze up of the pipes. These spikes appear in the ice temperature measurements but with increased damping as the depth of ice increases. These should not be corrected for in the data, but rather the linear regression analysis should be applied to the data as measured. Thus, any disturbances due to the spikes will be visible in the analysis for instance the L vs t plot.
3. The temperature probes that are closer to the ice surface feel the oscillations more, however, these oscillations are damped deeper in the ice

Lastly, the salinity of the solution was checked using a conductivity meter with a conductivity accuracy of ± 2 μS.cm^{-1} and temperature accuracy ± 0.6^{o}C, noting that the conductivity meter had its own thermocouple, which was separate from the temperature probes that were connected to the datalogger. The conductivity meter had to be constantly calibrated so that it could give more accurate readings. The calibration was performed using a solution whose salinity was known.

4.2.2 Experimental procedure

The first step involved preparing the artificial saltwater. This was done by dissolving Aquaforest Sea Salt in deionised water. It is important to note that for each experimental run, two experiments were performed concurrently at the same conditions. The first tank had temperature probes that spanned the length of the tank, and this was used for the analysis of the temperature evolution. The second tank had no temperature probes, and this was used for ice sampling for the analysis of the crystal structure and salinity profile at the end of the experiment. As two tanks were being used, the initial starting salinity had to be identical. Thus, 60 L of deionised water was decanted into a secondary 70 L cylindrical tank and the respective mass of Aquaforest sea salt was dissolved in it. The conversion used was that 1 PSU is equivalent to 1 g/cm^{3}. To prepare the 10 PSU, 20 PSU and 30 PSU solution in the 70 L

secondary tank, 600 g, 1 200 g and 1 800 g of salt were added respectively. Thereafter, the saltwater was manually mixed and left for 2 hours for the salt to adequately dissolve.

The salinity of the solution was checked using a conductivity meter (AZ instruments, model 8301 with a conductivity accuracy of ± 2 $\mu S.cm^{-1}$ and temperature accuracy ± 0.6°C). The conductivity meter measured the conductivity and temperature of the solution and the values obtained were converted to salinity using the PSS-78 standard (Lewis and Perkin, 1981). The saltwater solution once properly mixed and having the correct salinity was transferred to the 30 L freezing tanks. Noting that, the freezing tanks have a volume of 33 L but the working volume that was used is 30 L. The working volume is what is referenced in this work.

The freezing tanks were then placed on magnetic stirrer plates. The magnetic stirrers were placed inside the tanks, and these provided homogenous mixing of the solution. The temperature probes were then setup on a scaffold as shown in Figure 4.3. The side heating element's temperature probe was placed inside the bottom of the tank. The setpoint for the side heating temperature probe was the freezing temperature of the solution. Thereafter the side heating element was placed around the freezing tanks as shown in Figure 4.3. The reactors were insulated. The cold fan was switched on and positioned as highlighted in Figure 4.3.

The saltwater solution was then precooled prior to the onset of the experiment to prevent flash freezing. This was done by leaving the solution at 1°C over a period of 16 hours in the cold laboratory. Thereafter, the setpoint temperature of the cold laboratory was adjusted to be at the desired air temperature for the experiment. The surface temperature of the saltwater solution was then monitored until it had reached its freezing temperature.

Once the solution had reached its freezing temperature, the solution was seeded using ice shavings. The process of seeding presented points of nucleation to initiate freezing. After seeding the ice was left to grow over the desired growth period. At the end of the growth period, temperature measurements from the datalogger were extracted. The ice was sectioned into segments to obtain the salinity profile. Cross polarisation of the ice samples was done to check the crystal structure for confirmation that the growth conditions were simulating columnar ice.

Chapter 5 : Analysis of temperature- time data using the linearised model

5.1 Method of analysis

The experiment for artificial sea ice that was grown at a starting salinity of 10 PSU and constant air temperature of -20^{o}C will be used to confirm the validity for the development of a linear temperature profile model using the pseudo steady state assumption. The hypothesis is that a linear temperature profile exists within the ice. Therefore, it is possible to develop an analysis model for the prediction of the ice growth rate, conductive heat flux, surface temperature and the average thermal conductivity of a homogeneous ice sheet from the experimental measured temperature distribution of the ice by applying the linearised model at each instance in time using the temperature probes embedded in the ice.

The method of analysis used in this work follows from the developed Scilab code as shown in Appendix A1. Moreover, the analysis was developed based on the growth of columnar ice. This is substantiated by the cross polarised images shown in Figure C3 (Appendix C). The raw experimental results from the experimental set up (Figure 4.3) and procedure explained in Chapter 4 are produced in two variables over time. The variables include temperature and depth (position). This means that there are three ways of depicting the raw data. The raw data can be plotted as temperature vs time, position vs time and position vs temperature. In this work, only the temperature vs time and position vs temperature plots were considered.

Figure 5.1 shows the temperature versus time data that was collected for 160 hours. Similar temperature profiles were observed as in (Wettlaufer, Worster & Huppert, 1997). There are three main sections to note from Figure 5.1. The first is the air temperature. The next is the saltwater temperature, which will now be referred to as the underlying brine solution temperature, this is represented by the plateau. Lastly are the in-ice temperature measurements. These are sandwiched between the air temperature and the brine temperature curves as shown by the red arrow. The respective positions of the in-ice temperature are as shown in the legend of Figure 5.1. It is important to note that, at the start of the experiment, the air and ice surface temperature required 3 hours to stabilise. The data points recorded during this period are discarded in the analysis that is in accordance with the pseudo steady state assumption in the model that was used to analyse the data.

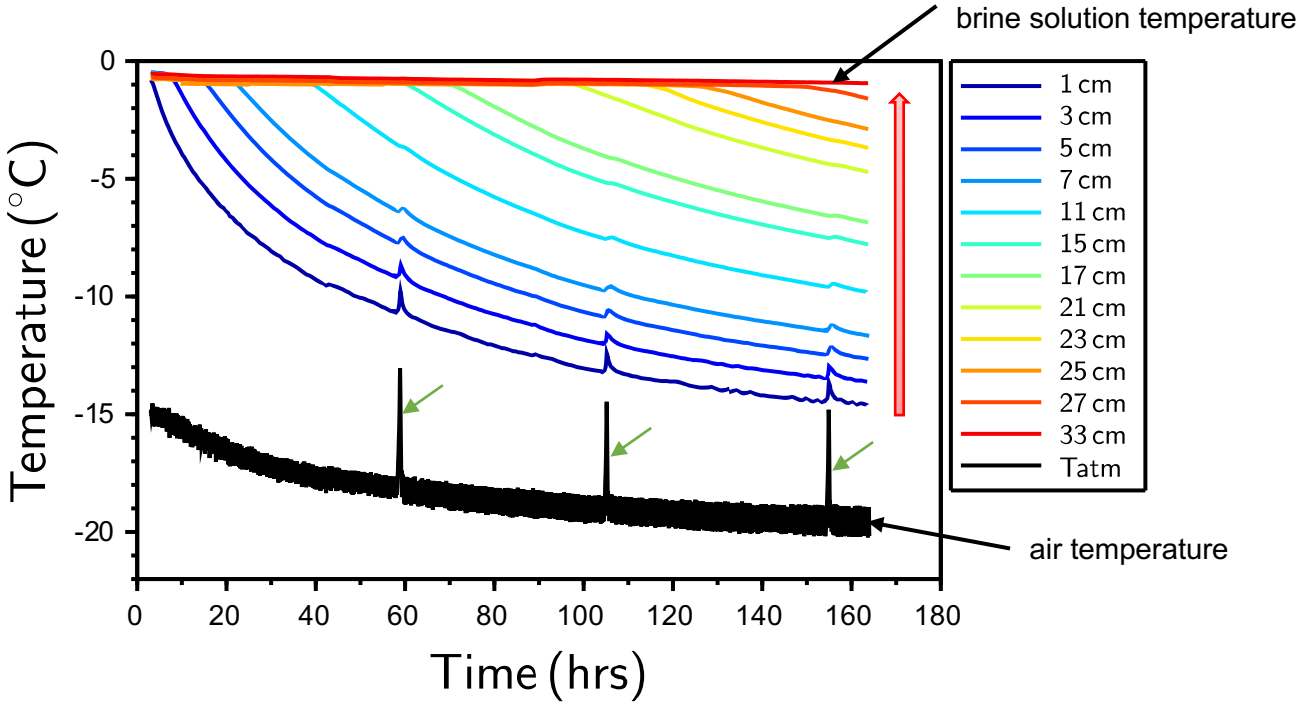


Figure 5.1: Experimental temperature profile for artificial sea ice grown at -20°C at 10PSU where each curve represents a different temperature probe location.

The air temperature, as measured by the atmospheric probe located 1 cm above the ice-air interface, initially measured the air temperature to be -15°C, thereafter it gradually decreases and stabilises at approximately -19°C. This is because as reported by Hall and Rampai, (2021), the temperature probe that controls the cooling within the cold laboratory is located near the cooling element which is the coldest place in the laboratory. Hence, the rest of the laboratory even with good circulation does not reach this temperature. This is the reason why the fan was used during the experiment, to promote an even convective cooling distribution within the cold laboratory and also increase heat transfer from the surface of the ice (Wiese, 2012; Roscoe et al., 2011).

The temperature increases that occur within the temperature profiles for a limited time duration as seen in Figure 5.1 correspond to defrost cycles. These are highlighted by the green arrows. Defrost cycles of the air cooler did not occur at the same time interval. However, the defrost cycles give an indication of the cooling rate of the cold laboratory. This is given by the time taken for the defrost cycle to drop from its peak temperature to the set point temperature of the cold laboratory. In this case it took 43 minutes for the cold laboratory to cool from -13°C to -19°C. This means that the cold laboratory had a cooling rate of 8°C/hour.

The freezing temperature which is the same as the brine temperature of the solution can be deduced from the plateau in Figure 5.1. Hence, it follows from Figure 5.1 that the freezing temperature of the solution was at -0.7 ± 0.1^{o}C. It should be noted that the expected freezing point of the solution was -0.5^{o}C based of the liquidus temperature relationship (Equation 2.3), for the measured starting salinity of 10 PSU (Worster & Jones, 2015). Nevertheless, the experimentally determined freezing point lies within the expected range from the mathematical relationship given in Equation 2.2. Moreover, the brine temperature at the onset of the experiment was at -0.7 ± 0.1^{o}C but it slightly drops towards the end of the experiment. The reason for the non-observable change in the brine temperature is because the expected decrease lies within the error of measurement. Hence it is difficult to see the brine temperature decrease as the ice freezes.

The temperature at each depth changes only when ice growth had occurred and the growth interface had moved past this point. It was thus observed that the ice grew from the surface going downwards. The ice started by forming at the probe located at a depth of 1 cm and lastly at the probe located at a depth of 27 cm. This suggests that the direction of the heat flux was predominantly in the vertical direction. There is a steep initial decrease of temperature recorded by the probes that are located at the cold upper boundary of the ice surface (1, 3 and 5 cm) relative to those located deeper in the tank (>5cm). Moreover, it can be noted from Figure 5.1 that the temperature drop away from the freezing point is rapid at the onset of the experiment as seen by the steep temperature descent of the temperature curve for the 1 cm temperature probe. However, the decrease in the slope of each curve, gradually slows down non-linearly overtime.

The data in Figure 5.1 seems to suggest that the curves are parallel to each other with the spacing between them corresponding to the placement of the temperature probes. This suggests that the temperature profile is linear. Moreover, this suggests that the thermal conductivity variation with position at any instant in time is small enough so that the linear approximation is obeyed. The second step in the analysis of the data involved transposing the temperature versus time data to temperature versus position at each instant in time.

Figure 5.2 is a different way of representing the raw data shown in Fig 5.1. Fig 5.2 shows the plot of temperature (T) versus position (z) at each instant in time. The colour pattern indicates that the temperature variation with position is nearly linear. Figure B13 (Appendix B6) shows the depth profiles for after every 1000th timestep, it indicates that the profiles are nearly linear. It follows from Figure 5.2 that there is a slowed decrease in the temperature with depth over

time as indicated by the decrease in the slope as indicated by the red arrow in Figure 5.2. The extrapolation to the brine temperature yields the position of the ice boundary.

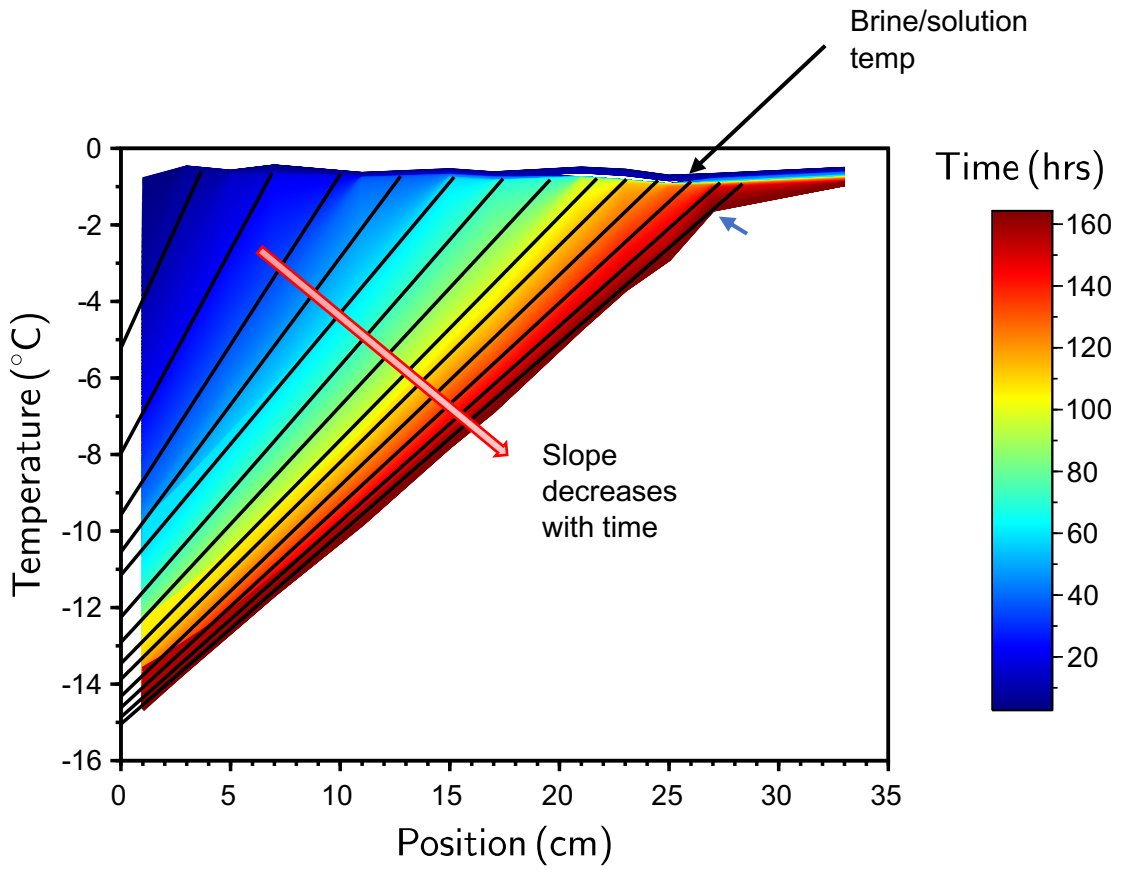


Figure 5.2: Temperature profile with depth for artificial sea ice grown at -20°C at 10PSU. This is raw data of Fig 5.1 which has now been put into the z coordinate system. The colour bar corresponds to each measurement in time. The black lines show that the temperature profiles are linear and these were extrapolated directly from the experimental data.

The deviation of the data from the linear behaviour as the brine temperature is approached can be described by the fact that the measurement points are stationary in time, while the ice-brine interface is moving with time. When extrapolating the linear profile to the brine temperature, this will indicate a depth of ice that lies between the measurement points and represents the last valid point to measure the ice temperature. This point has not been measured. However, the next temperature point that is measured, is at a greater depth than the linear extrapolation predicts and is still completely within the brine solution and thus cannot lie on the linear regression. Therefore, when joining the experimental points with lines, the last point will always be shifted off the linear extrapolation of the internal temperature measurements taken in the ice and leads to the observed deviation (bend) shown by the blue arrow. Secondly, the deviations of the data point from the linear model with position are

attributed to experimental error, which is the result of errors in the position of the thermocouples and errors in the temperature probe measurements. This is because there is measurement uncertainty from the spatial positioning of the temperature probes. The uncertainty in the positioning of the temperature probes was determined to be ±0.5 cm

The raw data in Figure 5.2 was then regressed. The temperature data recorded in the first 10 hours of the experiment was not used in the analysis. This is because the analysis can only start when two or more temperature probes are embedded in the ice. The y intercept of the extrapolated straight lines (as shown by the black straight lines) yielded the surface temperature at each time instant. The average squared error in fitting straight lines to all the data points is 0.0726. Furthermore, the average correlation coefficient of the straight-line fitting is 0.999. The variation of the correlation coefficient with time is shown in Figure B4 (Appendix B1). Figure 5.3 shows the variation of the surface temperature of the ice with time and it reflects on how it differs from the air temperature.

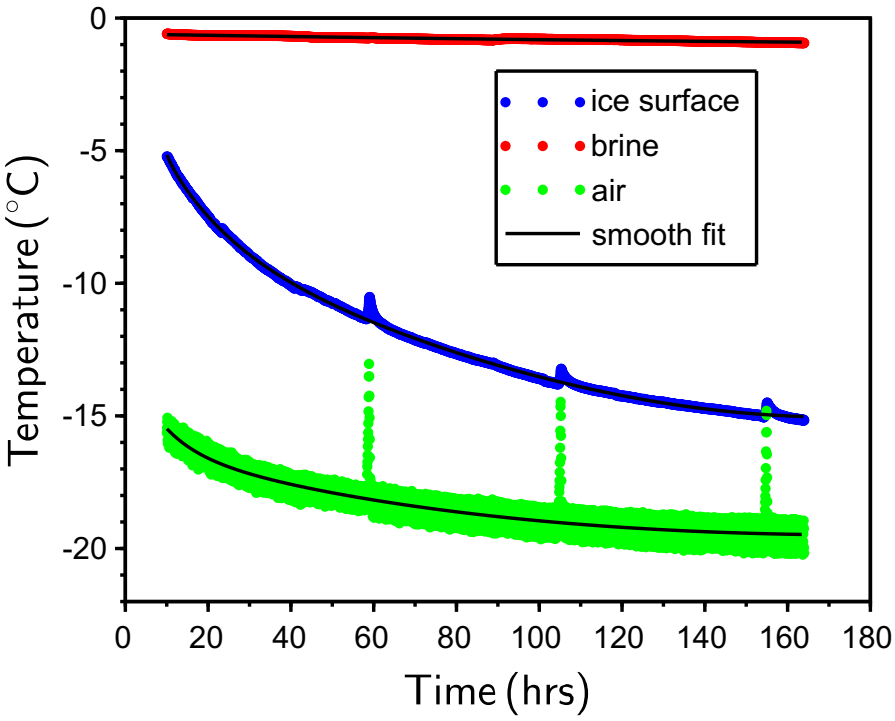


Figure 5.3: Analysis of the driving force for the growth of artificial sea ice at -20°C at 10PSU

This means that even in the absence of snow cover, the surface temperature of the ice is not same as the air temperature. This is due to the presence of the air film resistance to convective heat transfer. The deviation between the air and surface temperatures is purely due to assuming a linear temperature profile in the ice. The lowest surface temperature experienced for the experimental run was –14°C. Figure 5.3 indicates the overall driving force for heat

transfer which is the difference between the air temperature and the underlying solution temperature, remains fairly constant. The implication of stirring in the tank means that the saltwater within the tank is maintained at a uniform temperature, assuming that the tank is perfectly mixed. The growth profile of the ice was then inferred from the temperature measurements governed by Equation 4.23. Figure 5.4 shows the ice growth profile of the artificial sea ice. The experimental data fit an exponential curve where the blue curve indicates the predicted growth from the linearised model. Curve fitting was performed to the data through regression. The details of the fitting are in Appendix A1. This was done to obtain the exponential coefficients that fit the data. The spikes that appear in the data correspond to the defrost cycles that were observed in Figure 5.1.

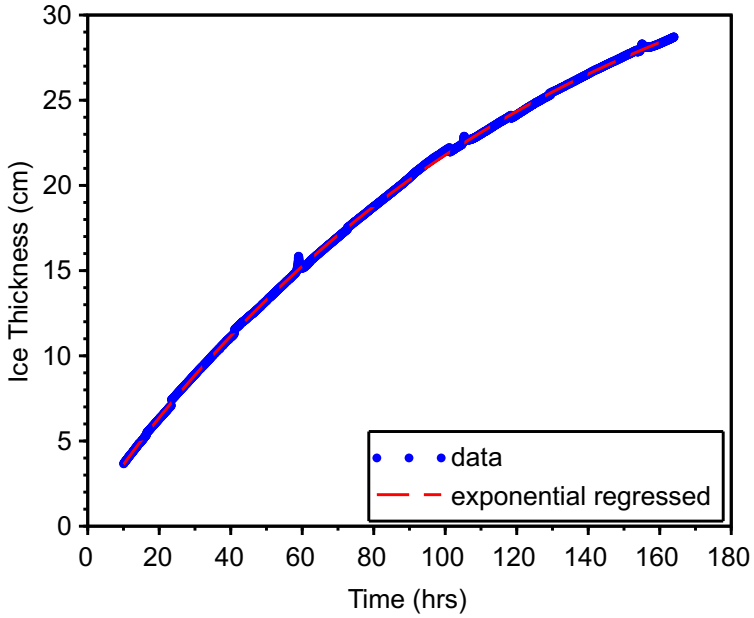


Figure 5.4:Ice growth profile for artificial sea ice grown at -20^{o}C and 10PSU

The growth curve is steep at the onset of the experiment. This means that fastest growth of the ice occurs during the initial stages of growth. After which it then gradually begins to slow down with time. This type of phenomenon was also observed by Cox &Weeks, (1975) in their artificial sea ice experiments. The gradient of the growth profile at each time instant gives the growth rate of the ice. Curve fitting for the growth rate profiles was done through linear regression. This was then compared with the curve obtained through the method of non-linear least squares. Figure 5.5 is the derivative of Figure 5.4. Thus, Figure 5.5 shows the growth rate profile of the ice. The highest growth rate is experienced at the onset of the experiment. This is indicated by the initial steep descent of the growth rate curve. Thereafter, it decreases non-linearly overtime.

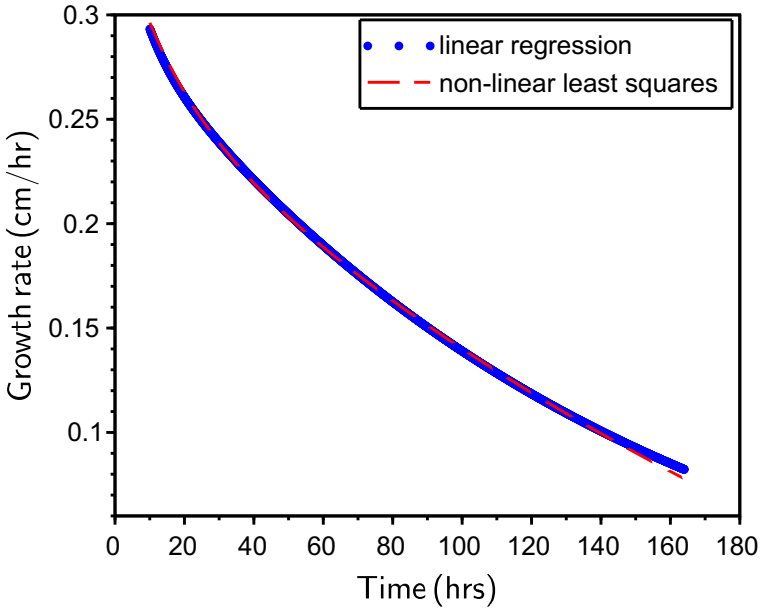


Figure 5.5 : Smoothed ice growth rate profile for artificial sea ice grown at -20°C and 10 PSU for a period of 160 hours.

Estimation of the ratio of $\frac{h}{k}$ was performed thereafter. Figure 5.6 shows that a plot of (1/alpha) plotted against ice thickness gives an approximately straight line. A straight line means that the thermal properties of the ice are constant in that region. The ratio of $\frac{h}{k}$ for this experiment is 12.1 ± 0.44 where 0.44 is the variance. Further assuming that h is 23 W/m^2.°C results in a k value of 1.90 (W/m.°C). This is the average k across the duration of the experiment

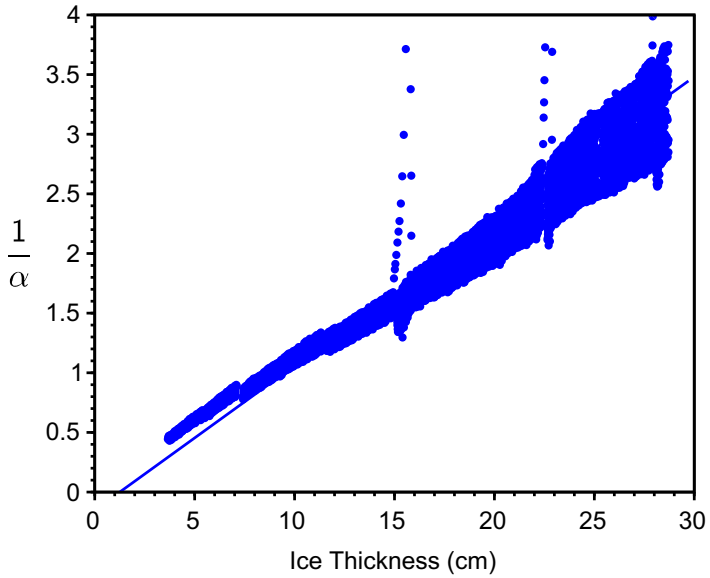


Figure 5.6: Estimation of h/k from the slope of 1/alpha vs ice thickness using regressed data for artificial sea ice grown at -20°C and 10 PSU for a period of 160 hours

The conductive heat flux was then inferred from the growth rate of the ice using Equation 4.24. Figure 5.7 shows the variation of the instantaneous conductive heat flux. Equation 4.24 shows that the growth rate of the ice is directly proportional to the heat flux liberated by the ice. Thus, the growth rate curve has the same shape as that for the conductive heat flux.

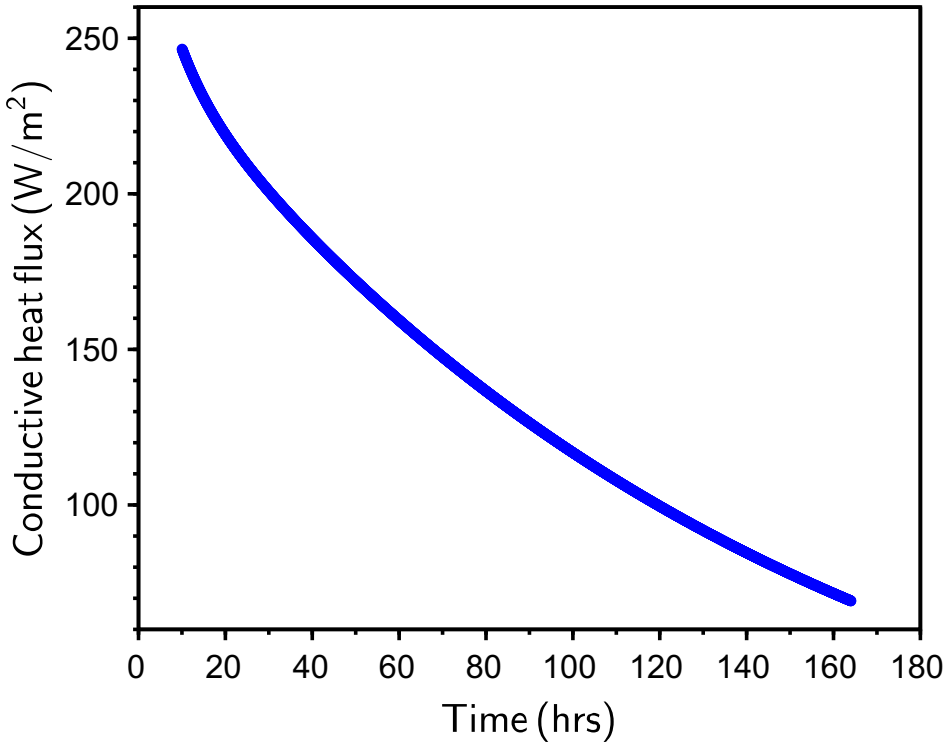


Figure 5.7: Conductive heat flux with time for artificial sea ice grown at -20°C at 10PSU using the pseudo steady state method

Figure 5.8. shows the salinity profiles for the ice melt at the end of the 160-hour growth period. The eight data points are indicative of the 8 segmented slices that were cut 3 cm long from the resulting ice at the end of the experiment. The shape of the salinity profile does not follow the expected “C” curve. The initial starting salinity of the freezing solution was measured to be 10.6 PSU. However, at the end of the experiment, the salinity of the underlying solution was found to be 15.9 PSU. The average salinity of the ice was found to be 3.60 PSU. This implies that salt was entrapped within the ice, but at much lower concentrations than in the freezing solution. The underlying solution salinity increased by 5.30 PSU. This is a 50% increase from the original starting solution salinity. However, this increase could also be attributed to gravity drainage from the ice as the ice was being sampled.

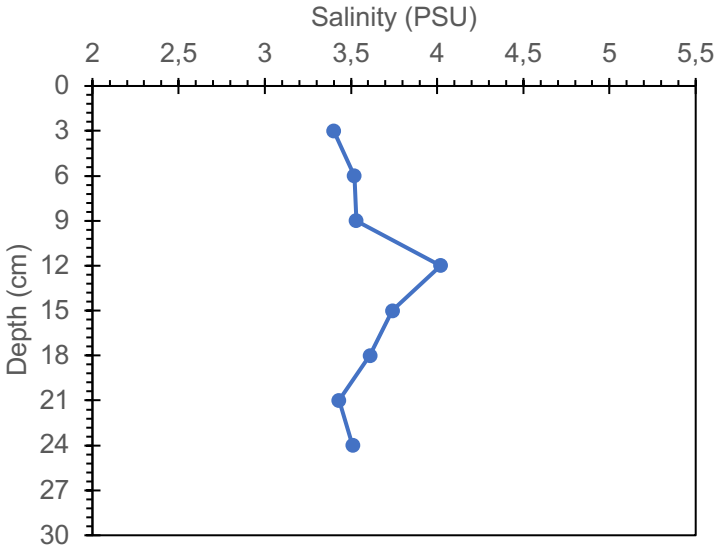


Figure 5.8: Salinity profile for artificial sea ice grown at 10PSU at -20^{O}C after 160 hours

A mass balance was conducted on the ice and underlying solution to determine the salt that was recovered at the end of the experiment. The mass of salt recovered after the experiment was 278 g. This means that 6.3% of the salt was lost, possibly during the ice cutting process.

5.2 Interpretation of results

The method of analysis was based on the existence of a linear temperature profile in the ice. Figure 5.2 proves that the temperature profiles within ice follow a linear trend with depth for artificial sea ice experiments. These observations have also been reported by (Notz, 2005),(Wiese, 2012) and (Weeks & Ackely, 1982). The existence of a linear temperature profile suggests that heat conduction within the ice occurs at pseudo steady state. This supports the argument of solving the heat conduction problem using the linearised approach reported in this work. The slope of $\frac{dT}{dz}$ decreases with increasing time. Consequently, the heat conducted from the brine solution as shown in Figure 5.7 decreases with increasing time. Thus, the growth rate of the ice as shown in Figure 5.5 is reduced with increasing time which is indicative of the slowed growth of ice with time which is seen in Figure 5.4.

Furthermore, the growth profile does not follow the square root of time that was proposed in literature. In this study the experimental data fits an exponential function rather than a parabolic function. Additionally, the growth profile of artificial sea ice shows that the fastest growth of the ice is experienced at the onset of the experiment. Thereafter, it gradually decreases with time. This means that the growth rate of the ice decreases with an increase in

the thickness of the ice. Qualitatively the decrease in ice growth rate has previously been attributed to the insulative properties of the ice. In this regard, the increase in the ice thickness causes a decrease in the growth rate of the ice because the heat exchange from the ice bottom to the atmosphere is reduced as ice acts as an insulator to heat transfer (Semtner Jr, 1976).

However, quantitative analysis of the presented experimental data indicates that, at pseudo steady state, the growth rate of the ice is directly proportional to the conductive heat flux that is linearly conducted through the ice. This relationship has been shown in Equation 4.23. It therefore follows that the heat exchanged at the air-ice interface is dependent on the driving force (T_a-T_L), the area (A) and the overall resistance to heat transfer (U). The driving force (T_a-T_L) has been shown to remain fairly constant throughout the duration of the experiment. Furthermore, the area available for heat transfer remains constant. As such the decrease in the heat exchanged is due to the increase in U. In this case, U increases with an increase in ice thickness. This implies that U increases with an increase in the length of the ice. The increased resistance to heat transfer thus results in the decrease in the growth rate of the ice. Consequently, this means that, when the ice thickness is small, there is rapid cooling of the ice. Hence the observed steep temperature time profiles at the onset of the experiment. However, as the ice thickness increases the cooling is slower, so the profiles are less steep.

The brine temperature decreases slightly towards the end of the experiment. This marginally decreased the freezing point of the solution. The slight decrease was expected because the underlying solution salinity increased by 50%, which proves that there was salt expulsion. The mechanism of salt expulsion has not been investigated in this work. However, Notz, (2005) proved that the salinity of the underlying water increases predominantly due to the process of gravity drainage.

The scatter in Figure 5.6 occurs due to the changes in the ice surface temperature. The change in the ice surface temperature is shown in Figure 5.3. The closer that To gets to Ta, the bigger is the noise in the data, hence a large variance. Moreover, the bigger the air oscillations are, the bigger the oscillations in the reciprocal of alpha.

The linearised pseudo steady state method differs from the classical Stefan’s law in that the Stephan's law measures the growth rate of the ice by assuming that the temperature profile is constant whereas the pseudo steady models (PSS) measures the ice temperature profile and does not assume that the ice temperature gradient is constant with all time. The PSS model assumes that the temperature profile is linear over all time. The Stefan’s law is then applied over a small time increment - that is the temperature profile is in PSS. The inversion of the

heat equations into linear equations allows for the determination of the linear equation coefficients which were used to estimate the growth rate using regression. The gradient decreases over time as the ice gets thicker. This is Stefan's law applied to data in which the temperature profile has been measured. It allows the estimation of more system parameters than if only the growth rate were measured

Lastly, it therefore follows from the above results that the temperature vs depth data has been successfully regressed using a linear model at every instant in time. Analysis of the regressed data can yield the:

1. Temperature of the surface of the ice with time
2. Depth of ice as a function of time
3. Heat passing through the ice Q(t)
4. Average convective to conductive heat resistance ratio
5. Growth rate of the ice
6. The technique can thus be reliably used to study the effects of varying the starting solution salinity, air temperature, and the tank size

Chapter 6 : Investigation of system parameters on the growth rate of artificial sea ice

This chapter presents the results and discussion on the effect of varying the growth conditions on the growth dynamics and conductive heat flux in artificial sea ice. The effect of varying the air temperature is presented in Section 6.1, the effect of varying the starting solution salinity in Section 6.2. Lastly the effect of varying the tank size is presented in Section 6.3. The experimental temperature output data was mathematically analysed using the linearised approach.

6.1 Variation of the air temperature

Three experiments were conducted where the air temperature was varied at -10^{o}C, -15^{o}C and -20^{o}C. The starting salinity of the freezing solution was kept constant at 10 PSU across these four experiments. The aim was to stop the experiments after the artificial sea ice had grown to a length of at least 18 cm. However, this was not always possible. Thus, the duration of the experiments was not constant. The experiments were run for 160 hours for the experiments performed at -15^{o}C and -20^{o}C. The experiment at -10^{o}C was run for a period of 94 hours. At the end of the experiments the underlying salinity of the solution, in-ice salinity and recorded temperature measurements were taken, and these are analysed and discussed as below.

Figure 6.1 gives a comparison of the temperature profiles for the three experiments. The blue curves represent the -10^{o}C experimental data, green curves for the -15^{o}C experimental data and lastly, the red /orange curves for the -20^{o}C experimental data. The purpose of Figure 6.1 is to show that the temperature profiles for the -20^{o}C experimental run are consistently steeper than the -15^{o}C and -10^{o}C. The steepness of the temperature descent decreases as the air temperature is increased. Figure B5, Figure B6 and Figure B7 in Appendix B shows the detailed locations over the growth period for the experimental runs at -15^{o}C, -10^{o}C and -20^{o}C respectively. Moreover, Figure 6.2 gives a comparison of the temperature with depth for the three experiments.

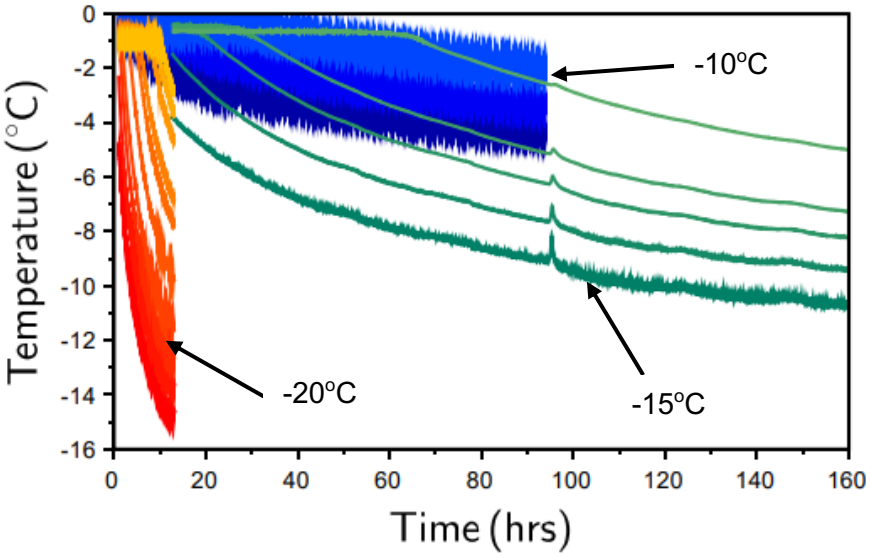


Figure 6.1: Temperature profiles for artificial sea ice grown at 10 PSU where the blue curves are for the experimental run at -10°C, green is for the experimental run at -15°C and red/orange is for the experimental run at -20°C. The data shown for the experimental run at -20°C is for the first 16 hours only. Refer to Figure 5.1 for the full temperature profile

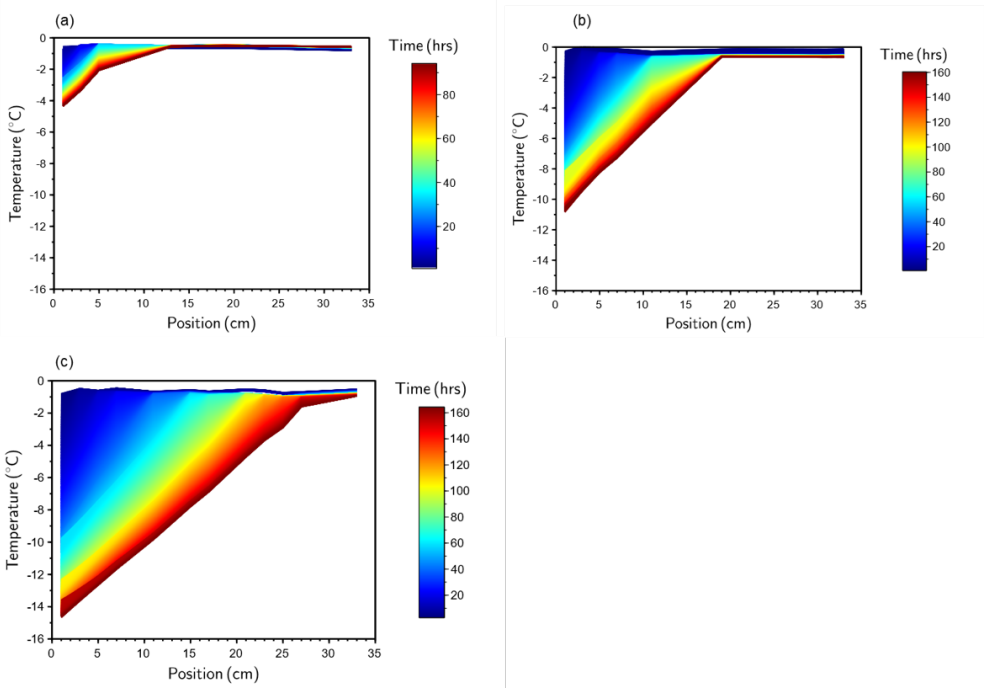


Figure 6.2: Temperature with depth profile for artificial sea ice that was grown at 10 PSU to show the effect of varying air temperature where the air temperature for (a) is -10°C, the air temperature for (b) is -15°C and the air temperature for (c) is -20°C

Figure 6.2 highlights that the linear temperature profile is maintained upon varying the air temperature. The slope of the linear profile decreases with time, the decrease is steeper at lower at temperatures. This is shown in Figure 6.3.

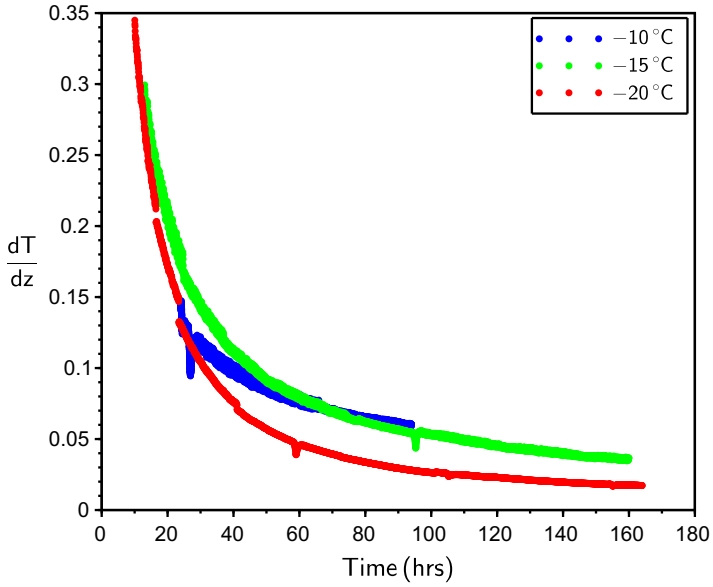


Figure 6.3: Variation in the change in the slope of dT/dz with units in °C/cm to show the effect of varying the ambient temperature.

Figure 6.4 shows the growth profiles for artificial sea ice that was grown at 10 PSU but at different air temperatures. The ice grew to 27.5 cm, 18 cm and 10 cm for the experimental run at -20°C, -15°C and -10°C respectively. As the ice did not reach the same depth, Figure 6.4 will be used to compare ice growth after 80 hours.

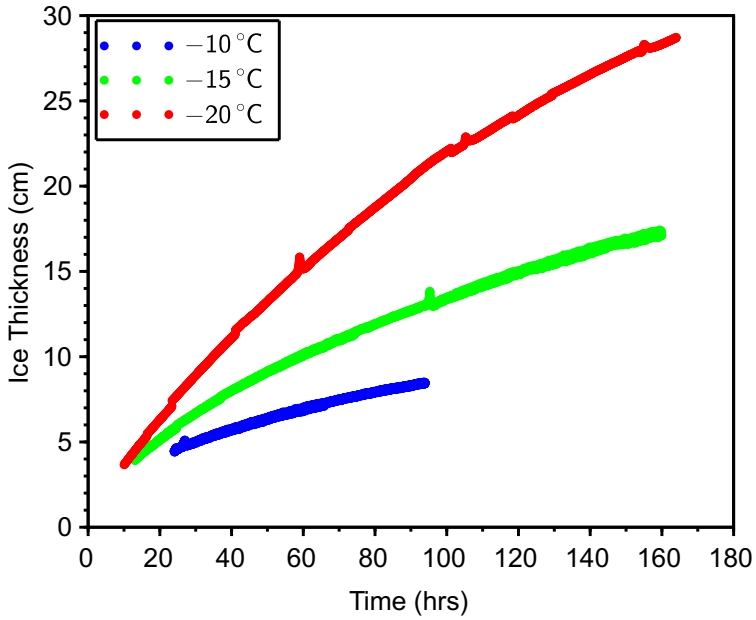


Figure 6.4: Growth profile for artificial sea ice that was grown at 10 PSU but at different air temperatures

The artificial sea ice that was grown at -20°C has the steepest growth profile. This is followed by the experimental run at -15°C and lastly -10°C. As the steepness of the slope from the growth profile is an indication of the growth rate, this suggests that the lower the ambient temperature, the higher is the growth rate. It is important to note that, the spikes that appear on the growth profile mean that the ice is melting, this is an error in the analysis technique that occurs when there is noise in the data.

Figure 6.5 shows the effect of varying the air temperature on the growth rate of ice. Faster growth rates are initially experienced when the air temperature is -20°C than when the temperature is at -15°C or at -10°C as seen by the steep slopes in Figure 6.5. This is due to the change in the driving force for ice growth. Thus, Figure 6.5 shows that the growth rate is highest at lowest ambient temperature. This supports the argument that a lower atmospheric temperature creates a greater temperature gradient and consequently a higher growth rate. (Weeks & Assur, 1967). The differences in the temperature gradient are shown in Figure 6.6.

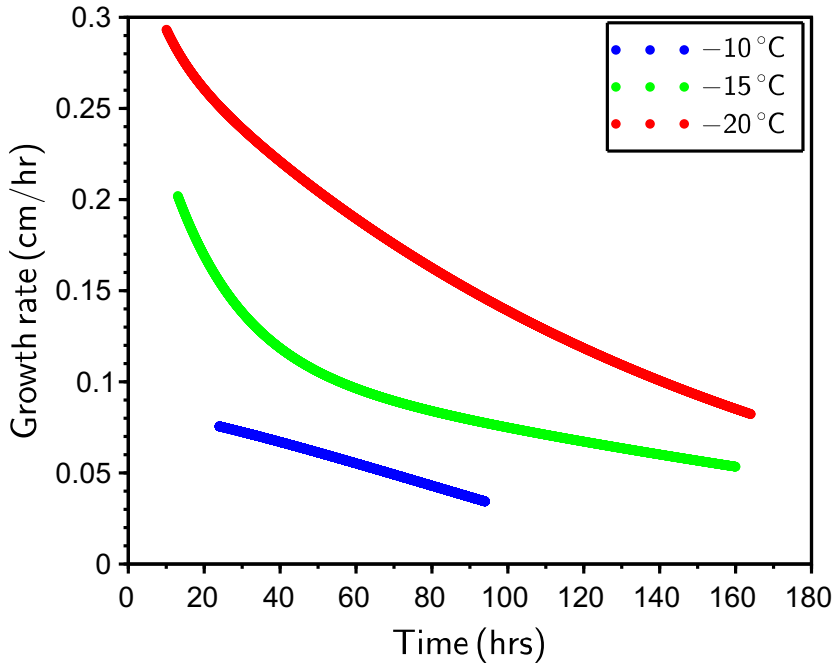


Figure 6.5: Smoothed ice growth rate profiles for artificial sea ice that was grown at 10 PSU but at different air temperatures to show the effect of varying the ambient temperature

Figure 6.6 shows the effect of varying the air temperature on the driving force. The overall driving force which is the difference between the air and brine temperature increases as the air temperature is decreased. Figure 6.7 shows the effect of varying the air temperature on the estimation of the $\frac{h}{k}$ ratio. Figure 6.7 indicates that the slope decreases with a decrease in the air temperature.

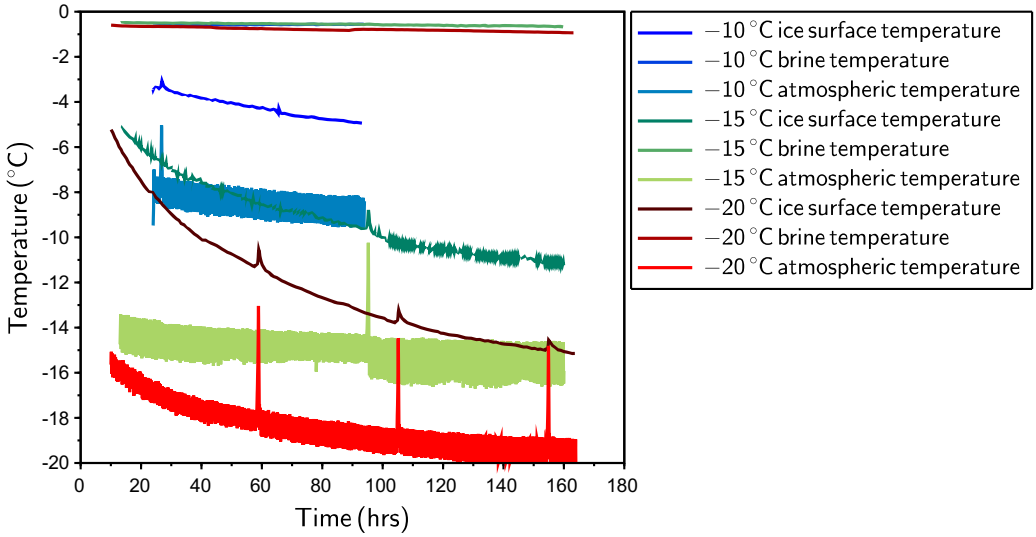


Figure 6.6: Evaluation of the driving force for artificial sea ice that was grown at 10 PSU but at varied air temperatures

Figure 6.7 shows that the ratio of $\frac{h}{k}$ is higher at higher temperatures and lower at lower temperatures. The quantification of k and $\frac{h}{k}$ is shown in Table 6.1. Moreover, Table 6.1 highlights the numerical variation $\frac{h}{k}$ reported with its variance. Table 6.1 shows that an increase in $\frac{h}{k}$ is associated with a decrease in k. This also means that the growth rate of ice decreases due to the decrease in the average value of k across the duration of the experiment.

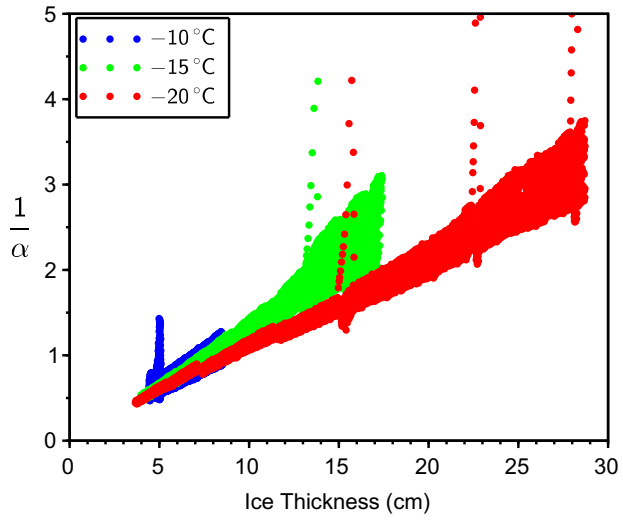


Figure 6.7: Estimation of h/k from the slope of 1/alpha vs ice thickness using regressed data for artificial sea ice that was grown at 10 PSU but at varied air temperatures

Table 6.1: Estimation of $\frac{h}{k}$ from temperature measurements for artificial sea ice

Set air temperature (°C)	**-10**	**-15**	**-20**
Starting solution salinity (PSU)	10	10	10
Tank size (L)	30	30	30
$\frac{h}{k}$ (m^{-1})	17.0 ± 0.06	16.3± 0.10	12.1± 0.44
h	23	23	23
k (W/m.°C)	1.35	1.41	1.90

Figure 6.8 shows the salinity profiles taken at the end of the experiments. Moreover, Table 6.2 shows the salinity uptake data to show the effect of varying the air temperature for solutions that have the same starting salinity of 10 PSU. Figure 6.8 shows that the sample at -20°C has a higher brine retention within the ice. This is followed by the sample at -15°C and lastly by the sample at -10°C.

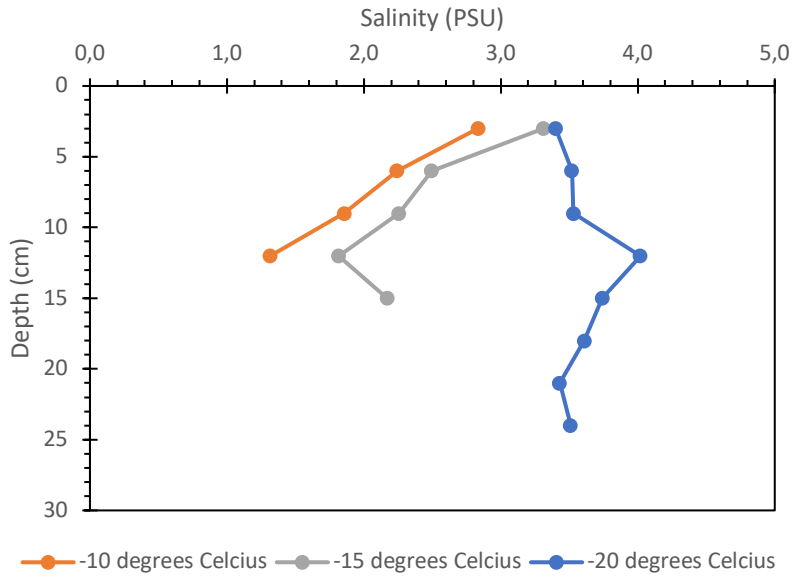


Figure 6.8: Salinity profile for artificial sea ice that was grown at 10 PSU at varied air temperatures

Table 6.2 shows that the sample at -20°C had the largest increase in the underlying solution salinity where the freezing solution salinity increased from 10 PSU to 15.9 PSU. Table 6.2 and Figure 6.8 show that the sample at -20°C experienced the largest increase in the average ice salinity relative to the sample at -15°C and -10°C.This is because the lower air temperature

results in greater artificial sea ice growth rates. This leads to the formation of smaller ice crystals with more brine inclusions (Weeks & Ackley, 1982). This means that there is higher brine retention in ice at lower temperatures than there is at higher temperatures (Gow et al., 1987). The brine solution for the experimental run at -10°C marginally increased by 1.1 PSU. This could be because the ice did not grow significantly relative to the other two experiments

Table 6.2: Salinity uptake data for artificial sea ice that was grown at 10 PSU at varied air temperature

Set air temperature (°C)	**-10**	**-15**	**-20**
Starting solution salinity (PSU)	10	10	10
Tank size (L)	30	30	30
Average ice salinity (PSU)	2.1	2.4	3.6
Underlying solution salinity at the end of the experiment (PSU)	11.2	14.1	15.9
Salt mass balance error (%)	7.2	4.4	6.3

Figure 6.9 shows the computed conductive heat flux for the experiments under investigation. It follows from Figure 6.9 that the conductive heat flux through the growing ice is a function of the air temperature. The conductive heat flux exchanged between the atmosphere and the ice interface is higher when the air temperature is at -20°C than when it is at -15°C and at -10°C

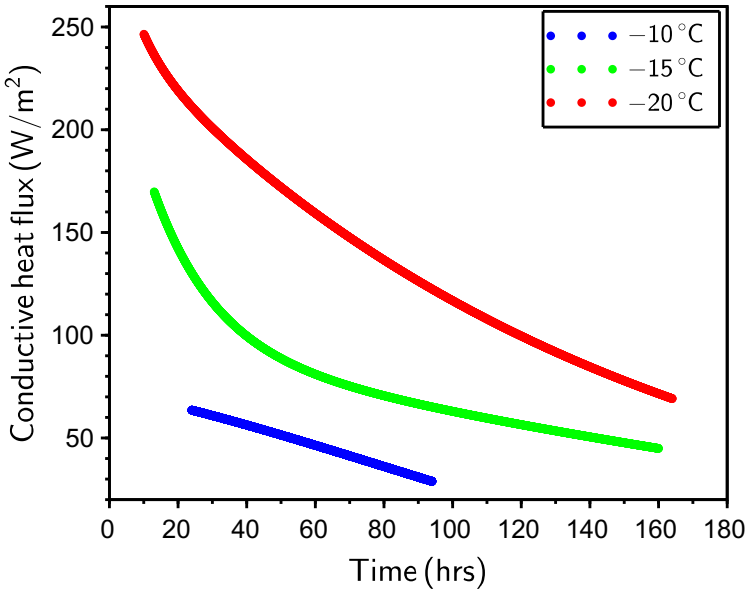


Figure 6.9: Conductive heat flux of artificial sea ice that was grown at 10PSU at varied air temperatures

6.2 Variation of the starting solution salinity

Three experiments are presented in this section, where the starting solution salinity was varied at 10 PSU, 20 PSU and 30 PSU. The air temperature for these experiments was kept constant at -20°C. The experiments were run until the artificial sea ice had reached a minimum thickness of 18 cm. The experiments were run for 160 hours, 120 hours and 140 hours for the 10 PSU, 20 PSU and 30 PSU respectively. At the end of the experiment the underlying salinity of the solution, in-ice salinity and recorded temperature measurements were taken, and these are analysed and discussed below.

Figure 6.10 shows the temperature with time profiles for artificial sea ice that is at a depth of 3 cm (solid lines) and 5 cm (dashed lines) to show the effect of varying the starting solution salinity. Figure B7, Figure B8 and Figure B9 (Appendix B) gives the detailed time evolution of the temperature recorded by probes at different locations over the growth period of the experiments.

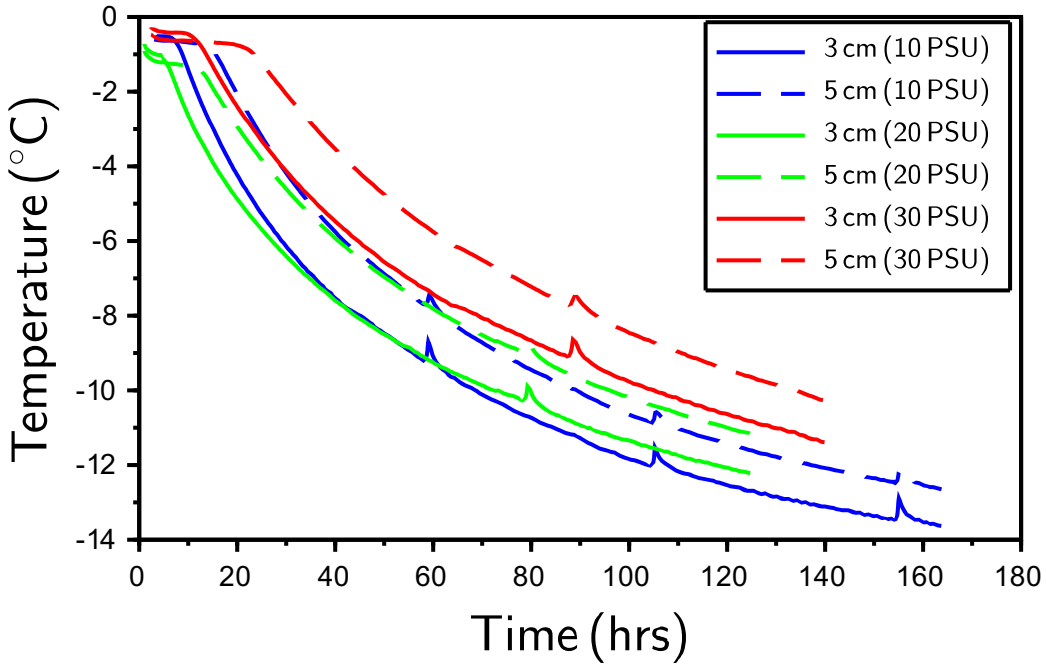


Figure 6.10: Temperature with time profile for artificial sea ice grown at -20°C to show the effect of varying the starting solution salinity. The solid lines are profiles for artificial sea ice at a depth of 3 cm and the dashed lines temperature profiles at 5 cm

Figure 6.10 shows that at a depth of 3 cm and 5 cm, the 30 PSU solution has a less steep temperature descent relative to the 10 PSU and 20 PSU experimental runs. The difference between the 10 PSU and 20 PSU solution is subtle. However, the 20 PSU solution initially has

a steep temperature decent relative to the 10 PSU solution, it overlaps then becomes less steep than the 10 PSU solution

Figure 6.10 shows that the ice interface reached 3 cm after 10 hours and it took a further 10 hours for the ice formation to reach 5 cm. However, it took 17 hours for 3 cm of ice to form in the 30 PSU tank and 13 more hours to grow to 5 cm. This observed difference between the temperature descent for the 10 PSU and 30 PSU solution means that increasing the starting solution salinity increases the time it takes for the ice interface to move from one growth location to another.

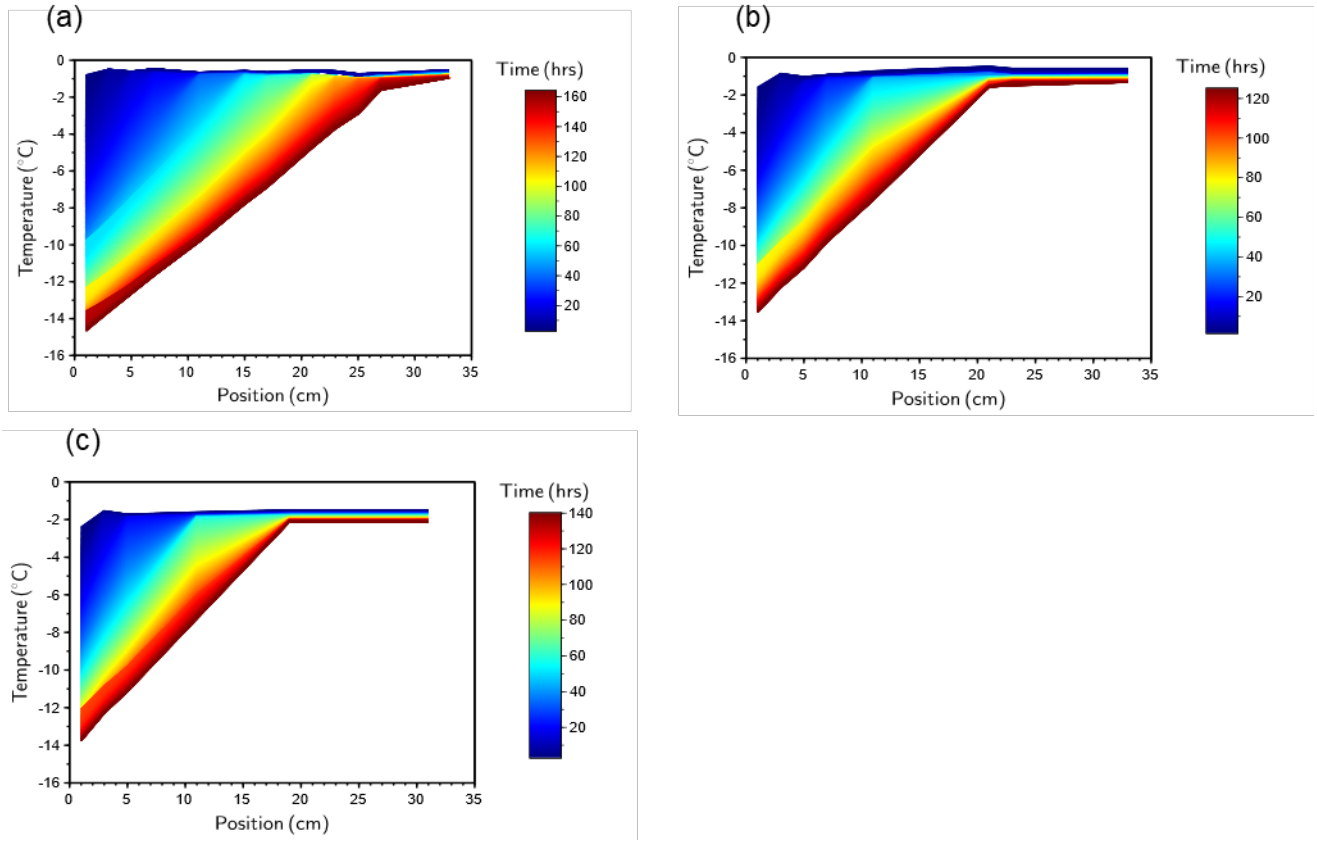


Figure 6.11: Temperature with depth profile for artificial sea ice that was grown at -20°C to show the effect of varying initial solution salinity where the starting solution salinity for (a) is 10 PSU, the starting solution for (b) is 20 PSU and the starting solution for (c) is 30 PSU

Figure 6.11 shows that all three experiments had a linear temperature profile with depth. Hence, the assumptions of the linearised model are valid in analysing the data. Figure 6.12 shows that the slope of the linear temperature profiles decreases non-linearly overtime. The 10 PSU and 20 PSU solutions have the steepest descent relative to the 30 PSU solution.

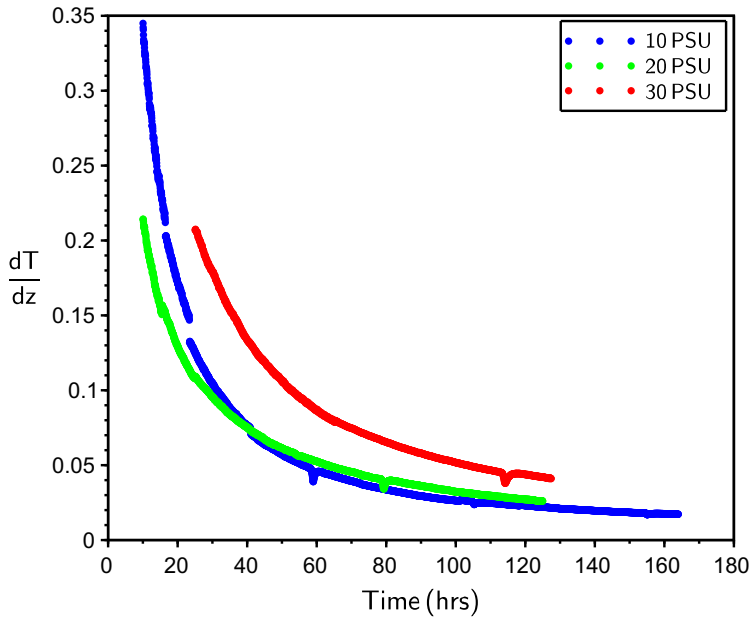


Figure 6.12: Variation in the change in the slope of dT/dz with units in °C/cm to show the effect of varying the starting solution salinity

Figure 6.13 shows the effect of varying the starting solution salinity on the growth profile of artificial sea ice. The ice grew to 27.5 cm, 21 cm and 19.5 cm for the 10 PSU, 20 PSU and 30 PSU experiments respectively.

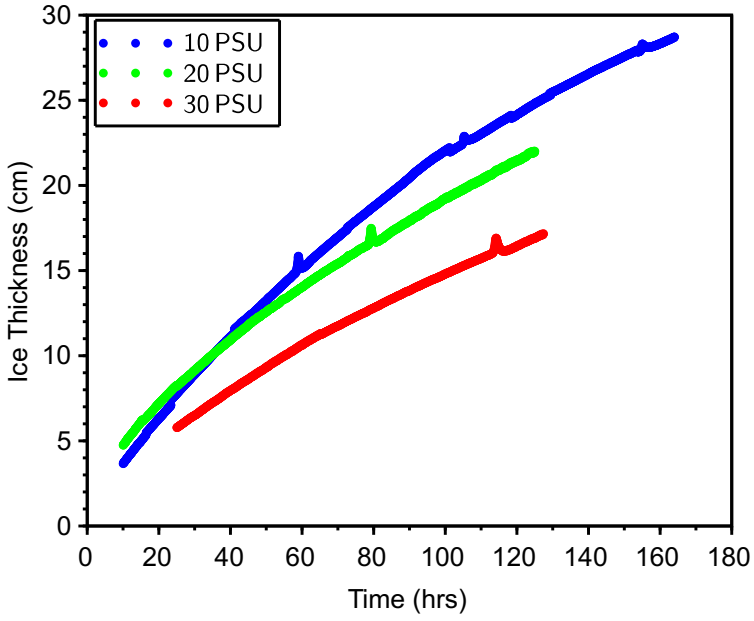


Figure 6.13: Growth profile for artificial sea ice that was grown at -20°C to show the effect of varying the starting salinity

Figure 6.13 shows that the 10 PSU solution has a steep growth profile. This is followed by the 20 PSU solution and lastly the 30 PSU solution. This indicates that an increase in the starting solution salinity results in a decrease in the growth of the ice. This implies that higher salinities will significantly slow down the growth of the ice. Consequently, this means that the growth rate of the ice decreases with an increase in the starting solution salinity.

The growth profile of the 10 PSU solution overlaps with the 20 PSU. This is because of the difference in the initial starting air temperature at t=0. The initial starting air temperature for the 10 PSU run is at approximately -15°C and it slowly decreases to -19°C (Figure B7, Appendix B). However, for the 20 PSU and 30 PSU run, the initial air temperature is at approximately -17°C and slowly decreases to -19°C (Figure B8 and Figure B9, Appendix B). Hence the growth rate of the ice in the 10 PSU was initially slower than expected due to the difference in the starting air temperature. Moreover, may have also have been due to subtle differences in the quality of the seed crystals. The effect of the quality of the seed crystals on the initial growth rate of the ice seeding has not been explored in this work. This is an area that can be further explored.

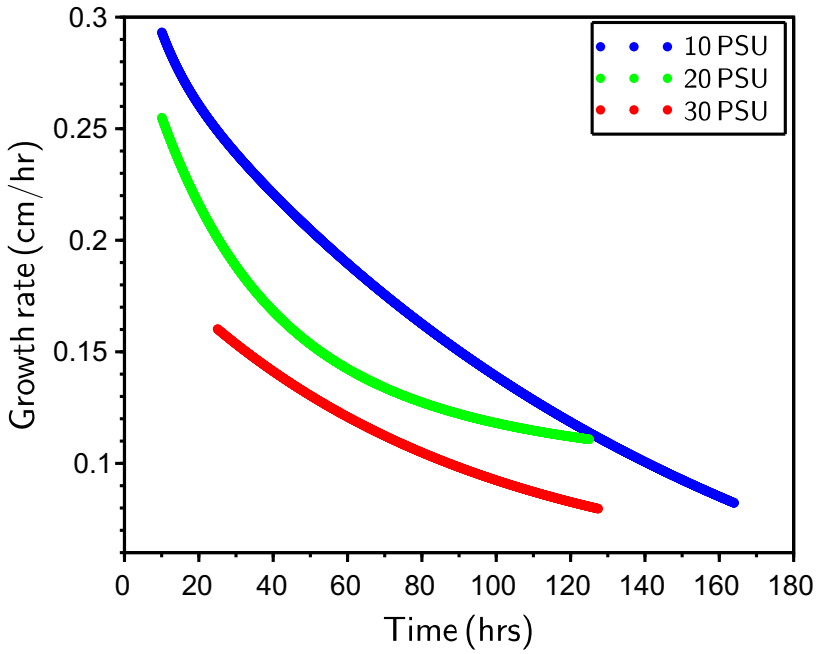


Figure 6.14: Smoothed ice growth rate profiles for artificial sea ice that was grown at -20°C but at different starting solution salinity

Figure 6.14 shows the effect of varying the starting solution salinity on the growth rate of the ice. The 10 PSU solution has the fastest growth rate followed by the 20 PSU and lastly the 30 PSU. The decrease in the growth rate of the ice as the starting solution salinity is increased

can be attributed to the the freezing point depression. The changes in the freezing point are shown in Figure 6.15.

Figure 6.15 indicates the freezing depression phenomenon that occurs when the starting salinity is increased from 10 PSU to 30 PSU. The 30 PSU solution had the lowest freezing point of -1.8°C relative to the 20 PSU solution whose freezing point was -1.0°C and the 10 PSU solution whose freezing point was -0.70°C. The freezing point of the solution decreases with an increase in salinity based on the liquidus temperature relationship to maintain local thermodynamic equilibrium (Feltham et al., 2006). Hence, the decrease in the freezing point reduces delta T, which is the driving force for energy transfer and consequently the growth rate of the ice. This is because in Section 6.1, it has been shown that a large driving force results in faster growth rates. The reverse holds true.

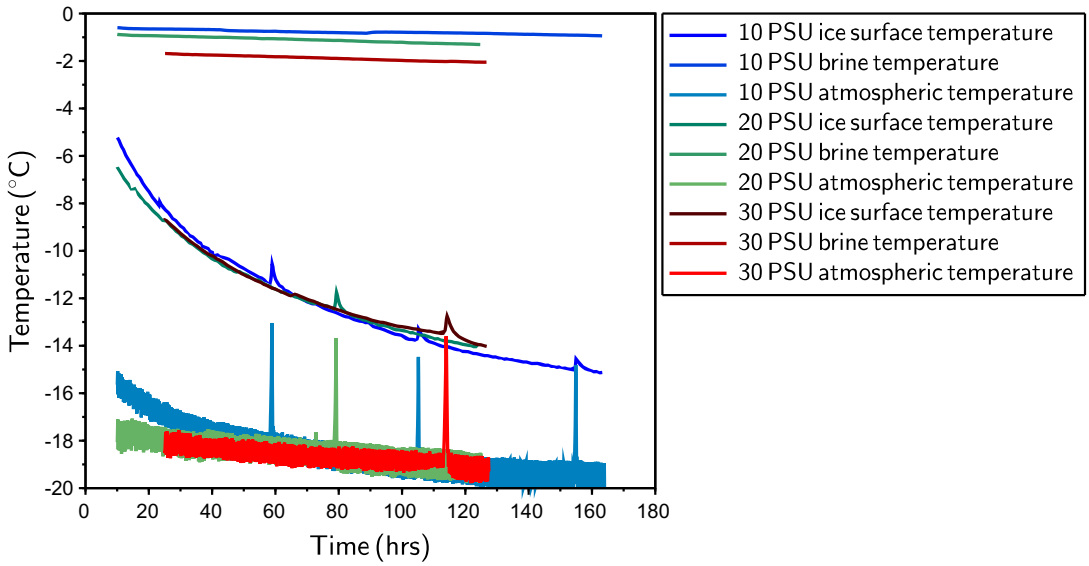


Figure 6.15: Evaluation of the driving force for artificial sea ice that was grown at -20°C to show the effect of varying the starting salinity

Figure 6.16 shows the straight-line fitting in estimating the $\frac{h}{k}$ ratio whilst

Table 6.3 shows the numerical values.

Table 6.3 highlights that $\frac{h}{k}$ increases with an increase in the starting solution salinity. Moreover,

Table 6.3 shows that k decreases upon increasing the starting solution salinity. It is important to note that the same value for h was used in each case. The decrease in the average value

of k across results in the observed slowed growth rates of the ice upon increasing the starting solution salinity.

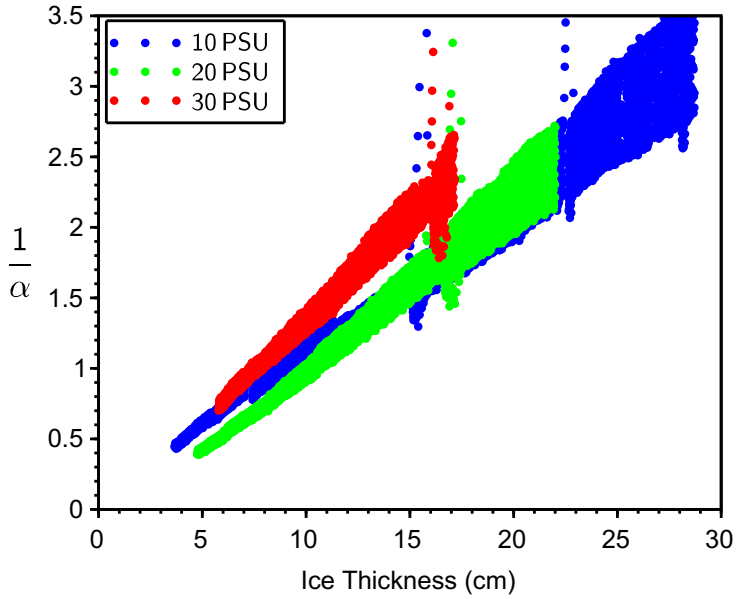


Figure 6.16: Estimation of h/k from the slope of 1/alpha vs ice thickness using regressed data for artificial sea ice that was grown at -20°C to show the effect of varying the starting solution salinity

Table 6.3: Thermal conductivity estimation from temperature measurements for artificial sea ice

Set air temperature (°C)	-20	-20	-20
Starting solution salinity (PSU)	**10**	**20**	**30**
Tank size (L)	30	30	30
$\frac{h}{k}$ (m^{-1})	12.1 ± 0.44	12.2 ± 0.06	15.5 ± 0.41
h ($W/m^2.°C$)	23.0	23.0	23.0
k (W/m.°C)	1.90	1.88	1.48

The increase in $\frac{h}{k}$ relates to the decrease in the average thermal conductivity of the ice as the starting solution salinity increases. Thus, this means that, the decrease in the growth rate of the ice is also due to the decrease in the average thermal conductivity of the ice. The decrease in the average thermal conductivity implies that there is increased resistance to heat flow.

Moreover, the change in the thermal conductivity upon variation of the starting solution salinity means that ice's thermal conductivity is a function of the starting solution salinity. Figure 6.17 shows the effect of varying the starting solution salinity on the conductive heat flux.

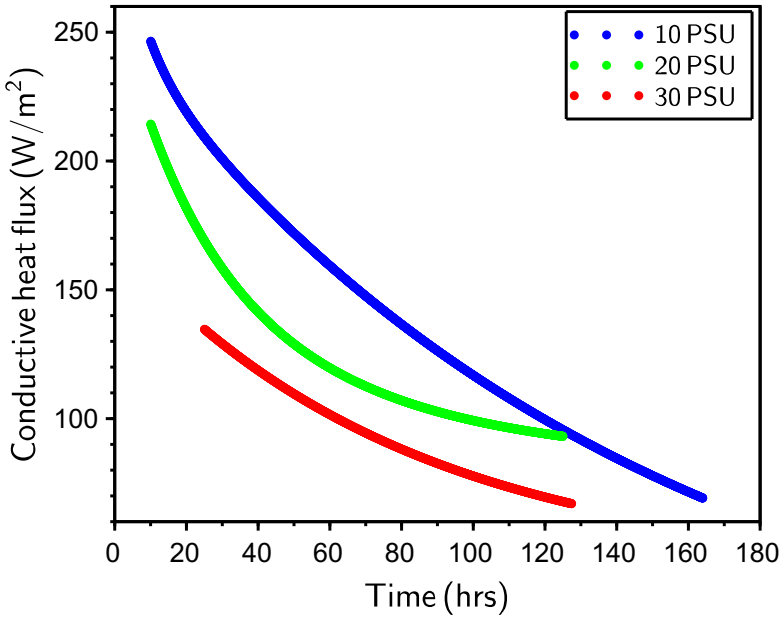


Figure 6.17: Conductive heat flux of artificial sea ice that was grown at -20°C to show the effect of varying the starting salinity

The conductive heat flux decreases as the starting solution salinity is increased. Figure 6.17 supports the argument presented earlier that as the salinity of the solution increases, there is increased resistance to heat flow.

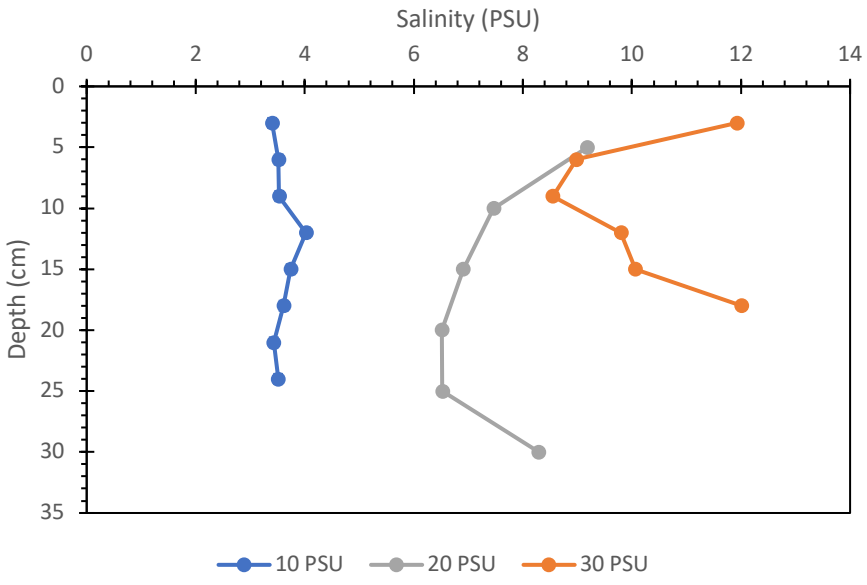


Figure 6.18: Salinity profile for artificial sea ice that was grown at -20°C to show the effect of varying starting salinity

Figure 6.18 shows the salinity profile that was recorded at the end of the experiments. The salinity profile at 20 PSU and 30 PSU displayed a “C” shaped curve. This is characteristic of young and first year sea ice salinity curve which is expected of first year ice in both the Arctic and Antarctic (Eicken, 1992). However, the salinity profile for the 10 PSU solution displayed an “I” curve. The “C” shaped profiles have also been observed by Notz and Worster (2008). Table 6.4 shows that underlying solution salinity increased by 5.9 PSU for a starting solution of 10 PSU, and it increased by 16.1 PSU for the solution that had a starting salinity of 20 PSU. Lastly, it increased by 9.5 PSU for the solution that had a starting salinity of 30 PSU.

Table 6.4: Salinity uptake data for artificial sea ice that was grown at -20°C to show the effect of varying starting salinity

Air temperature (°C)	-20	-20	-20
Starting solution salinity (PSU)	**10**	**20**	**30**
Tank size (L)	30	30	30
Average ice salinity (PSU)	3.6	7.5	10.2
Underlying solution salinity at the end of the experiment (PSU)	15.9	36.1	39.5
Salt mass balance error (%)	6.3	6.4	9.4

The ratio of the starting solution salinity is the same the average ice salinity ratio of 1:2:3, this implies that the average ice salinity ratio is linearly related to the starting solution salinity. The ratio of the average ice salinity to the underlying solution salinity is not the same for the 30 PSU solution. This could be due to the difference in the length of the ice that was grown.

6.3 Variation of the tank size

This section focuses on investigating the effect of the tank size on the growth dynamics in artificial sea ice. This effect was investigated using a 3 L, 30 L and 300 L tank. The artificial sea ice was grown at -20°C at 30 PSU. The air temperature for these experiments was kept constant at -20°C. The results obtained are as discussed below:

Figure B9, Figure B10 and Figure B11 show that at the same depth, the time taken for the solution to freeze increases as the size of the tank increases. The 3 L tank takes the least amount of time to cool per given depth, followed by the 30 L tank and lastly the 300 L tank. Moreover the 300 L tank has less steep temperature profiles at each depth relative to the 30 L and 3 L tanks. The 3 L tank shows steep temperature descents throughout the experiment. The trend in the temperature profile with depth is shown in Figure 6.19.

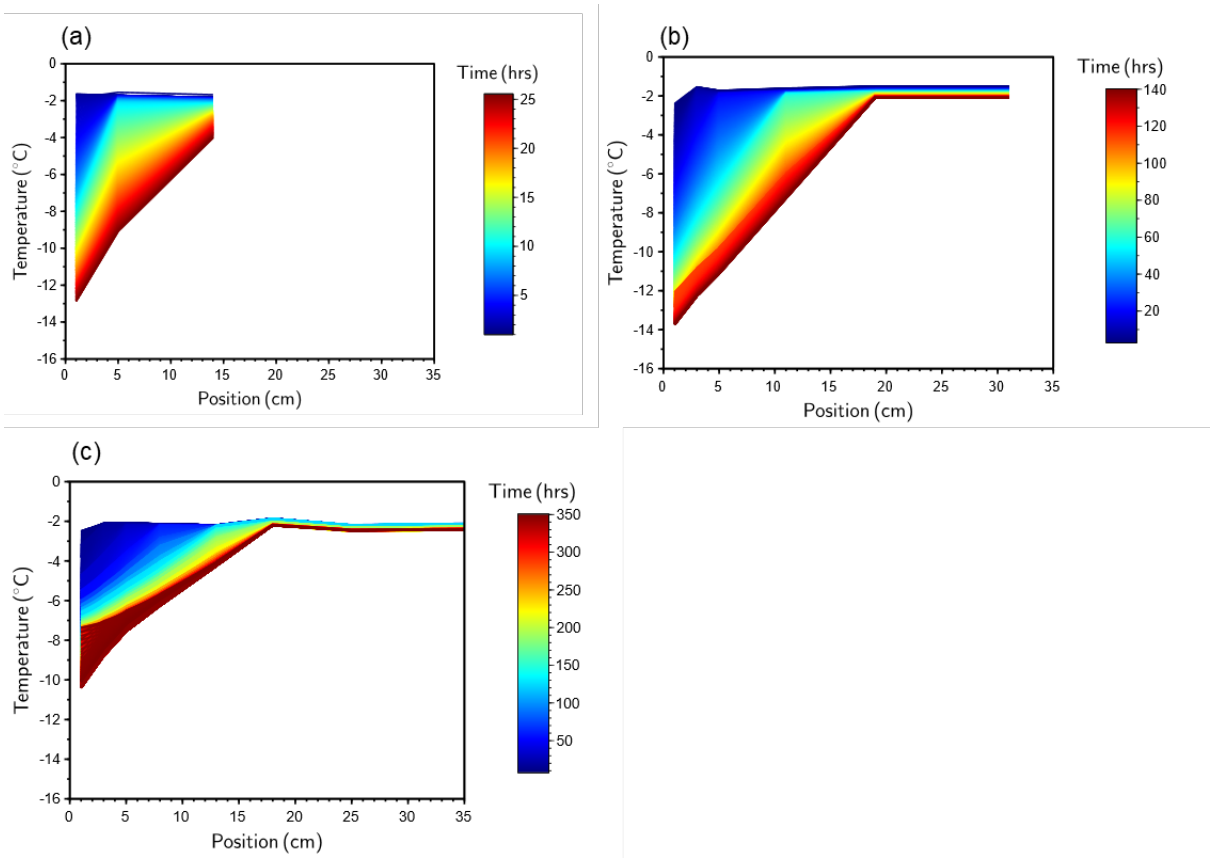


Figure 6.19: Temperature profile with depth for artificial sea ice grown at -20°C and 30 PSU to show the effect of tank size where the tank size for (a) is 3 L, the tank size for (b) is 30 L and the tank size for (c) is 300 L

The 300 L tank does not have a linear temperature profile with depth. The data for the experiment in the 300 L tank was obtained from a previous experiment on the UCT MARiS

database. The defrost cycles experienced in the 300 L tank, distort the linearity of the data. Hence, the data does not conform to the assumptions of the linearised model. The 3 L tank has insufficient in ice temperature measurements for detailed analysis using the linearised model. However, an attempt to extrapolate the growth profiles using the linearised model was performed. It can be noted from Figure 6.19 that the steepness in the slope for the same time interval decreases as the size of the tank is increased. The 3 L tank has the steepest slopes relative to the 30 L tank and the 300 L tank. The growth profile of the 300 L tank is distorted. This is due to the large spikes in the defrost cycles which propagate into the ice.

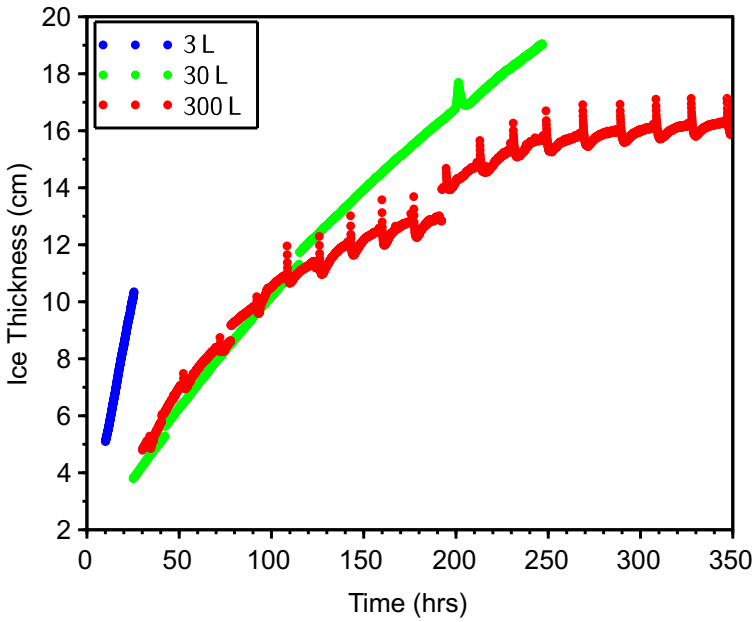


Figure 6.20: Growth profile for artificial sea ice that was grown at -20°C to show the effect of varying the starting salinity

The effect of the defrost cycles on the growth profile of the 300 L introduces the question of how daily variations in the ambient temperature affect the growth profile. This may present another limitation to the linearised model. However, this was beyond the scope of the project. This effect can be investigated in further research. The 3 L tank data has insufficient in-ice temperature measurements for linear regression to be performed. This can be combated by using thermistors which have a reduced physical footprint in the tank. The pseudo steady sate linearised model is one dimensional, it does not account for the area and volume of the tank. Hence, the differences in the growth profiles are due to external factors that have not been investigated in this project. Thus, the question of how the tank size affects the growth dynamics of sea ice remains an area that needs further exploration.

Figure 6.21 shows the effect of varying the tank size on the salinity profile whereas Table 6.5 shows the average ice salinity. The 3 L and 30 L tank samples both exhibit a “C” shaped salinity profile. The curve is more defined for the 3 L sample than it is for the 30 L sample. The salinity profile for the 300 L tank displays a reversed “S” shaped profile.

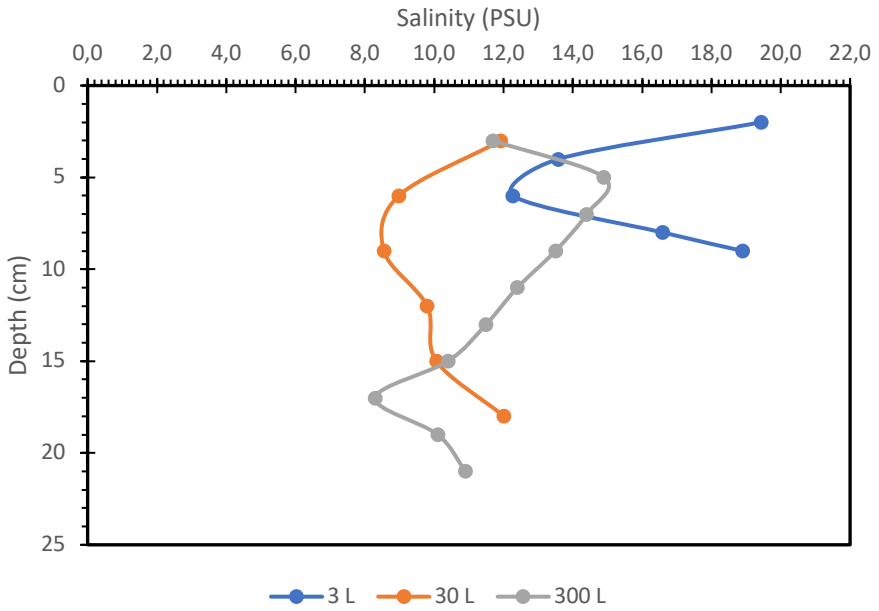


Figure 6.21: Salinity profile for artificial sea ice grown at -20°C and 30 PSU to show the effect of tank size on the growth dynamics of artificial sea ice

Table 6.5: Salinity uptake data for artificial sea ice that was grown at -20°C and 30 PSU to show the effect of varying the tank size

Air temperature (°C)	-20	-20	-20
Starting solution salinity (PSU)	30	30	30
Tank size (L)	**3**	**30**	**300**
Average ice salinity (PSU)	16.2	10.2	11.8
Underlying solution salinity at the end of the experiment (PSU)	43.8	39.5	44.2
Salt mass balance error (%)	8.3	9.4	9.1

Figure 6.21 also shows that there is high brine retention in the 3 L tank. Table 6.5 shows that the 3 L tank has the highest average ice salinity. The underlying solution salinity increases by 13.8 PSU for the 3 L tank.

The results presented in Section 6.1 have shown that at lower air temperatures, the cooling rate of the freezing solution is significantly increased. This is due to the higher driving force that is present at lower air temperatures. Hence, temperature has a significant effect on the growth dynamics of the ice.

Additionally, the results presented in this Section 6.3 have shown that increasing the starting solution salinity results in a decrease in the growth rate of the ice. This is due to the decrease in the temperature difference between the underlying solution and the air. Moreover, it has been shown that the average ice salinity ratio is linearly related to the starting solution salinity. This implies that increasing the starting solution salinity results in an increase in brine inclusions regardless of the growth rate of the ice. However, this relationship requires further investigation and it implies the need to have continuous salinity measurements that can substantiate the argument further.

Lastly, in Section 6.3 it has been shown that, the experimental data for the 300 L tank shows the limitation of the linearised model when there is noise in the data. However, the difference in the temperature with time profiles suggests that changing the tank size affects the steepness of the temperature profiles. The differences cannot be accounted for by the linearised model as it is a one-dimensional model which does not account for tank geometry. The differences are due to external factors which require further exploration.

Chapter 7 : Dynamic model to solving the temperature field for sea ice

7.1 Method of analysis for the dynamic model

The focus of this chapter is to present the results and analysis for solving the temperature field of sea ice from the heat diffusion equation. This is the direct analysis of solving the heat diffusion PDE at unsteady state. This was done by assuming constant thermal properties of the ice. Table 7.1 gives the parameters that were assumed to be constant in the dynamic model. The ratio of $\frac{h}{k}$ was based of the experimental results in Chapter 5.

Table 7.1: Parameters used in the dynamic model

Parameter	Value
Underlying solution temperature (^oC)	-0.5
Ambient temperature (^oC)	-20
Thermal conductivity (W/m.^oC)	1.90
Convective heat transfer coefficient (W/m^2.^oC)	23.0
Density(kg/m^3)	917
Specific heat capacity (kJ/kg)	2.12
Latent heat of fusion (kJ/kg)	330

The simulated temperature field was obtained using the growth conditions for artificial sea ice that was grown at a starting salinity of 10 PSU and constant air temperature of -20^{o}C. The dynamic model was solved using the method of orthogonal collocation and using a DAE solver in Scilab. Orthogonal collocation was used to approximate the spatial direction in discrete quantities. The dynamic model used 7 collocation points and 1 000 time points. The results from the base case simulation are as presented below.

Figure B12 (Appendix B5) shows the normalised position in ice plotted against temperature, where 0 is the normalised position at the surface of the ice (the ice-air interface) and 1 is the normalised position of the ice at the ice-brine interface. The scale on the x axis is between 0 and 1 as the position within the ice was first converted into a dimensionless number using the dimensionless quantity that $x = \frac{z}{L}$, which enabled the problem to be solved in the x coordinate system. However, since ice growth has been shown to occur in the axial (z) direction, the modelled results were thus converted back into the z coordinate system. The results are shown in Figure 7.1. Figure 7.1 exhibits the same trend as in Figure B12 (Appendix B5) Figure 7.1 shows the temperature profile with depth where all the temperature nodes of the position discretisation are within the ice. The only difference is that the position of the ice is now in the z coordinate system. Moreover, Figure 7.1, clearly shows that the ice reaches a depth of 31 cm in a period of 160 hours. The corresponding temperature with time profile for Figure 7.1 is shown in Figure 7.2.

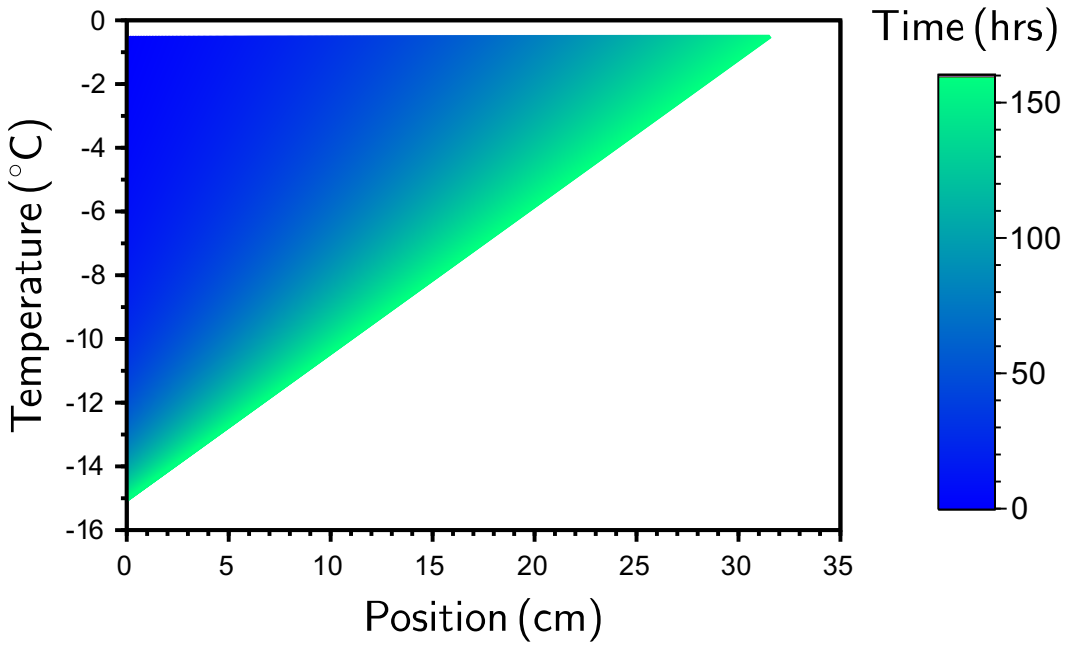


Figure 7.1: Simulated temperature with depth profile for artificial sea ice growing at -20°C where all the temperature nodes are within the ice

Figure 7.2 shows the temperature evolution with time for the modelled experiment. It can be seen from Figure 7.2 that the temperature nodes all diverge from -0.5°C. This is because, it was assumed that there is perfect mixing in the tank and that the freezing solution was at its freezing point. Hence, initially all the temperature nodes were simulated to record the freezing temperature. As such, the temperature nodes start experiencing a temperature drop once they are embedded in the ice. The trend in the temperature profile shows that the temperature decreases non-linearly with time. It is important to note that results presented in Figure 7.2

are for the moving coordinate system in the z direction. As such the modelled data was then inverted into the stationary coordinate system using an interpolating polynomial of the 8th order. The results are shown in Figure 7.3 which shows the modelled temperature evolution with time at constant position.

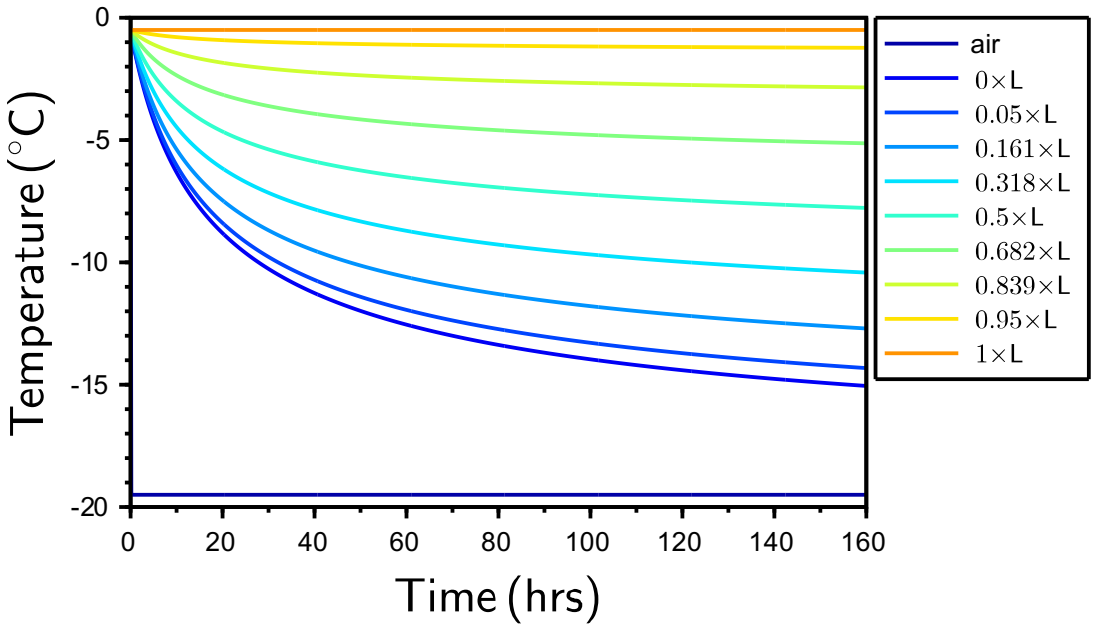


Figure 7.2: Simulated temperature evolution with time for artificial sea ice growing at -20°C where all the nodes are within the growing ice. The nodes are always at the same position relative to the length of ice, L(t)

The trend observed in Figure 7.3 of the simulated temperature evolution with time from the dynamic model is the same as that observed in the experimental data (Chapter 5, Figure 5.1). The corresponding temperature evolution with depth from the dynamic model is shown in Figure 7.4. It is important to note that Figure 7.4 shows the temperature profiles at the same fixed locations within the tank as those that were used in the experimental measurements. Thus, not all the temperature nodes are embedded in the ice. As such Figure 7.4 reflects the true temperature distribution within the modelled tank from the ice surface through to the underlying brine solution.

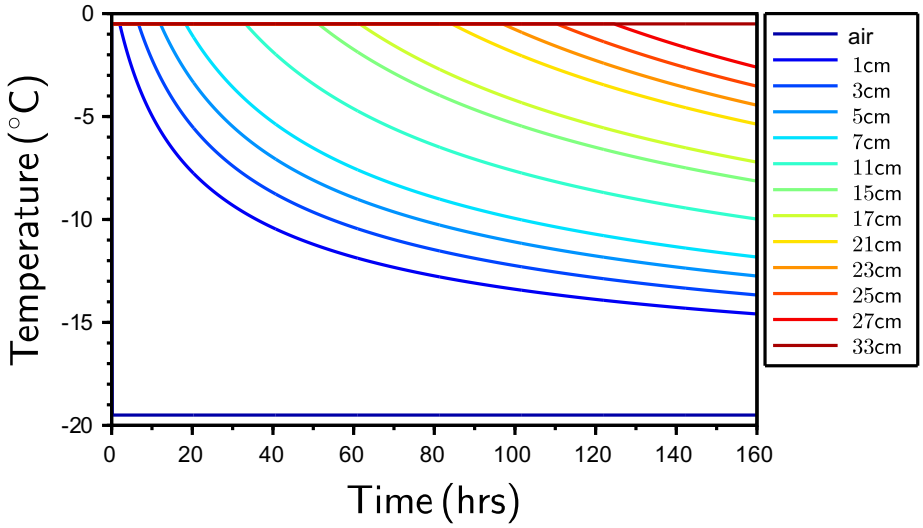


Figure 7.3: Simulated temperature evolution with time for artificial sea ice growing at -20°C where the temperature profiles are reported at the same fixed locations within the tank as were used in the experimental measurements.

Applying the linearised approach to the simulated data in Figure 7.3 yields Figure 7.4. It follows from Figure 7.4 that the dynamic model predicts that a linear temperature profile exists within the ice. The bend that occurs in the simulated experimental data (as shown by the black arrow) reflect temperature measurements in the brine where the ice front has not moved to that location. This is the same phenomenon that was observed in Chapter 5.

.

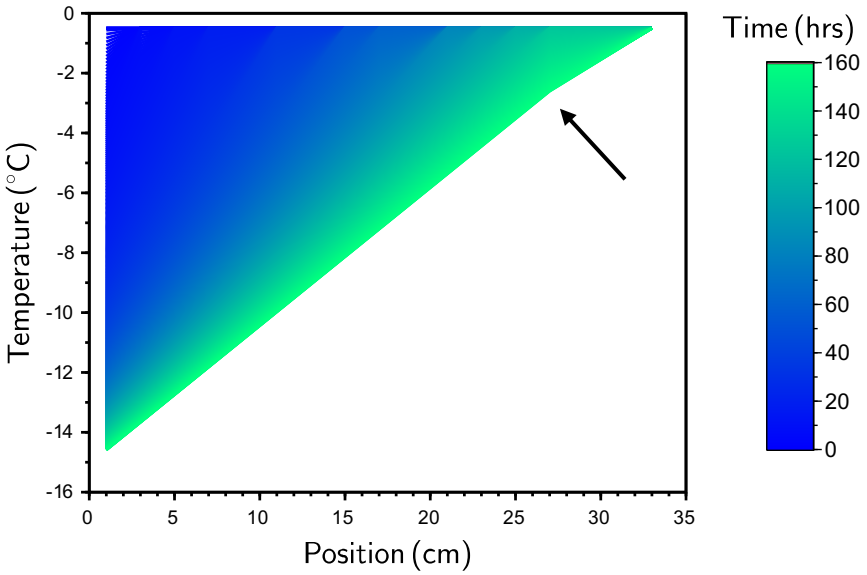


Figure 7.4: Simulated temperature with depth profile for artificial sea ice growing at -20°C where the thermocouples stationary and the growing ice front is moving past them

7.2 Comparison of dynamic model data and experimental data

As both the thermal conductivity and the convective heat transfer coefficient had been estimated, it was imperative to determine the optimum parameter conditions that would result in an overlap in the experimental and modelled data. This was done by varying the ratio of $\frac{h}{k}$.. The best estimate of the convective heat transfer coefficient and the thermal conductivity were found to be to be 20 W/m^2.^{o}C and 2.25 W/m.^{o}C respectively. This corresponds to an $\frac{h}{k}$ ratio of 8.9. This differs from the experimental $\frac{h}{k}$. of 12.1 ± 0.44.

The growth profile was then inferred from the simulated temperature measurements. Figure 7.5 shows the simulated growth profile. It can be noted that the dynamic model predicts the growth profile to follow the same shape as the experimental data. The growth curve from the dynamic model is steeper relative to the growth curve from the experimental data presented in Chapter 5. This means that the dynamic model overestimates the growth rate of the ice.

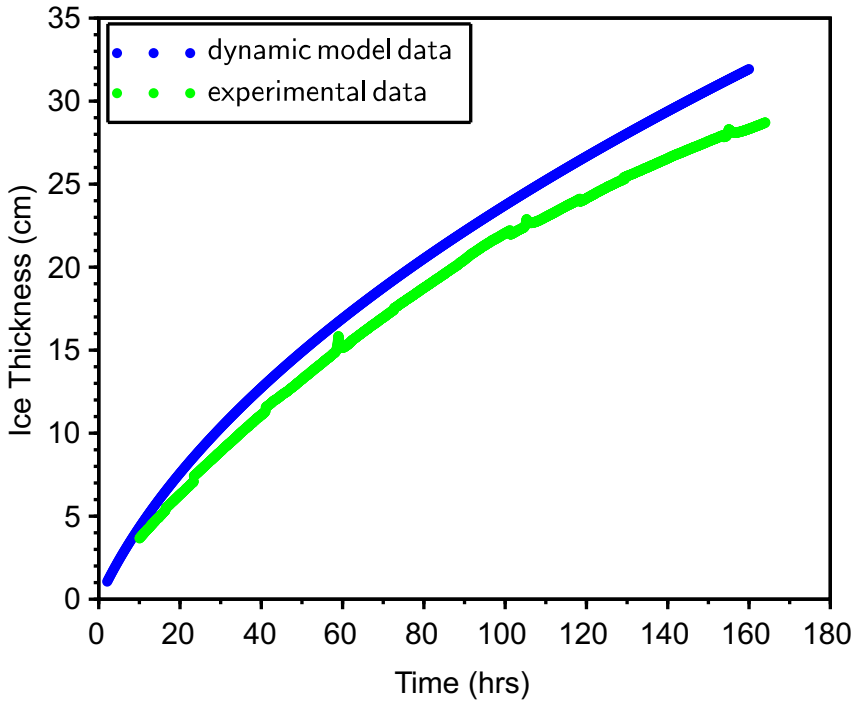


Figure 7.5: Modelled ice growth profile for artificial sea ice that was simulated at -19.5^{o}C at a starting solution salinity of 10 PSU

Figure 7.6 shows the growth rate data which was deduced from the derivative of the growth profile. Figure 7.6 shows that the modelled growth rate from the dynamic model is higher than that from the experimental data. This is due to the higher thermal conductivity. The section in

Figure 7.6 where the growth rate from the dynamic model data is the same as from the experimental data corresponds to the point where the growth profiles are parallel to each other.

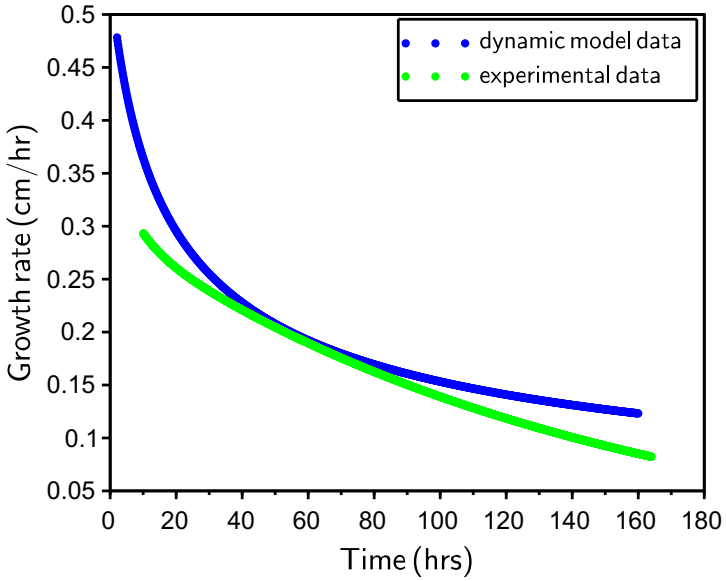


Figure 7.6: Modelled growth rate for artificial sea ice that was simulated at -20°C at a starting solution salinity of 10 PSU.

Figure 7.7 shows the comparison of the optimised modelled temperature data with the experimental data. The average least squares error per time point for between the modelled and experimental temperature data is 0.31°C.

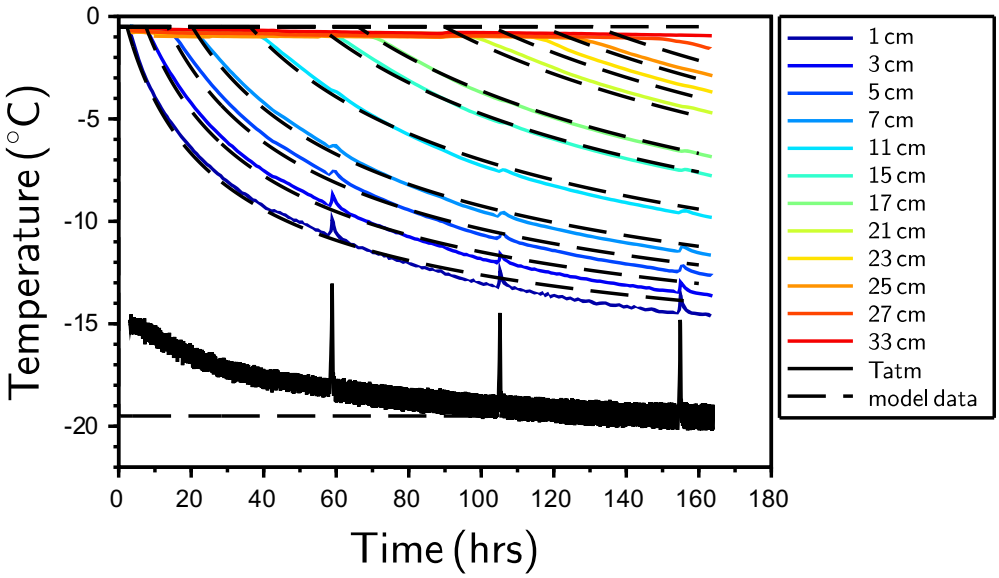


Figure 7.7:Comparison of the modelled vs experimental temperature time profile

7.2.1 Sensitivity analysis of the linearised model in the determination of the thermal conductivity

The dynamic model data was further analysed using the linearised model. This was done exactly the same as with the experimental data presented in Chapter 5. The average instantaneous k and h were individually determined. Figure 7.8 and Figure 7.9 gives a comparison of the average instantaneous k and h that was calculated using the linearised model from the experimental data and the dynamic model data respectively. Figure 7.8 and Figure 7.9 shows that k and h calculated using the simulated dynamic model is approximately constant. This was expected since these were assumed to be constant in the dynamic model. However, the experimental data's output for k and h has fluctuations where k and h gradually decrease with time. This difference highlights the limitations of the linearised model in predicting the average k at that time instant, and h when there is noise in the data.

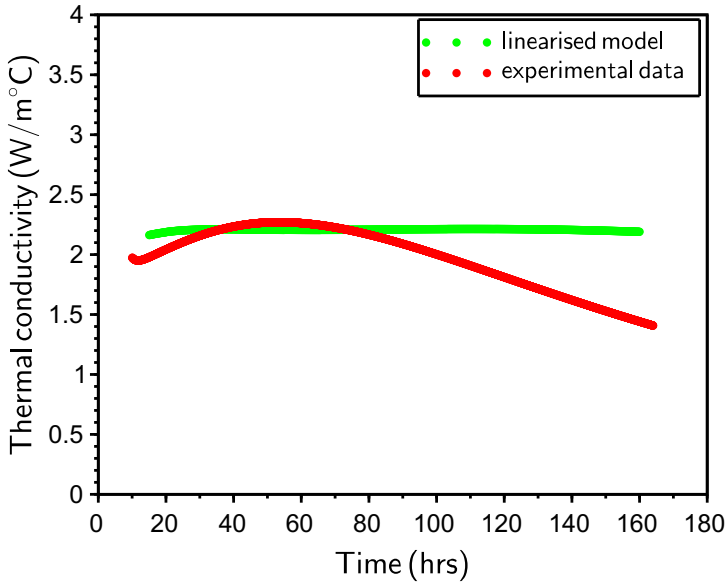


Figure 7.8: Estimation of the average k for the length of ice that has grown by that time from the linearised model using the dynamic model data and the experimental data for artificial sea ice grown at -20°C at 10 PSU

The fluctuations in k and h are not property variations but these are due to the noise in the data. Hence, it is highly improbable that the average instantaneous k values will have such a large range due to physical variation. Moreover, h does not depend on ice properties and is expected to be constant over the duration of the experiment. The temperature oscillations that propagate into the ice distort the growth curves. These oscillations affect the straight-line fitting. Curve fitting of the temperature profiles increases the distortion, whereas for the dynamic model, only L(t) and the growth rate is given directly by the dynamic model. In the

linearised model, k and h require the derivative of the growth rate, and the linearised model takes a differential approach by solving for the growth rate numerically from the noisy data. Hence, the error that is introduced by the noise in the data is amplified (Brenan et al., 1996).

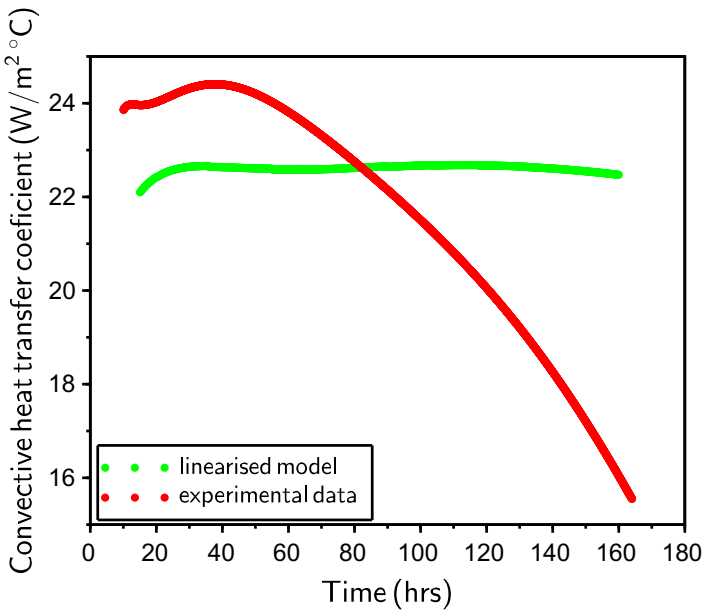


Figure 7.9: Estimation of the average h when the air temperature is at -20°C from the linearised model using the dynamic model data and the experimental data for artificial sea ice grown at 10 PSU

The linearised model can predict the growth rate and growth profiles reliably but to be able to extrapolate the instantaneous k and h from the experimental data, the prediction of k and h requires experimental data with minimum noise. The ratio of $\frac{h}{k}$ from the linearised model is more reliable than the individual determination of the average instantaneous k and h as it is an average ratio across the duration of the experiment. Thus, the linearised model provides a technique of analysing experimental data. It provides robust results when there is no noise in the data.

It therefore follows from the above results that the developed dynamic model solves the temperature distribution within artificial sea ice. The modelled temperature profiles mimic the experimentally determined temperature and growth profiles. However, for the dynamic model to accurately predict the experimental profiles, the input data for k and h has to be known. The linearised approach reliably allows for the determination of $\frac{h}{k}$.

7.3 Effect of varying parameters on the average instantaneous thermal parameters (k and h)

It has been noted that the accuracy of the linearised model in estimating the average instantaneous k is limited by the noise in the experimental data. This section aims to look at the general trend in the behaviour of the system upon variation of k and h.

7.3.1 Effect of varying the starting salinity on the thermal parameters

Figure 7.10 shows the effect of varying the starting solution salinity on the average instantaneous k of artificial sea ice that was grown at -20°C. The observed trend is that the average instantaneous k decreases with an increase in the starting solution salinity.

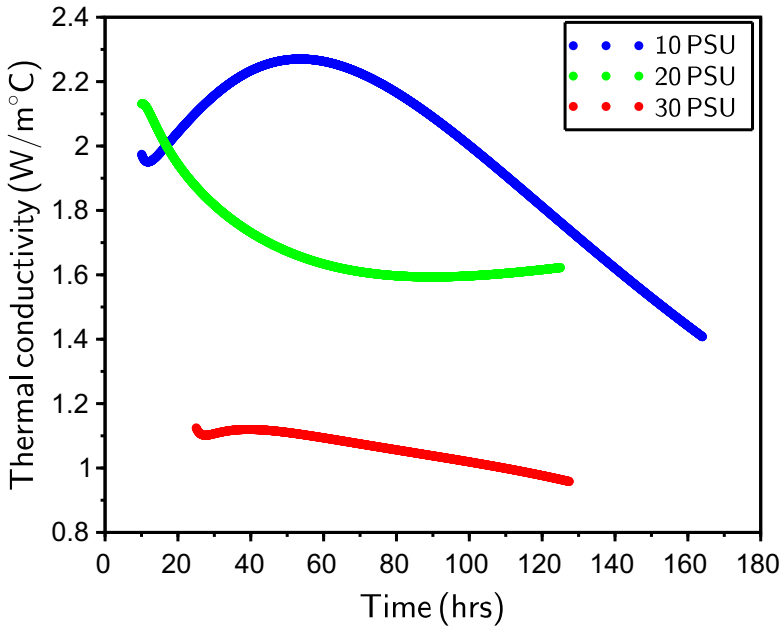


Figure 7.10: Average instantaneous variation of k for artificial sea ice that was grown at -20°C to show the effect of varying the starting solution salinity

Figure 7.11 shows the instantaneous variation of h when the starting solution salinity is varied. The observed trend is that h decreases with an increase in the starting solution salinity. This trend was not expected. The heat transfer coefficient should be the same when varying the starting solution salinity. This is because the air temperature was kept constant when the starting solution salinity was varied. The trend shown in Figure 7.11 is due to the limitation of the linearised model in estimating the average instantaneous thermal conductivity. As such to keep the ratio of $\frac{h}{k}$ constant, when k decreases, h simultaneously decreases.

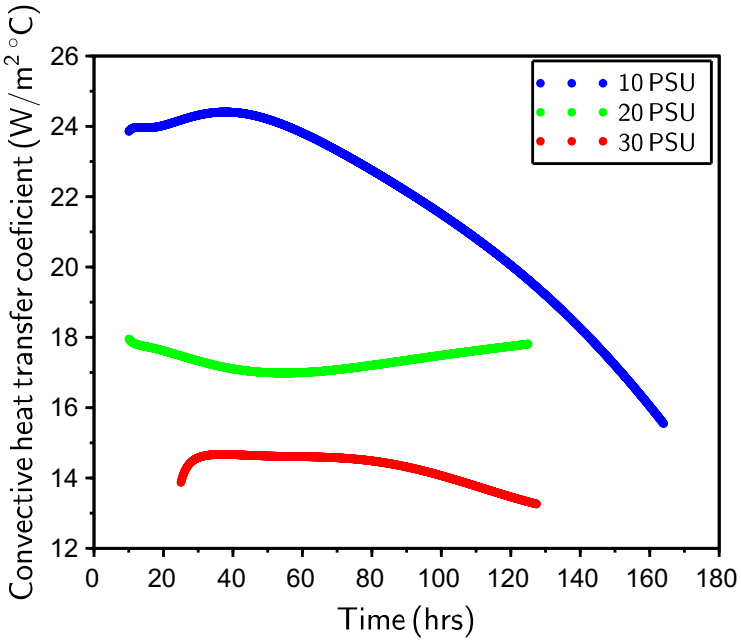


Figure 7.11: Average instantaneous variation of the convective heat transfer coefficient for artificial sea ice that was grown at -20°C to show the effect of varying the starting salinity

7.3.2 Effect of varying the ambient temperature on the thermal parameters

Figure 7.12 shows the effect of varying the ambient temperature on the thermal conductivity of artificial sea ice that was grown at 10 PSU. The observed trend is that the thermal conductivity increases with a decrease in the ambient temperature.

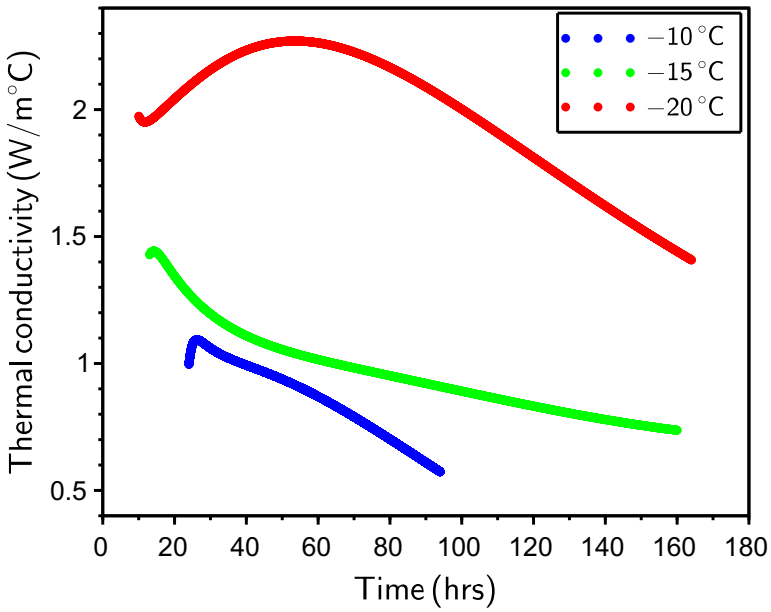


Figure 7.12: Average instantaneous variation of thermal conductivity for artificial sea ice that was grown at 10 PSU to show the effect of varying the ambient temperature

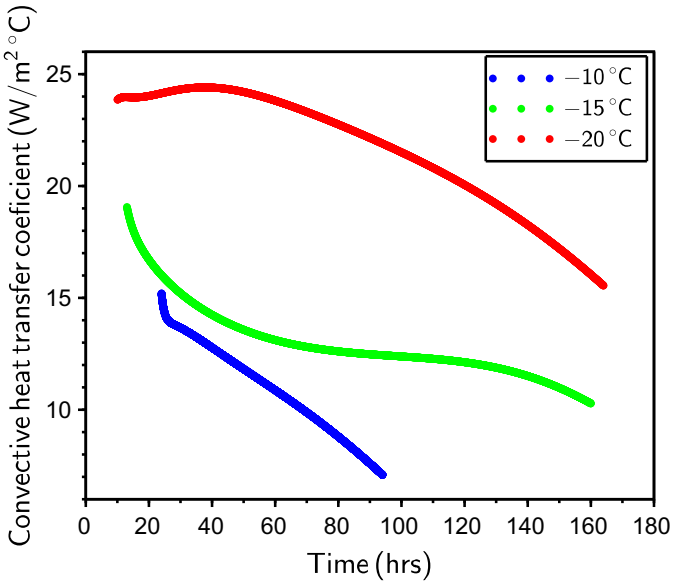


Figure 7.13: Average instantaneous variation of the convective heat transfer coefficient for artificial sea ice that was grown at 10 PSU to show the effect of varying the ambient temperature

Figure 7.13 shows the instantaneous variation of h when the starting solution salinity is varied. The observed trend is that h decreases with an increase in air temperature. The convective heat transfer coefficient was not expected to vary at different air temperatures. The decrease in the average instantaneous k is accompanied a simultaneous change in h.

7.3.3 Summary of trends in average k upon variation of air temperature and starting solution salinity in a 30 L tank

Figure 7.14 shows the variation of the average k across the duration of the experiment for artificial sea ice that was grown at -20°C whilst varying the starting solution salinity. Figure 7.15 shows the variation of the average k for artificial sea ice that was grown at 10 PSU whilst varying the air temperature. Figure 7.14 and Figure 7.15 follows the same trend as Figure 7.10 and Figure 7.12 respectively.

Figure 7.15, shows that the average k is higher at lower temperatures. Figure 7.14 shows that the average k is higher at lower starting solution salinities. Hence, it can be deduced that the average k of artificial sea ice decreases with an increase in starting solution salinity and temperature. The lower the temperature and salinity of the solution is the higher is the average k. Referencing this to Section 6.1 and Section 6.2 shows that the higher the average k, the higher is the growth rate of the ice.

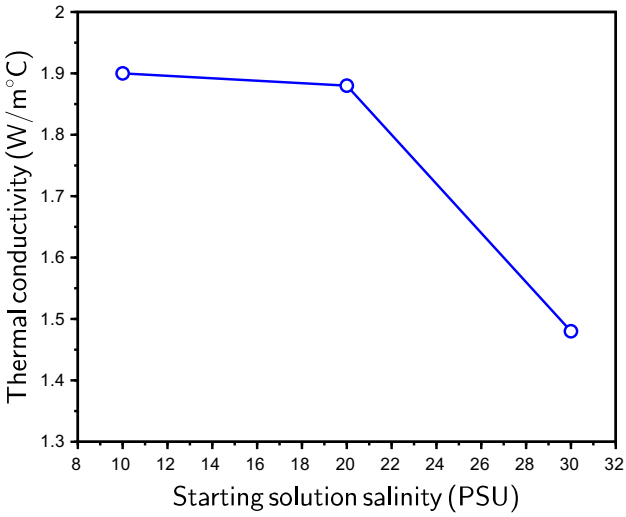


Figure 7.14: Variation of the average thermal conductivity across the duration of the experiment for artificial sea ice that was grown at -20°C in a 30 L tank but at varied starting solution salinities

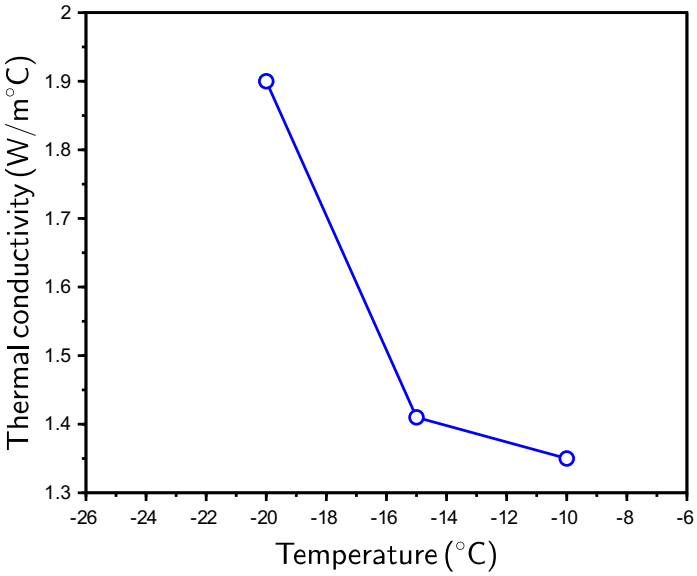


Figure 7.15: Variation of the average thermal conductivity across the duration of the experiment for artificial sea ice that was grown at 10 PSU in a 30 L tank but at varied temperatures

Lastly, the results presented in Chapter 7 show that the using the model parameters obtained from the linearised model, a 1-D model variable boundary constant parameter dynamic model is able to predict the dynamic growth of ice, within a least squares error of 0.31°C. The accuracy of the linearised model in predicting the average instantaneous k is dependent on the quality of the data.

Chapter 8 : Conclusions and Recommendation

8.1 Conclusions

The following conclusions can be deduced from this work:

1. Heat transfer through artificial sea ice grown at constant air temperatures can be assumed to be at pseudo steady state due to the presence of linear temperature profiles with depth. As such the average thermal conductivity, ice surface temperature and heat linearly conducted through the ice can be computed through regression of experimental temperature output data. Regression is performed at each measured time point.
2. The surface temperature of the ice differs from the air temperature and the underlying solution temperature. This means that even in the absence of snow cover, it is not accurate to assume that the surface temperature is the same as the air temperature as has been done. This is due to the presence of the air film resistance to convective heat transfer.
3. The air temperature is the primary driving force for heat transfer in saline ice. The lower the air temperature, the faster is the growth rate of the ice and the more the brine is trapped between the ice.
4. An increase in salinity decreases the growth rate of ice due to the decrease in the freezing point of the solution.
5. The higher the growth rate of the ice, the more the salt that is trapped in the ice.
6. The higher the salt content trapped in the ice, the lower is the thermal conductivity.
7. Thermal conductivity of artificial sea ice grown at constant air temperature decreases with an increase in starting solution salinity. Moreover, it also decreases when the air temperature is varied.
8. The thermal conductivity is a function of both temperature and starting solution salinity.
9. At pseudo steady state, the growth rate of the ice is directly proportional to the conductive heat flux. This is possible by assuming that the heat of crystallisation of the ice is constant.
10. Using the model parameters obtained from the linearised model, a 1-D model variable boundary constant parameter dynamic model is able to predict the dynamic growth of ice. The accuracy of the linearised model in predicting the instantaneous thermal conductivity and heat transfer coefficient of artificial sea ice is dependent on the quality of the temperature input data. When there is no noise in the data, the accuracy of the linearised model in predicting the thermal parameters is improved.

8.2 Recommendations

The following recommendations can be implemented to further improve the work done in this project. These include:

1. Optimisation of the dynamic model so that it uses the actual air and brine temperature as input parameters. Moreover, to perform more experiments as input for the dynamic model so that the model can be extended to accurately predict the thermal conductivity of natural sea ice
2. Quantification of heat loss through the walls
3. Quantification of the effect of seed crystals
4. Building a new laboratory where there are NO oscillations
5. Study the effect of tank geometry but keeping the volume constant or adjusting the volume of the tank but keep the depth the same
6. Using non-destructive methods of measuring the salinity of the ice
7. Introduction of a thermal source into the laboratory to simulate the conditions of night and day

References

Allison, I. 1981. Antarctic sea ice growth and oceanic heat flux. *Sea level, ice and climatic change*. 131:161–170.

Anderson, D.L. 1961. Growth rate of sea ice. *Journal of Glaciology*. 3(30):1170–1172.

Ashton, G.D. 1989. Thin ice growth. *Water Resources Research*, 25(3):564–566.

Assur, A. 1960. Composition of Sea Ice and its Tensile Strength. *SIPRE Research Report*. 44:54.

Brenan, K.E., Campbell, S.L. and Petzold, L.R., 1996. Numerical Solution of Initial-value Problems in Differential-algebraic Equations (Vol. 14). SIAM.

Butler, B.M., Papadimitriou, S., Santoro, A. & Kennedy, H. 2016. Mirabilite solubility in equilibrium sea ice brines. *Geochimica et Cosmochimica Acta*. 182:40–54. DOI: 10.1016/j.gca.2016.03.008.

Cottier, F., Eicken, H. & Wadhams, P. 1999. Linkages between salinity and brine channel distribution in young sea ice. *Polar Research*. 104:859–871.

Cox, G.F.N. & Weeks, W.F. 1975. Brine Drainage and Initial Salt Entrapment in Sodium Chloride Ice. *US Army Corps Eng Cold Reg Res Eng Lab Res Rep*. (345).

Curry, J.A., Schramm, J.L. & Ebert, E.E. 1995. Sea ice-albedo climate feedback mechanism. *Journal of Climate*. 8(2):240–247.

Doble, M.J., Coon, M.D. & Wadhams, P. 2003. Pancake ice formation in the Weddell Sea. *Journal of Geophysical Research C: Oceans*. 108(7):2–1. DOI: 10.1029/2002jc001373.

Eicken, H. 1992. Salinity Profiles of Antarctic Sea Ice: Field Data and Model Results. *Geophysical Research*. 97(92).

Eicken, H. & Lange, M.A. 1989. Development and properties of sea ice in the coastal regime of the southeastern Weddell Sea. 94:8193–8206.

Feltham, D.L., Untersteiner, N., Wettlaufer, J.S. & Worster, M.G. 2006. Sea ice is a mushy layer. *Geophysical Research Letters*. 33(14):4–7. DOI: 10.1029/2006GL026290.

Fransson, L. 2009. Ice Handbook for Engineers. 31. Available: http://static1.1.sqspcdn.com/static/f/572109/15210238/1321785520853/ice_handbook_2009-1.pdf?token=a21YScBT45KpmE0TXGlpLToBNBA=.

Freitag, J. 1999. The hydraulic properties of arctic sea-ice: implications for the small scale particle transport. *Reports on polar research*. 325.

Gough, A.J., Mahoney, A.R., Langhorne, P.J., Williams, M.J.. . & Haskell, T.G. 2012. Sea ice salinity and structure: A winter time series of salinity and its distribution.pdf. *Journal of Geophysical Research*.

Gow, A.J., Ackley, S.F., Buck, K.R. & Golden, K.M. 1987. CRREL Report 87-14. (August).

Haas, C. 1999. Ice tank investigations of the microstructure of artificial sea ice grown under different boundary conditions during INTERICE II.

Hall, B.A., 2021. *Design of a Small-Scale System for the Growth of Artificial Sea Ice* (Master's thesis, Faculty of Engineering and the Built Environment).

Hunke, E.C., Notz, D., Turner, A.K. & Vancoppenolle, M. 2011. The multiphase physics of sea ice: A review for model developers. *Cryosphere*. 5(4):989–1009. DOI: 10.5194/tc-5-989-2011.

IPCC. 2019. *Special Report on the Ocean and Cryosphere in a Changing Climate —*.

Kawano, Y. & Ohashi, T. 2009. A mesoscopic numerical study of sea ice crystal growth and texture development. *Cold Regions Science and Technology*. DOI: 10.1016/j.coldregions.2009.02.001.

Lepparanta, M. 1993. A review of analytical models of sea-ice growth. *Atmosphere - Ocean*. DOI: 10.1080/07055900.1993.9649465.

Light, B., Maykut, G.A. & Grenfell, T.C. 2003. Effects of temperature on the microstructure of first-year Arctic sea ice. *Journal of Geophysical Research: Oceans*. 108(2):1–16. DOI: 10.1029/2001jc000887.

Løset, S., Shkhinek, K.N., Gudmestad, O.T. & Høyland, K. V. 2006. *Actions from ice on Arctic offshore and coastal structures*. St. Petersburg, Moscow, Krasnodar.

Marks, A.A., Lamare, M.L. & King, M.D. 2017. Optical properties of sea ice doped with black carbon -An experimental and radiative-Transfer modelling comparison. *Cryosphere*. 11(6):2867–2881. DOI: 10.5194/tc-11-2867-2017.

Maykut, G.A. 1985b. An Introduction to Ice in the Polar Oceans.

Maykut, G.A., Grenfell, T.C. & Weeks, W.F. 1992. On estimating spatial and temporal variations in the properties of ice in the polar oceans. *Journal of Marine Systems*. 3:41–72. DOI: 10.1016/0924-7963(92)90030-C.

Maykut, G. A. & Untersteiner, N. 1971. Some results from a time-dependent thermodynamic model of sea ice. Journal of Geophysical Research, 76(6):1550–1575.

McPhee, M.G. & Untersteiner, N. 1982. Using Sea Ice To Measure Vertical Heat Flux in the Ocean. *Journal of Geophysical Research*. 87(C3):2071–2074. DOI: 10.1029/JC087iC03p02071.

Middleton, C.A., Thomas, C., De Wit, A. & Tison, J.L. 2016. Visualizing brine channel development and convective processes during artificial sea-ice growth using Schlieren optical methods. *Journal of Glaciology*. 62(231):1–17. DOI: 10.1017/jog.2015.1.

Mukaromah, A.H., Kadja, G.T.M., Mukti, R.R., Pratama, I.R., Zulfikar, M.A. & Buchari. 2016. Surface-to-volume ratio of synthesis tank vessel governing low temperature crystallization of ZSM-5. *Journal of Mathematical and Fundamental Sciences*. 48(3):241–251. DOI: 10.5614/j.math.fund.sci.2016.48.3.5.

Naumann, A.K., Notz, D., Håvik, L. & Sirevaag, A. 2012. Laboratory study of initial sea-ice growth: properties of grease ice and nilas. *The Cryosphere*. 6(4):729–741.

Neufeld, J.A. & Wettlaufer, J.S. 2008. Shear-enhanced convection in a mushy layer. *Journal of Fluid Mechanics*. 612(2008):339–361. DOI: 10.1017/S0022112008002991.

Nomura, D., Yoshikawa-Inoue, H. & Toyota, T. 2006. The effect of sea-ice growth on air-sea CO2 flux in a tank experiment. *Tellus, Series B: Chemical and Physical Meteorology*. 58(5):418–426. DOI: 10.1111/j.1600-0889.2006.00204.x.

Notz, D. 2005. Thermodynamic and fluid-dynamical processes in sea ice. *University of Cambridge*. (May):238.

Notz, D. & Grae Worster, M. 2008. In situ measurements of the evolution of young sea ice. *Journal of Geophysical Research: Oceans*. 113(3). DOI: 10.1029/2007JC004333.

De Paoli, M., Alipour, M. & Soldati, A. 2020. How non-Darcy effects influence scaling laws in Hele-Shaw convection experiments. *Journal of Fluid Mechanics*. DOI: 10.1017/jfm.2020.229.

Peppin, S.S.L., Aussillous, P., Huppert, H.E. & Worster, M.G. 2007. Steady-state mushy layers: Experiments and theory. *Journal of Fluid Mechanics*. 570(2007):69–77. DOI: 10.1017/S0022112006003028.

Perovich, D.K. & Grenfell, T.C. 1981. Laboratory Studies of the Optical Properties of Young Sea Ice. *Journal of Glaciology*. 27(96):331–346. DOI: DOI: 10.3189/S0022143000015410.

Petrich, C. & Eicken, H. 2017. Overview of sea ice growth and properties. In *Sea Ice*. Third ed. D.N. Thomas, Ed. Chichester, UK: John Wiley & Sons, Ltd. 1–37. DOI: 10.1002/9781118778371.

Randall, D.G., Nathoo, J. & Lewis, A.E. 2009. Seeding for selective salt recovery during eutectic freeze crystallization. In *International Mine Water Conference*. 19–22.

Rinke, A., Maslowski, W., Dethloff, K. & Clement, J. 2006. Influence of sea ice on the atmosphere: A study with an Arctic atmospheric regional climate model. *Journal of Geophysical Research Atmospheres*. DOI: 10.1029/2005JD006957.

Roscoe, H.K., Brooks, B., Jackson, A. V, Smith, M.H., Walker, S.J., Obbard, R.W. & Wolff, E.W. 2011. Frost flowers in the laboratory: Growth, characteristics, aerosol, and the underlying sea ice. *Journal of Geophysical Research: Atmospheres*. 116(D12).

Rozmanov, D. & Kusalik, P.G. 2011. Temperature dependence of crystal growth of hexagonal ice (I h). *Physical Chemistry Chemical Physics*. 13(34):15501–15511. DOI: 10.1039/c1cp21210a.

Schulson, E.M., Renshaw, C.E. & Snyder, S.A. 2015. Effect of Deformation Damage on the Mechanical Behavior of Sea Ice : Ductile-Brittle Transition , Elastic Modulus and Brittle Compressive Strength. (July).

Schulze, T.P. & Worster, M.G. 2005. A time-dependent formulation of the mushy-zone free-boundary problem. *Journal of Fluid Mechanics*. 541:193–202. DOI: 10.1017/S0022112005006221.

Schwarz, J. & Weeks, W.F. 1977. Engineering Properties of Sea Ice. *Journal of Glaciology*. 19(81):499–531. DOI: DOI: 10.3189/S0022143000029476.

Schwerdtfeger, P. 1963. The Thermal Properties of Sea Ice. *Journal of Glaciology*. DOI: 10.3189/s0022143000028379.

Semtner Jr, A.J. 1976. A model for the thermodynamic growth of sea ice in numerical

investigations of climate. *Journal of Physical Oceanography*. 6(3):379–389.

Talley, L.D. 2002. Salinity Patterns in the Ocean. *Encyclopedia of Global Environmental Change*. 1(1):1–11.

Tervola, P. 1989. A method to determine the thermal conductivity from measured temperature profiles. *International Journal of Heat and Mass Transfer*. 32(8):1425–1430. DOI: 10.1016/0017-9310(89)90066-5.

Texas Instruments. 2019. The Engineer's Guide to Temperature Sensing. *Technical Report*.

Thomas, D.N. & Dieckmann, G.S. 2010. *Sea ice*. V. 4.

Thorndike, A.S. 1992. Estimates of sea ice thickness distribution using observations and theory. *Journal of Geophysical Research: Oceans*. 97(C8):12601–12605.

Trodahl, H., Wilkinson, S., Mcguinness, M. & Haskell, T. 2001. Thermal conductivity of sea ice; Dependence on temperature and depth. *Geophysical Research Letters - GEOPHYS RES LETT*. 28:1279–1282. DOI: 10.1029/2000GL012088.

Trodahl, H.J., McGuinness, M.J., Langhorne, P.J., Collins, K., Pantoja, A.E., Smith, I.J. & Haskell, T.G. 2000. Heat transport in McMurdo Sound first-year fast ice. *Journal of Geophysical Research: Oceans*. 105(C5):11347–11358.

Tucker III, W.B., Gow, A.J. & Weeks, W.F. 1987. Physical properties of summer sea ice in the Fram Strait. *Journal of Geophysical Research: Oceans*. 92(C7):6787–6803.

Vancoppenolle, M., Fichefet, T. & Goosse, H. 2009. Simulating the mass balance and salinity of Arctic and Antarctic sea ice. 2. Importance of sea ice salinity variations. *Ocean Modelling*. 27(1–2):54–69. DOI: 10.1016/j.ocemod.2008.11.003.

Wadhams, P. 2000. *Ice in the Ocean*.

Weeks, W.F. 1962. Tensile Strength of NaCl Ice. *Journal of Glaciology*. 4(31):25–52. DOI: 10.3189/s0022143000018190.

Weeks & Ackely. 1982. The growth, structure and properties of sea ice.

Weeks, W.. & Ackley, S.. 1982. *The growth, structure, and properties of sea ice*. Hanover, New Hampshire.

Weeks, W. & Hibler, W.D. 2010. *On sea ice*. University of Alaska Press

Weeks, W.F. & Ackley, S.F. 1986. The growth, structure, and properties of sea ice. In *The geophysics of sea ice*. Springer. 9–164.

Weeks, W.F. & Assur, A. 1967. The Mechanical Properties of Sea Ice. *Cold Regions Research & Engineering Laboratory*. (September):96.

Weeks, W.F. & Cox, G.F.N. 1974. Laboratory preparation of artificial sea and salt ice. *Technical Report, Hanover,N.H.*

Weissenberger, J., Dieckmann, G., Gradinger, R. & Spindler, M. 1992. Sea ice: A cast technique to examine and analyze brine pockets and channel structure. *Limnology and Oceanography*. 37(1):179–183. DOI: 10.4319/lo.1992.37.1.0179.

Wettlaufer, J.S., Worster, M.G. & Huppert, H.E. 1997. Natural convection during solidification of an alloy from above with application to the evolution of sea ice. *Journal of Fluid Mechanics*. 344:291–316. DOI: 10.1017/S0022112097006022.

Wiese, M. 2012. Laboratory experiments on the thermodynamics of melting sea ice. (September):72.

Wiese, M., Griewank, P. & Notz, D. 2015. On the thermodynamics of melting sea ice versus melting freshwater ice. *Annals of Glaciology*. 56(69):191–199.

Worster, M.G. 1996. *Convection in Mushy Layers*.

Worster, M.G. & Jones, D.W.R. 2015. Sea-ice thermodynamics and brine drainage. *Philosophical Transactions of the Royal Society A: Mathematical, Physical and Engineering Sciences*. 373(2045). DOI: 10.1098/rsta.2014.0166.

Yang, C.Y. 1999. Estimation of the temperature-dependent thermal conductivity in inverse heat conduction problems. *Applied Mathematical Modelling*. 23(6):469–478. DOI: 10.1016/S0307-904X(98)10093-8.

Yen, Y.-C. 1981. *Review of thermal properties of snow, ice, and sea ice*. V. 81. US Army, Corps of Engineers, Cold Regions Research and Engineering Laboratory.

Appendices

Appendix A: Scilab CODES

A1: Code for proof-of-concept analysis

```
clear;clc()
disp("reading data")
Ta=readxls('2010 proof.xls');
disp("data read")

//raw data
//read the ALL t data first for analysis
c=5;f=3941   //the excel data block data ranges
t=Ta(1)(c:f,2);  //read all the data
tskip=3 //skip first 3 hours, the initial stabilisaing zone, clearly visible
nskip=find(t>tskip,1)  //the t value is entered here
c=5+nskip-1
t=Ta(1)(c:f,2);  //the stable T,t data can now be read
n=length(t)
T1atm=Ta(1)(c:f,21);
T1=Ta(1)(c:f,13);
T3=Ta(1)(c:f,14)-0.1;  //minor correction probably not needed
T5=Ta(1)(c:f,15);
T7=Ta(1)(c:f,16)-0.6;  //major correction this is an obvious error and is needed
T11=Ta(1)(c:f,18);
T15=Ta(1)(c:f,3);
T17=Ta(1)(c:f,4);
T21=Ta(1)(c:f,7);
T23=Ta(1)(c:f,8);
T25=Ta(1)(c:f,9);
T27=Ta(1)(c:f,11);
T33=Ta(1)(c:f,19);

//assign the matrices for analysis and plotting
T=[T1 T3 T5 T7 T11 T15 T17 T21 T23 T25 T27 T33]
z=[1,3,5,7,11,15,17,21,23,25,27,33]';

// plotting the temperature time smoothed data for tank 1
ff=scf(1);clf
ff.figure_size=[600 500]
drawlater()

ga=gca()
ga.thickness=2
ga.font_size=3
cmap=jetcolormap(13)
plot(t,T,"color",cmap)
plot(t,T1atm,"blk")
xlabel('$\Large\mathsf{Time\,(hrs)}$',"fontsize",4)
ylabel('$\Large\mathsf{Temperature\,(^\circ C)}$',"fontsize",4)
legend1=['$\mathsf{1\,cm}$';'$\mathsf{3\,cm}$';'$\mathsf{5\,cm}$';'$\mathsf{7\,cm}$';'$\mathsf{11\,cm}$';'$\mathsf{15\,cm}$';'$\mathsf{17\,cm}$';'$\mathsf{21\,cm}$';'$\mathsf{23\,cm}$';'$\mathsf{25\,cm}$';'$\mathsf{27\,cm}$';'$\mathsf{33\,cm}$';'$\mathsf{Tatm}$']
legend(legend1,-1)
drawnow()

//plotting the temperature depth smoothed data for tank 1
ff=scf(2);clf
ff.figure_size=[700 600]
ga=gca()
ga.thickness=2
ga.font_size=3.5
```

```
ga.data_bounds = [0,-16;35,0]
drawlater()
nn=1:1:n
gcf().color_map = jetcolormap(length(nn))
cmap=jetcolormap(length(nn))
//plot(z, T(nn,:)',"color",cmap)  //plot2D much faster
plot2d(z,T(nn,:)',axesflag=1)
xlabel('$\Large\mathsf{Position\,(cm)}$',"fontsize",3.5)
ylabel('$\Large\mathsf{Temperature\,(^\circ C)}$',"fontsize",3.5)
//xstring(20,-14,"A")
colorbar(t(1),t($))
gce().title.text='$\Large\mathsf{Time\,(hrs)}$'//"Time (hrs)"
gce().title.font_size = 3.5
gce().font_size = 3.5
drawnow()

//tstart and Tice must be carefully choose to avoid NaN output
//Its easiest to set Tice and then estimate valid tstart from the
//output of
tstart=10
nstart=find(t>tstart,1)  //the t value is entered here
Tice=-1.2

//linear regression of the T vs x data at each t point between nstart and n
//using a skip factor as needed (here it is 1)
k=nstart:1:n
kk=length(k)
err=[]
for j=1:kk
   A=[]
   b=[]
   for i=1:length(z)-1
      if T(k(j),i)<Tice then
         A=[A;1 z(i)]
         b=[b;T(k(j),i)]// b values aare the actual measured values
      end
   end
   x=A\b// A*x gives the predicted values
   bpredict=A*x
   err=[err;b-bpredict]
   MX(j)=correl(b,bpredict)
   Tss(j)=x(1)  //this is a
   bss(j)=x(2)// this is b (the gradient from regression)
   alpha(j)=(T1atm(k(j))-x(1))/(x(1)-T33(k(j)))  //T39 is TL
   L(j)=(T33(k(j))-x(1))/x(2) // growth of ice/length of ice
   thermalcond(j)=0.003*(alpha(j)*L(j))
end
err2=(err'*err)/length(err)//average error of all regression lines, error in the measured temperature
err2=sqrt(err2)//uncertainity in the regression points
disp(err2)
//disp([t(k) Tss alpha L bss thermalcond Q])
check=find(L==%inf)
if check<>[] thenplot
   disp("%inf in output, set tstart >= "+string(t(k(check($)+1))))
   abort
end

kx=nstart:300:n
kxx=kx-nstart+1
//add straight lines to T vs z plot
plot([zeros(length(kx),1) L(kxx)]', [Tss(kxx) T33(kx)]',"-blk")
ff=scf(12);clf// plot of ice growth with time
ff.figure_size=[600 600]
ga=gca()
ga.thickness=2
ga.font_size=4
```

```
plot(t(k),MX,"-blue")
xlabel("Time (hrs)","fontsize",4)
ylabel("Correlation coeficient","fontsize",4)

ff=scf(3);clf// plot of ice growth with time
ff.figure_size=[600 600]
ga=gca()
ga.thickness=2
ga.font_size=4
plot(t(k),L,".blue")
xlabel("Time (hrs)","fontsize",4)
ylabel("Ice Thickness (cm)","fontsize",4)

//fit equation to growth curve and predict dL/dt curve
ttx=t(k)
Ltx=L
//stage 1, linear regression
a1=0.6;a2=10
A=[ones(length(ttx),1)  ttx/ttx($) exp(-a1*ttx/ttx($)) exp(-a2*ttx/ttx($))]
x=A\Ltx
Ltt=A*x
A=[ones(length(ttx),1)/ttx($) -a1/ttx($)*exp(-a1*ttx/ttx($)) -a2/ttx($)*exp(-a2*ttx/ttx($)) ]
dLdtt=A*x(2:$)

//stage 2 non-linear regression
function f=modelx(x)
   f=x(1)+x(6)*ttx/ttx($) + x(2)*exp(-x(3)*ttx/ttx($)) + x(4)*exp(-x(5)*ttx/ttx($))
endfunction
function f=modeldx(x)
   f=x(6)/ttx($) - x(2)*x(3)/ttx($)*exp(-x(3)*ttx/ttx($)) - x(4)*x(5)/ttx($)*exp(-x(5)*ttx/ttx($))
endfunction
function f=fitx(x, m)
   f=modelx(x)-Ltx
endfunction
x0=[x(1) x(3) a1 x(3) a2 x(2)]'
[x ferr info]=lsqrsolve(x0,fitx,length(ttx))
Ltx=modelx(x)
dLdtx=modeldx(x)
plot(ttx,Ltx,"--red")
legend("data","exponential regressed",4)

ff=scf(7);clf// plot of the growth rate
ff.figure_size=[600 600]
ga=gca()
ga.thickness=2
ga.font_size=4
plot(t(k),dLdtx,".blue")
plot(ttx,dLdtt,"--red")
xlabel('$\Large\mathsf{Time\,(hrs)}$',"fontsize",3.5)
ylabel('$\Large\mathsf{Growth\,rate\,(cm/hr)}$',"fontsize",3.5)

rho=917
Hc=330000
Q=(rho*Hc*dLdtx)/360000

ff=scf(8);clf
ff.figure_size=[600 600]
ga=gca()
ga.thickness=2
ga.font_size=4
A=[ones(kk,1) t(k) exp(-(0.1*t(k))/t($)) exp(-(1*t(k)/t($)))  exp(-(10*t(k)/t($))) exp(-(100*t(k)/t($))) ]
b=Tss
x=A\b
Tssm=A*x
A=[ones(kk,1) t(k) exp(-(t(k))/t($)) exp(-(5*t(k)/t($)))  exp(-(20*t(k)/t($)))]
b=T1atm(k)
```

```
x=A\b
T1atmm(k)=A*x
A=[ones(kk,1) t(k) t(k).^2 t(k)]
b=T33(k)
x=A\b
T33m(k)=A*x
h=-(Q./(T1atmm(k)-Tssm))
h1=-(Q./(Area*(T1atm(k)-Tss)))
A=[ones(kk,1) t(k) t(k).^2 t(k).^3]
b=L/100
x=A\b
Lm=A*x
kc=-(Q.*Ltx./(Tssm-T33m(k)))/100

plot(t(k),kc, ".blue")
xlabel('$\Large\mathsf{Time\,(hrs)}$',"fontsize",3.5)
ylabel('$\Large\mathsf{Thermal\,conductivity\,(W/m^\circ C)}$',"fontsize",3.5)

ff=scf(9);clf
ff.figure_size=[600 600]
ga=gca()
ga.thickness=2
ga.font_size=4
plot(t(k),h,".blue")// no fitting of curves
xlabel('$\Large\mathsf{Time\,(hrs)}$',"fontsize",3.5)
ylabel('$\Large\mathsf{Convective\,heat\,transfer\,coeeficient\,(W/m^2^\circ C)}$',"fontsize",2)

ff=scf(4);clf//plot for the extrapolation of the thermal conductivity
ff.figure_size=[600 600]
ga=gca()
ga.thickness=2
ga.font_size=4
plot(L,(1)./alpha,".")
ylabel("$\mathsf{\dfrac{1}{\alpha}}$","fontsize",5)
gca().y_label.font_angle = 0
xlabel("Ice Thickness (cm)","fontsize",4)
A=[ones(kk,1) L]
ATA=A'*A
b=(1)./alpha
x=A\b//experimental coeeficients
ypredict=A*x
r=b-ypredict// starting variance calculation
invATA=ATA\eye(2,2)
sigma=diag(sqrt((r'*r/length(b))*invATA))// calculating the variance
disp(real(sigma))
LL=linspace(0,L($)+1,10)'
A=[ones(10,1) LL]
y=A*x//predicted
plot(LL,y,"-")

ff=scf(5);clf// plot of surface, air and water temperature
ff.figure_size=[600 600]
ga=gca()
ga.thickness=2
ga.font_size=4
plot(t(k),Tss,".blue")
plot(t(k),T33(k),".red")
plot(t(k),T1atm(k),".green")
plot(t(k),T33m(k),"-blk")
plot(t(k),Tssm,"-blk")
plot(t(k),T1atmm(k),"-blk")
xlabel('$\Large\mathsf{Time\,(hrs)}$',"fontsize",4)
ylabel('$\Large\mathsf{Temperature\,(^\circ C)}$',"fontsize",4)
legend("ice surface","brine","air","smooth fit",[90,-2])

ff=scf(6);clf// plot for the instantaneous heat duty
```

```
ff.figure_size=[600 600]
ga=gca()
ga.thickness=2
ga.font_size=4
plot(t(k),Q,".blue")
xlabel('$\Large\mathsf{Time\,(hrs)}$',"fontsize",3.5)
ylabel('$\Large\mathsf{Conductive\,heat\,flux\,(W/m^2)}$',"fontsize",3.5)
```

A2: Code for the dynamic model of solving for the temperature field

```
//Given Data
h=23  // W/m2.K heat transfer coefficient assumed value from Hall pg43
    //h = 12.12-1.16*v+11.6*v^0.5, v(m/s) h(w/m2.K), engineering toolbox
Ta=-20  // degrees celcius
Tb=-0.5   // degrees celcius brine temperature determined from temperature probe
Ts=-15  //Will change
k=2.25  //W/m.K thermal conductivity, 2.22 is fir pure ice
ro=917    //kg/m3 density, pure ice
Cp=2108   //J/kg.C heat capacity, pure ice
alpha=k/(ro*Cp)
//L    length changes with time
Hc=330000   // J/kg, pure ice

//loading collocation libraries
exec('.\collocation\colloc.sci');
exec('.\collocation\jcobi.sci');
exec('.\collocation\radau.sci');
exec('.\collocation\intrp.sci');
exec('.\collocation\dfopr.sci');

nc=7    //number of interior collocation points
n0=1    //x0 is included as an interpolation point (1=yes, 0=no)
n1=1    //x1 is included as an interpolation point (1=yes, 0=no)
Nc=nc+n0+n1  //total collocation points
al=0
be=0
s=0
sx=0
BCincl=%T
[Ac,Bc,W,xc,dif1]=colloc(nc,n0,n1,al,be,s,sx,BCincl);
xpos1="$"+string(round(xc*1000)/1000)+"$"+"$\mathsf{\times L}$"
xpos1=["air";xpos1]
pwr=ones(Nc,1)*(0:Nc-1)
Ax=(xc*ones(1,Nc)).^pwr

//pde function
aa=1000
function [f, ires]=model(t, y, dy)
   //t : time
   //y : T = y(1:Nc)
   //    L=y(Nc+1)
   //dy: dT/dt = dy(1:Nc)
   //    dL/dt = dy(Nc+1)
   T=y(1:Nc)
   L=y(Nc+1)
   dT=dy(1:Nc)
   dL=dy(Nc+1)

   Tat=Tb+(Ta-Tb)*(1-exp(-aa*t^2))
   f1=h*(Tat-T(1))+(k/L)*Ac(1,:)*T
   f2=(alpha/L^2)*Bc(2:Nc-1,:)*T-dT(2:Nc-1)
   f3=T(Nc)-Tb
   f4=(-(k/(L*ro*Hc))*Ac(Nc,:)*T)+dL
   f=[f1;f2;f3;f4]
   ires=0
endfunction

function f=xcross(t, y, dy)
endfunction

//initial temp
T0(1:Nc)=Tb
dT0(1:Nc)=0
```

```
L0=0.0001  //1mm thick ice
dL0=0
t0=0

t=linspace(0,160*3600,1000)'  //160h
//t=logspace(-1,6,1000);t=[t0 t]'
Nt=length(t)  //time points
ng=0
y0=[T0;L0]
dy0=[dT0;dL0]
tic()
[r,ng]=dasrt([y0,dy0],t0,t,model,ng, xcross)
disp(toc())
Tat=Tb+(Ta-Tb)*(1-exp(-aa*t'.^2))
tt=r(1,:)  //time
Tx=r(2:Nc+1,:)  //temperature map
Lt=r(Nc+2,:)  //position of the ice interface
dLdt=r(2*Nc+3,:)
xt=Lt.*.xc  //actual position of Tx
//the next target is to plot the profiles versus actual position
//the postion moves with L
//Thus interpolation is needed to get the T values at constant L
//each t data set is a polynomial of order nc+1 in xc
//its best to work with Tx' data, where
//Lx=[0.01 0.03 0.05 0.08 0.13 0.18 0.25 0.39]'  //the position of the temperature measurements
Lx=[0.01 0.03 0.05 0.07 0.11 0.15 0.17 0.21 0.23 0.25 0.27 0.33]'  //the position of the temperature measurements
nx=length(Lx)
xpos="$"+string(round(Lx*1000)/10)+"$"+"$\mathsf{cm}$"
xpos=["air";xpos]
Rx=Lx.*.(Lt.^-1)  //Rx=Lx/Lt for all times points
            //Rx < 1 the temperature is measured in the ice
            //Rx >1 the temperature is in the brine
[row,col]=size(Rx)
kk=find(Rx>1)
Rx(kk)=1   //Rx max is 1 for interpolation
//get interpolation coefficients at each time step
a=Ax\Tx  //poly coeff's for all the x data at each t

Tt(1:row,1:col)=Tb  //define Tt the same shape as Tx, Rx etc and set T=Tb
[krow,kcol]=find(Rx<1)  //all values <1
nk=length(krow)
k=find(Rx<1)
//find A
pwrx=ones(nk,1)*(0:Nc-1)
A=(Rx(k)'*ones(1,Nc)).^pwrx   //interpolation matrix
for i=1:nk
   Tt(k(i))=A(i,:)*a(:,kcol(i))  //interpolation for all Rx<1
end
disp(toc())

//===========================================
//plot the model data
ff=scf(11);clf//T vs t
ff.figure_size=[600 500]
ga=gca()
ga.thickness=2
ga.font_size=3
cmap=jetcolormap(13)
plot((tt/3600)',[Tat' Tx'],"color",cmap)
xlabel('$\Large\mathsf{Time\,(hrs)}$',"fontsize",4)
ylabel('$\Large\mathsf{Temperature\,(^\circ C)}$',"fontsize",4)
legend(xpos1,-1)

[xxxx,nx]=max(dLdt)
ttx=tt(nx+20:$)'
Ltx=Lt(nx+20:$)'
```

```
tref=3600
a1=0.6;a2=10;a3=20
A=[ones(length(ttx),1)  ttx/ttx($) exp(-a1*ttx/ttx($)) exp(-a2*ttx/ttx($))]
x=A\Ltx
Ltt=A*x
A=[ones(length(ttx),1)/ttx($) -a1/ttx($)*exp(-a1*ttx/ttx($)) -a2/ttx($)*exp(-a2*ttx/ttx($)) ]
dLdtt=A*x(2:$)

function f=modelx(x)
   f=x(1)+x(6)*ttx/ttx($) + x(2)*exp(-x(3)*ttx/ttx($)) + x(4)*exp(-x(5)*ttx/ttx($))
endfunction
function f=modeldx(x)
   f=x(6)/ttx($) - x(2)*x(3)/ttx($)*exp(-x(3)*ttx/ttx($)) - x(4)*x(5)/ttx($)*exp(-x(5)*ttx/ttx($))
endfunction
function f=fitx(x, m)
   f=modelx(x)-Ltx
endfunction
x0=[x(1) x(3) a1 x(3) a2 x(2)]'
x=lsqrsolve(x0,fitx,length(ttx))
Ltx=modelx(x)
dLdtx=modeldx(x)

ff=scf(12);clf// plot of ice growth with time
ff.figure_size=[600 600]
ga=gca()
ga.thickness=2
ga.font_size=4
plot((tt/3600),Lt*100,"o")
plot(ttx/3600,Ltt*100,"--green")
plot(ttx/3600,Ltx*100,"--red")
xlabel("Time (hrs)","fontsize",4)
ylabel("Ice Thickness (cm)","fontsize",4)

ff=scf(17);clf// plot of growth rate
ff.figure_size=[600 600]
ga=gca()
ga.thickness=2
ga.font_size=4
plot(tt/3600,dLdt*360000,"red")
plot(ttx/3600,dLdtt*360000,"--green")
plot(ttx/3600,dLdtx*360000,"--blue")
xlabel("Time (hrs)","fontsize",4)
ylabel("Growth rate (cm/hr))","fontsize",4)

Area=0.0697464 //m^2, this is the area of the tank in the direction that ice grows
Q= (Area*ro*Hc*dLdt)
kc1=-(Q.*Lt./(Area*(Tt(1,:)-Tt(10,:))))
h1=-(Q./(Area*(Tat-Tt(1,:))))
slope=h1./kc1
disp(slope)

//legend("","thermal conductivity")
ff=scf(8);clf
ff.figure_size=[600 600]
ga=gca()
ga.thickness=2
ga.font_size=4
plot(tt'/3600,kc1,"red")// no fitting of curves
xlabel('$\Large\mathsf{Time\,(hrs)}$',"fontsize",3.5)
ylabel('$\Large\mathsf{Thermal\,conductivity\,(W/m^\circ C)}$',"fontsize",2)

ff=scf(9);clf// convective heat transfer coeeficient
ff.figure_size=[600 600]
ga=gca()
ga.thickness=2
ga.font_size=4
```

```
plot(tt'/3600,h1,"green")// no fitting of curves
xlabel('$\Large\mathsf{Time\,(hrs)}$',"fontsize",3.5)
ylabel('$\Large\mathsf{Convective\,heat\,transfer\,coeeficient\,(W/m^2^\circ C)}$',"fontsize",2)

ff=scf(13);clf  //T vs xc
ff.figure_size=[700 600]
ga=gca()
ga.thickness=2
ga.font_size=3.5
n=length(tt)
nn=1:1:n
felix=1
cmap=[((n-nn')/n).^felix  ((n-nn')/n).^felix  ones(n,1)]
gcf().color_map =wintercolormap(length(nn))
cmap=wintercolormap(length(nn))
//ga.data_bounds = [0,-16;35,0]
drawlater()
plot(xc,Tx,"color",cmap)
xlabel('$\Large\mathsf{Normalised\,position\,in\,ice}$',"fontsize",3.5)
ylabel('$\Large\mathsf{Temperature\,(^\circ C)}$',"fontsize",3.5)
colorbar(0,(tt($)/3600))
gce().title.text='$\Large\mathsf{Time\,(hrs)}$'//"Time (hrs)"
gce().title.font_size = 3.5
gce().font_size = 3.5
drawnow()

ff=scf(14);clf//plot the model data at fixed Lx
ff.figure_size=[600 500]
ga=gca()
ga.thickness=2
ga.font_size=3
n=length(tt)
nn=1:1:n
felix=1
cmap=[((n-nn')/n).^felix  ((n-nn')/n).^felix  ones(n,1)]
gcf().color_map =wintercolormap(length(nn))
cmap=wintercolormap(length(nn))
drawlater()
plot((xt*100),Tx,"color",cmap)
xlabel('$\Large\mathsf{Position\,(cm)}$',"fontsize",3.5)
ylabel('$\Large\mathsf{Temperature\,(^\circ C)}$',"fontsize",3.5)
colorbar(0,(tt($)/3600))
gce().title.text='$\Large\mathsf{Time\,(hrs)}$'//"Time (hrs)"
gce().title.font_size = 3.5
gce().font_size = 3.5
drawnow()

ff=scf(15);clf//plot the model data at fixed Lx
ff.figure_size=[600 500]
ga=gca()
ga.thickness=2
ga.font_size=3
cmap=jetcolormap(13)
plot((tt/3600)',[Tat' Tt'],"color",cmap)
xlabel('$\Large\mathsf{Time\,(hrs)}$',"fontsize",4)
ylabel('$\Large\mathsf{Temperature\,(^\circ C)}$',"fontsize",4)
legend(xpos,-1)

ff=scf(16);clf  //T vs Lx
ff.figure_size=[700 600]
ga=gca()
ga.thickness=2
ga.font_size=3
ga.data_bounds = [0,-16;35,0]
n=length(tt)
nn=1:1:n
```

```
felix=1
cmap=[((n-nn')/n).^felix  ((n-nn')/n).^felix  ones(n,1)]
gcf().color_map =wintercolormap(length(nn))
cmap=wintercolormap(length(nn))
drawlater()
plot((Lx*100),Tt,"color",cmap)
xlabel('$\Large\mathsf{Position\,(cm)}$',"fontsize",3.5)
ylabel('$\Large\mathsf{Temperature\,(^\circ C)}$',"fontsize",3.5)
colorbar(tt(1)/3600,(tt($)/3600))
gce().title.text='$\Large\mathsf{Time\,(hrs)}$'//"Time (hrs)"
gce().title.font_size = 3.5
gce().font_size = 3.5
drawnow()
```

Appendix B: Experimental temperature output data

B1: Uncertainty in temperature measurements

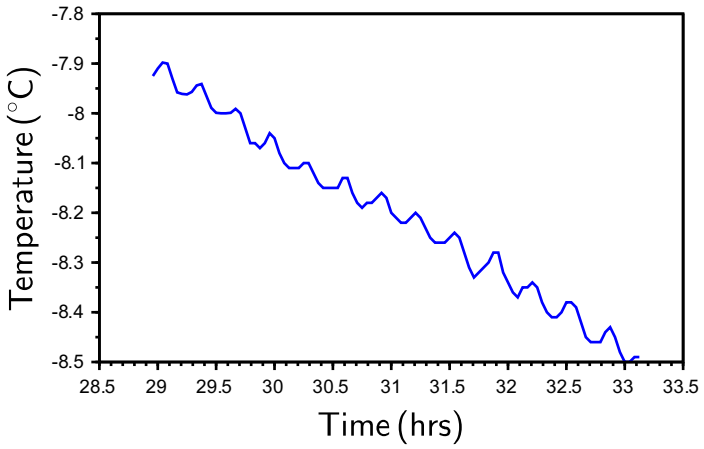


Figure B1: Zoomed in temperature time profile for artificial sea ice showing the temperature fluctuations as recorded by the temperature probe located 1 cm within the growing ice- to show the uncertainty in the temperature measurements

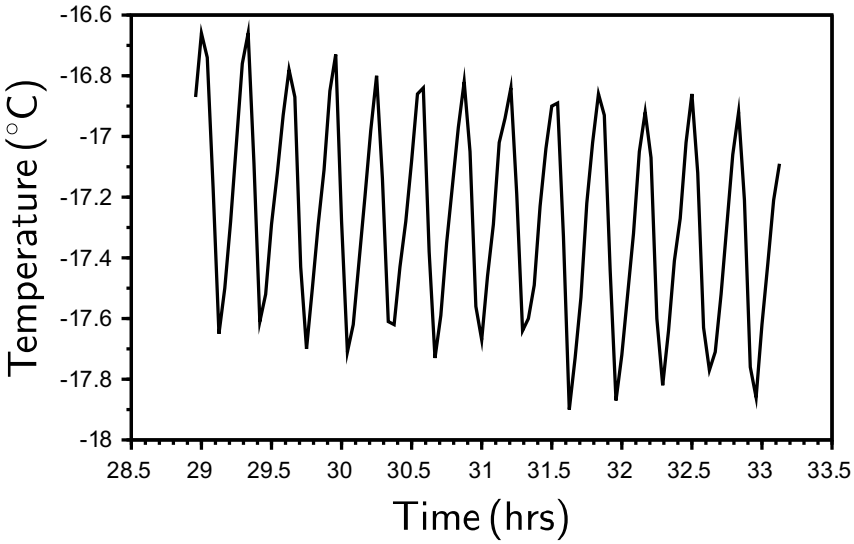


Figure B2: Zoomed in temperature time profile for artificial sea ice showing the temperature fluctuations as recorded by the temperature probe located 1 cm above the ice surface to measure the air temperature within the growing ice- to show the uncertainty in the temperature measurement

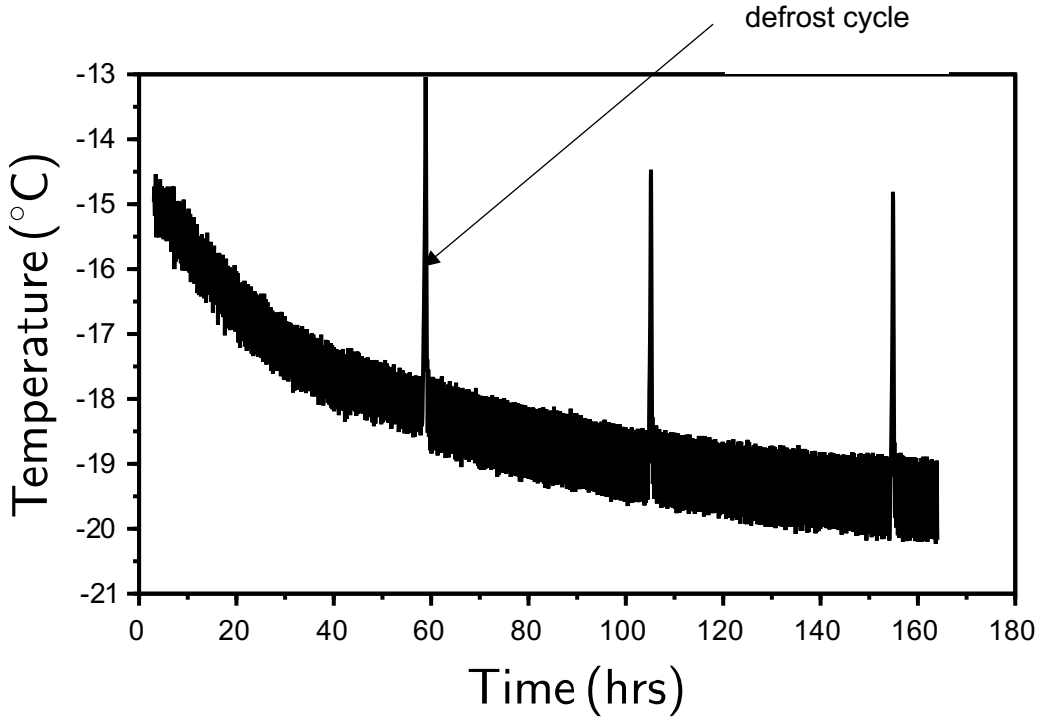


Figure B3: Temperature time profile showing the defrost cycles as recorded by the temperature probe located 1 cm above the ice surface to measure the air temperature within the growing ice

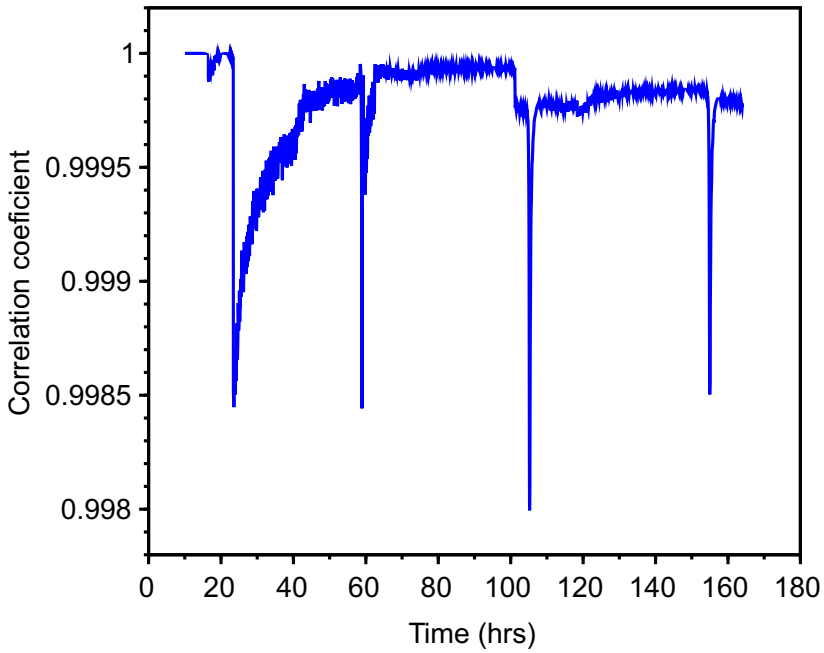


Figure B4: Variation of the correlation coefficient of the linear regression of the temperature vs depth data at each time point in Figure 5.2. (this is for the experiment that was performed at -20°C at 10 PSU)

B2: Temperature profiles to analyse the effect of varying the air temperature on the growth dynamics and conductive heat flux of artificial sea ice

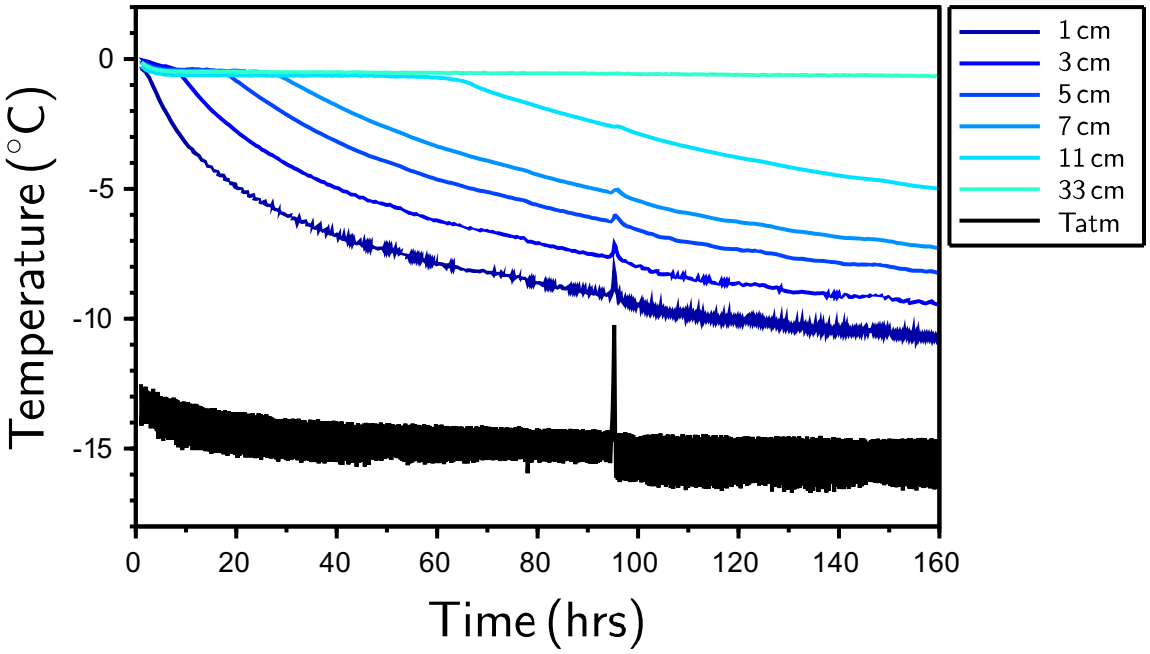


Figure B5: Temperature-time profile for artificial sea ice grown at 10 PSU at -15°C for 160 hours

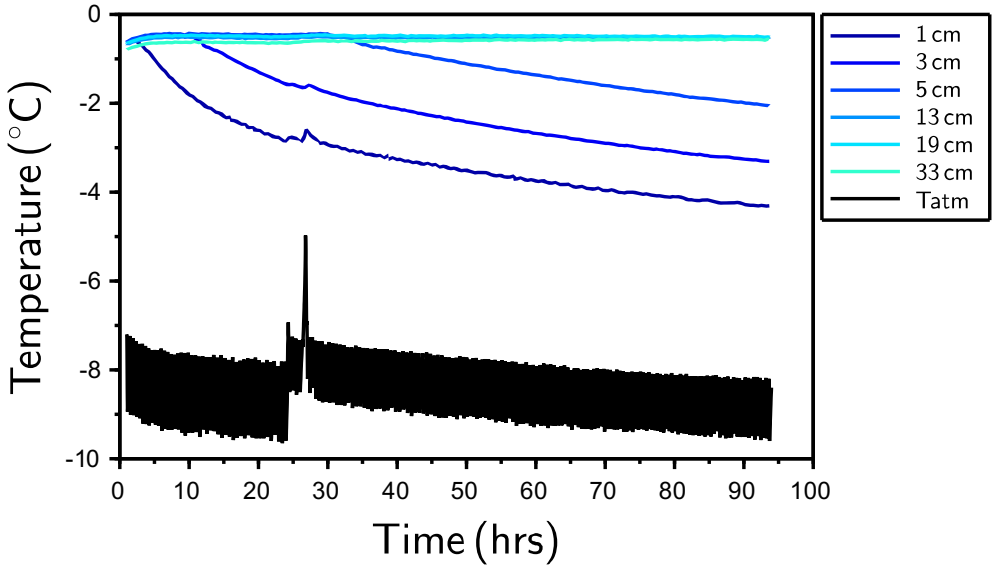


Figure B6:Temperature- time profiles for artificial sea ice grown at 10 PSU at -10°C for 94 hours

B3: Temperature profiles to analyse the effect of varying the starting solution salinity on the growth dynamics and conductive heat flux of artificial sea ice

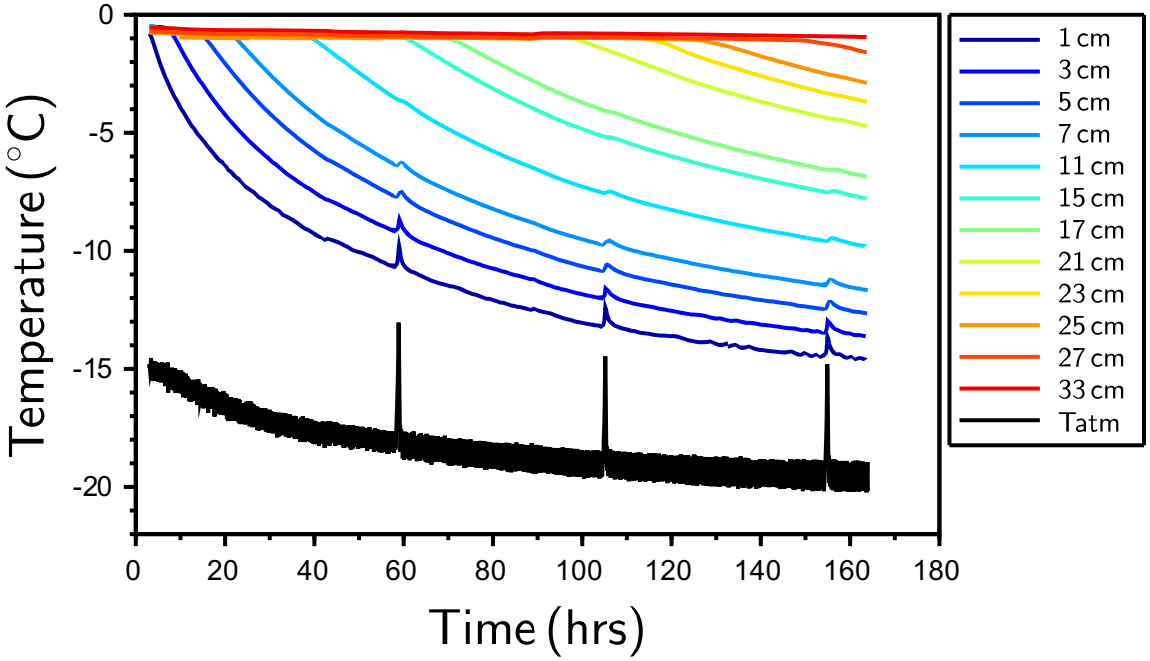


Figure B7:Temperature-time profile for artificial sea ice grown at 10 PSU at -20°C for 140 hours in 30 L tank

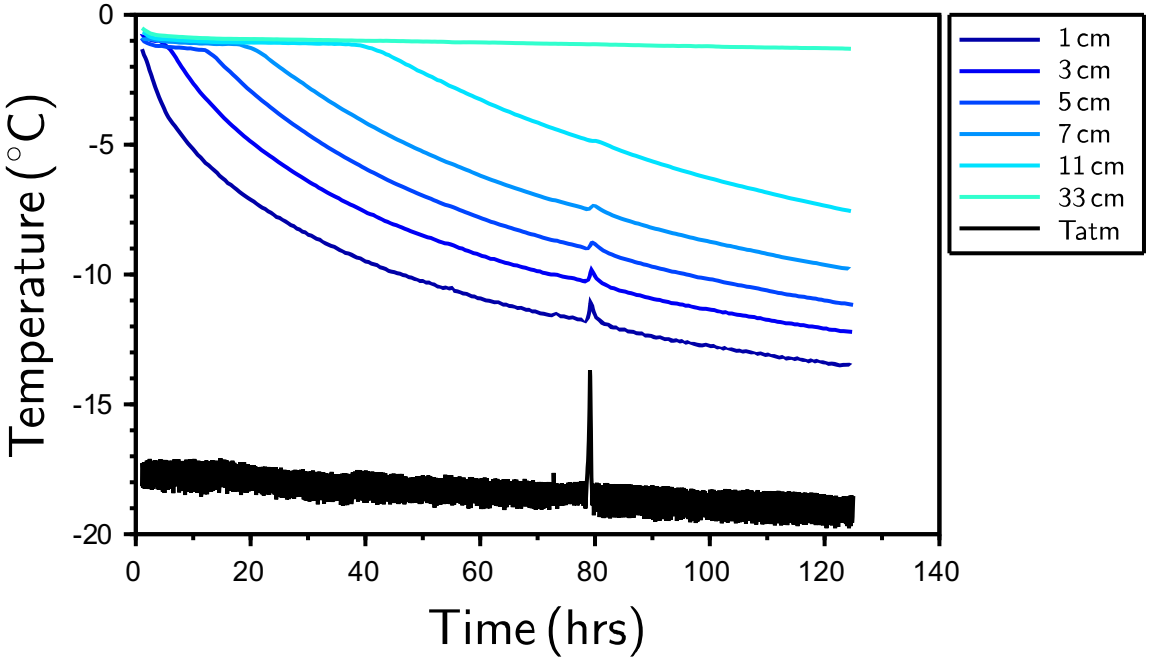


Figure B8:Temperature-time profile for artificial sea ice grown at 20 PSU at -20°C for 125 hours in 30 L tank

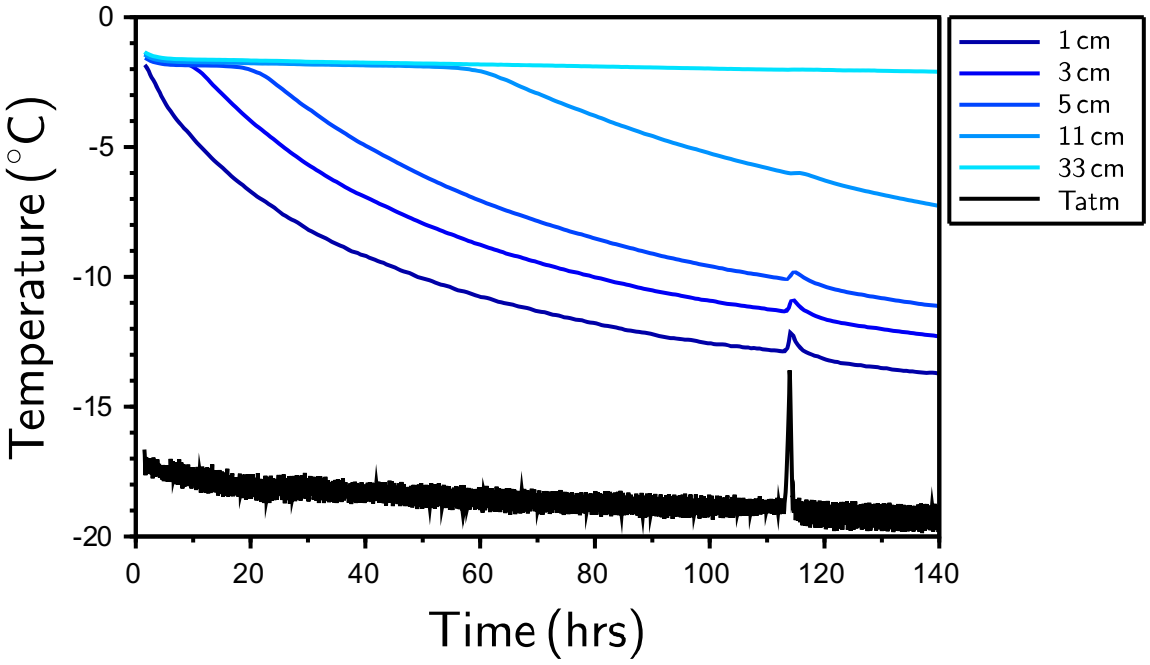


Figure B9:Temperature-time profile for artificial sea ice grown at 30 PSU at -20ºC for 248 hours in 30 L tank

B4: Temperature profiles to analyse the effect of varying the tank on the growth dynamics and conductive heat flux of artificial sea ice

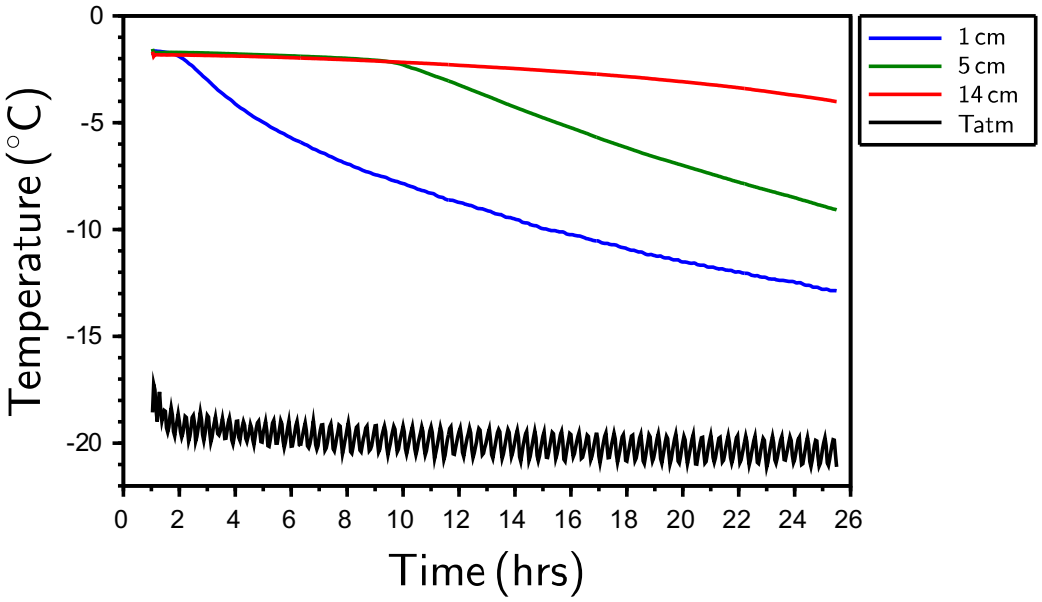


Figure B10: Temperature-time profile for artificial sea ice grown at 30 PSU at -20ºC for 25 hours in a 3 L tank

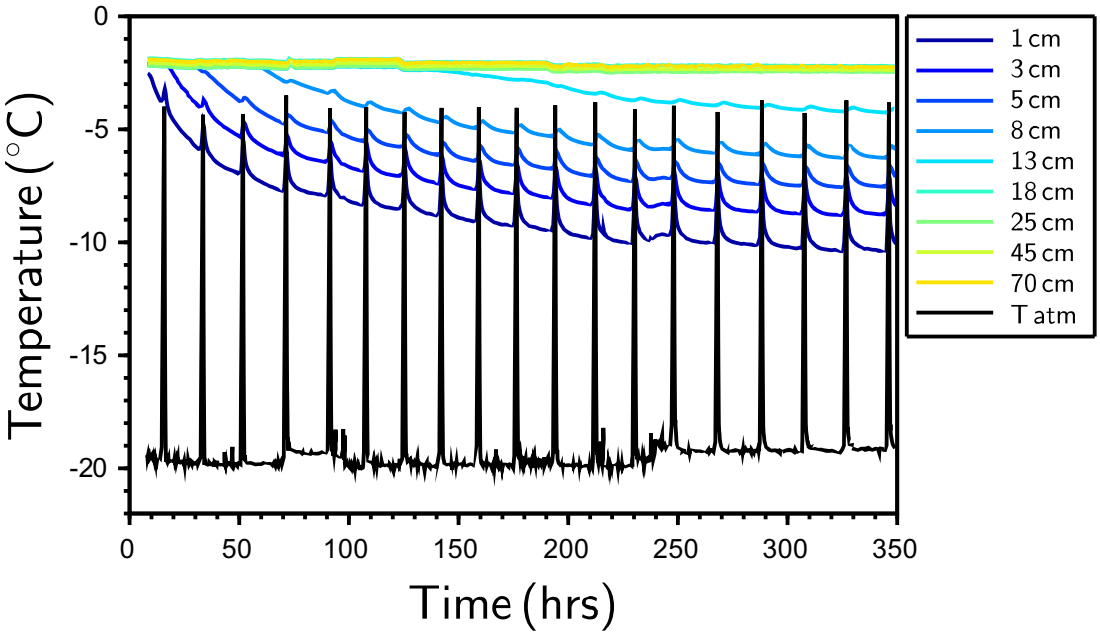


Figure B11: Temperature-time profile for artificial sea ice grown at 30 PSU at -20°C for 350 hours in a 300 L tank

B5: Dynamic model output data

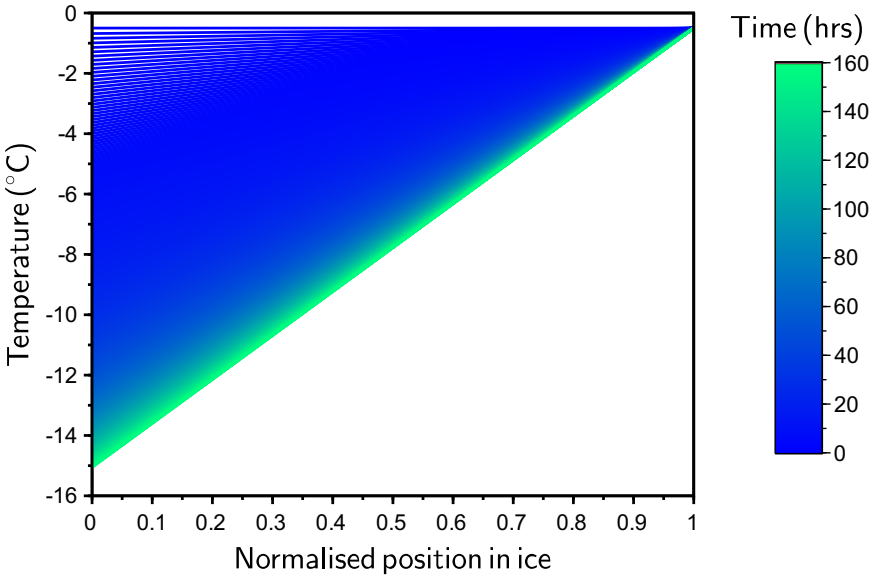


Figure B12: Simulated temperature with normalised depth profile for artificial sea ice growing at -20°C where all the temperature normalised nodes are within the ice

B6: Sample Temperature- Depth Profile to prove that the temperature profile within the artificial se ice is linear

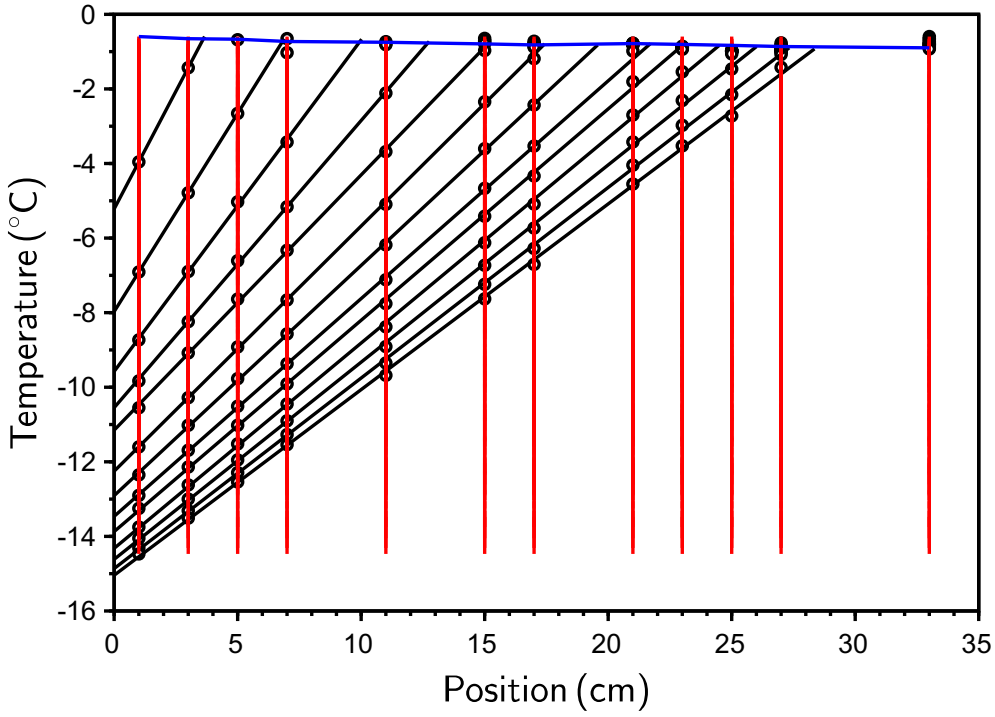


Figure B13: Temperature profile with depth for artificial sea ice grown at -20°C at 10PSU. This is raw data of Fig 5.1 which has now been put into the z coordinate system. The blue lines show the brine temperature, the red vertical lines correspond to the position of the thermocouple. The black lines show the linear profile of the ice after every 1000th time step. The black lines are the same as those that were shown in Figure 5.2. Thus, they correspond to the same timestamp as in Fig 5.2. The circles represent the measured temperature at each location at a specific time

Appendix C: Cross polarised images for artificial sea ice

The following are cross polarised images of artificial sea ice that was grown at different growth conditions. Their purpose is to support the argument that the artificial sea ice that was grown is columnar.

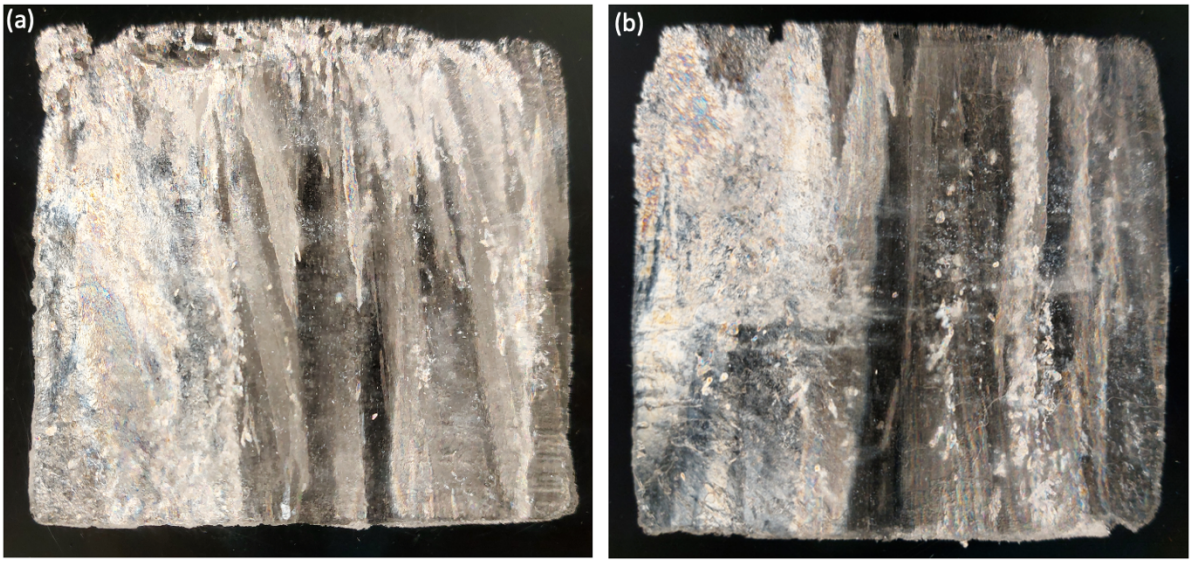


Figure C1: Cross polarised sample for artificial sea ice that was grown at -20^{o}C at 30 PSU in the 30 L tank where (a) represents the top section of the ice and (b) represents the bottom segment of the ice

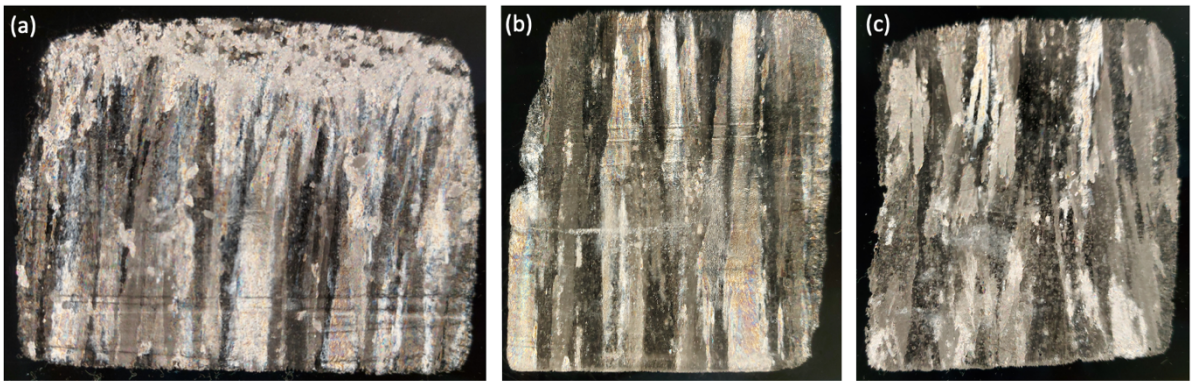


Figure C2: Cross polarised sample for artificial sea ice that was grown at -20^{o}C at 20 PSU in the 30 L tank where (a) represents the top section of the ice and (b) represents the middle segment of the ice and (c) represents the bottom segment of the ice

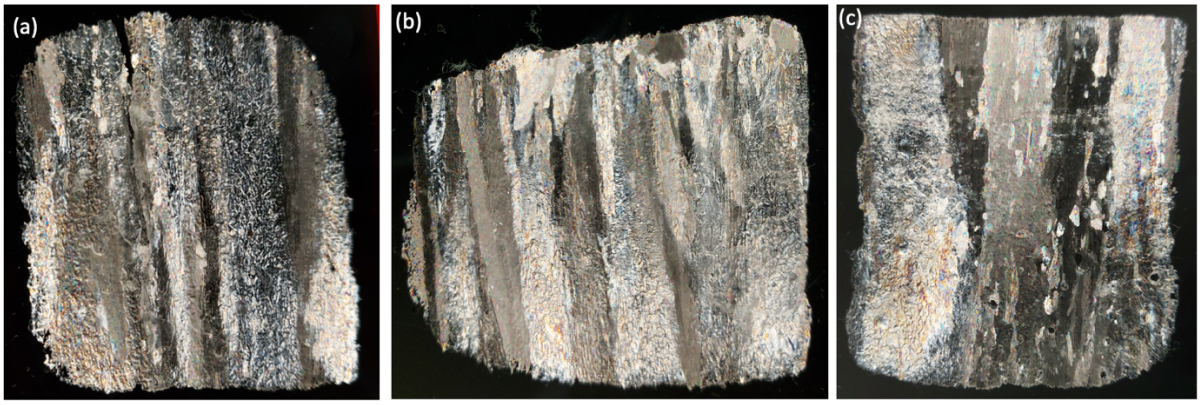


Figure C3: Cross polarised sample for artificial sea ice that was grown at -20°C at 10 PSU in the 30 L tank where (a) represents the top section of the ice and (b) represents the bottom segment of the ice

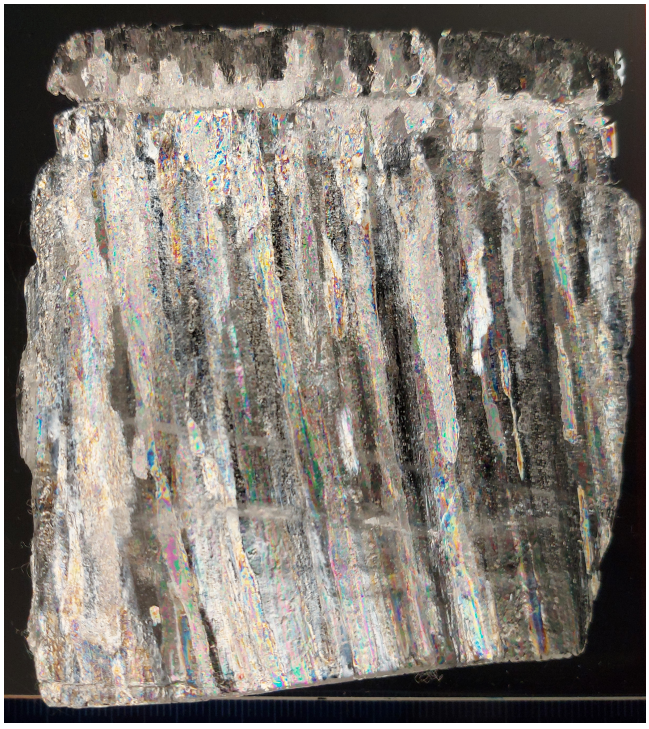
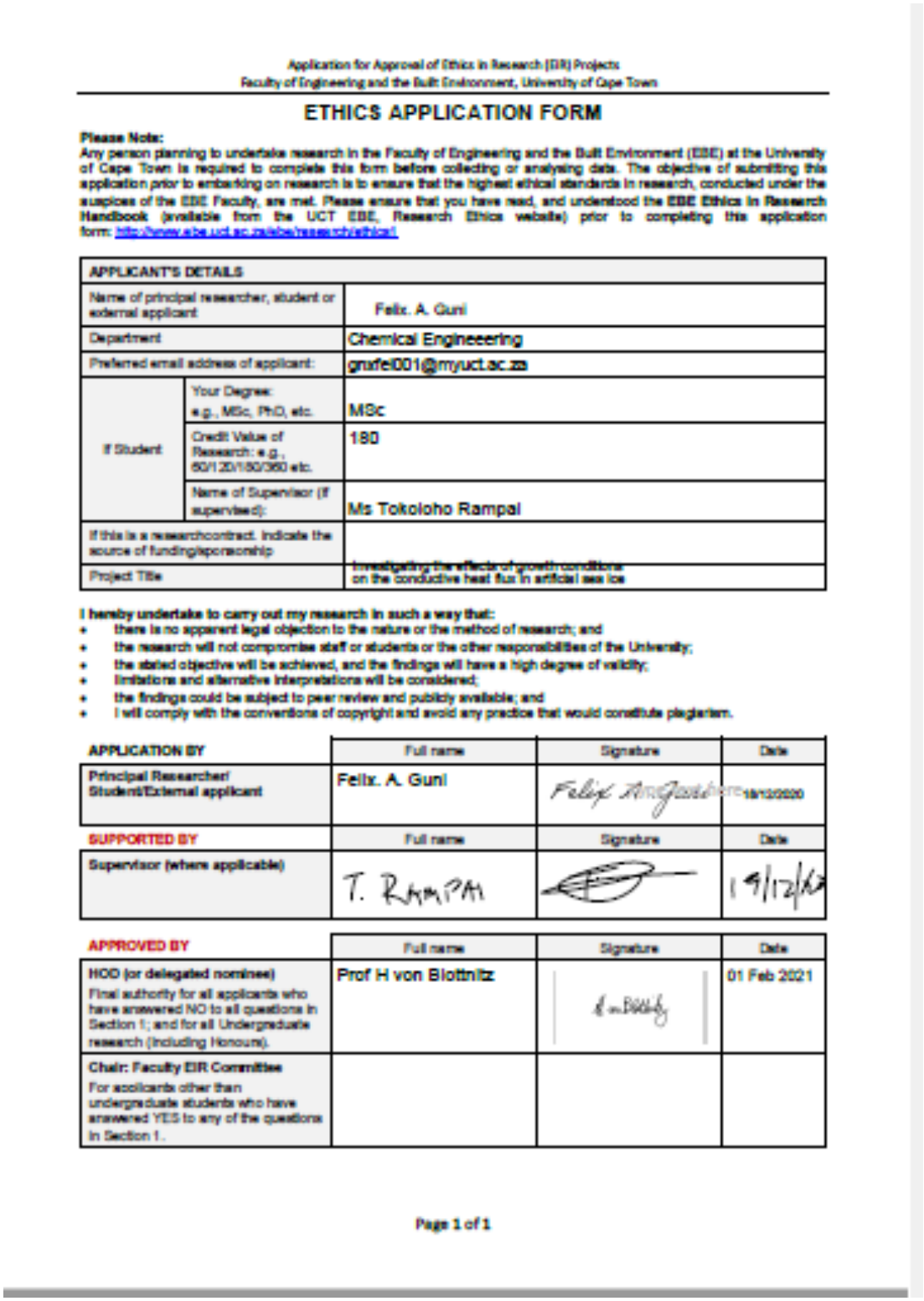


Figure C4: Cross polarised sample for artificial sea ice that was grown at -10°C at 10 PSU in the 30 L tank

Appendix D: Ethics Approval

This project met the requirements and guidelines as set by UCT. There were no ethical considerations for this project It was approved by the relevant authorities. This is shown below:



Application for Approval of Ethics in Research (EIR) Projects
Faculty of Engineering and the Built Environment, University of Cape Town

ETHICS APPLICATION FORM

Please Note:
Any person planning to undertake research in the Faculty of Engineering and the Built Environment (EBE) at the University of Cape Town is required to complete this form before collecting or analysing data. The objective of submitting this application *prior* to embarking on research is to ensure that the highest ethical standards in research, conducted under the auspices of the EBE Faculty, are met. Please ensure that you have read, and understood the **EBE Ethics in Research Handbook** (available from the UCT EBE, Research Ethics website) prior to completing this application form: http://www.ebe.uct.ac.za/ebe/research/ethics/

APPLICANT'S DETAILS		
Name of principal researcher, student or external applicant		Felix. A. Guni
Department		Chemical Engineeering
Preferred email address of applicant:		gnafel001@myuct.ac.za
If Student	Your Degree: e.g., MSc, PhD, etc.	MSc
	Credit Value of Research: e.g., 60/120/180/360 etc.	180
	Name of Supervisor (if supervised):	Ms Tokoloho Rampai
If this is a research contract, indicate the source of funding/sponsorship		
Project Title		Investigating the effects of growth conditions on the conductive heat flux in artificial sea ice

I hereby undertake to carry out my research in such a way that:
- there is no apparent legal objection to the nature or the method of research; and
- the research will not compromise staff or students or the other responsibilities of the University;
- the stated objective will be achieved, and the findings will have a high degree of validity;
- limitations and alternative interpretations will be considered;
- the findings could be subject to peer review and publicly available; and
- I will comply with the conventions of copyright and avoid any practice that would constitute plagiarism.

APPLICATION BY	Full name	Signature	Date
Principal Researcher/ Student/External applicant	Felix. A. Guni	Felix A. Guni	19/12/2020
SUPPORTED BY	Full name	Signature	Date
Supervisor (where applicable)	T. RAMPAI		19/12/20

APPROVED BY	Full name	Signature	Date
HOD (or delegated nominee) Final authority for all applicants who have answered NO to all questions in Section 1; and for all Undergraduate research (including Honours).	Prof H von Blottnitz		01 Feb 2021
Chair: Faculty EIR Committee For applicants other than undergraduate students who have answered YES to any of the questions in Section 1.			

Page 1 of 1